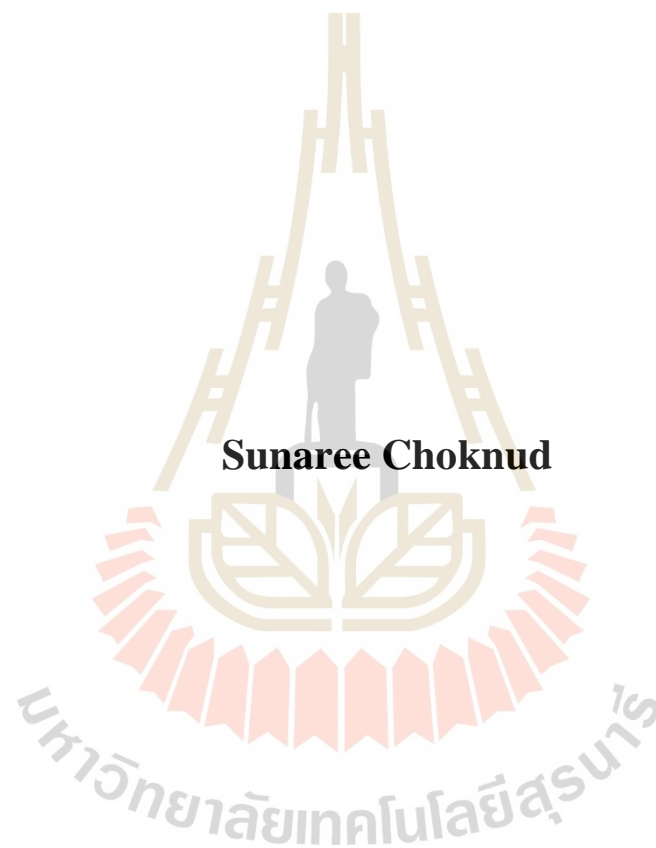


**TRANSGLYCOSYLATION BY RICE  $\beta$ -GLUCOSIDASES  
AND  $\beta$ -TRANSGLYCOSIDASE VARIANTS**



**Sunaree Choknud**

**A Thesis Submitted in Partial Fulfillment of the Requirements for the  
Degree of Doctor of Philosophy in Biochemistry and Biochemical Technology**

**Suranaree University of Technology**

**Academic Year 2020**

ปฏิบัติการย้ายกลุโคสโดยเอนไซม์เบต้ากลูโคซิเดสและ  
เบต้าทรานส์กลูโคซิเดสจากข้าว



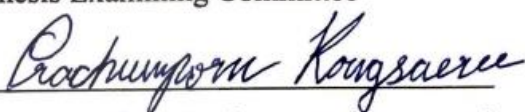
ว่าที่ร้อยตรีหญิงสุนารี โชนัด

วิทยานิพนธ์นี้เป็นส่วนหนึ่งของการศึกษาตามหลักสูตรปริญญาวิทยาศาสตรดุษฎีบัณฑิต  
สาขาวิชาชีวเคมีและเทคโนโลยีชีวเคมี  
มหาวิทยาลัยเทคโนโลยีสุรนารี  
ปีการศึกษา 2563

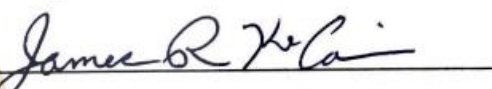
**TRANSGLYCOSYLATION BY RICE  $\beta$ -GLUCOSIDASES AND  
 $\beta$ -TRANSGLYCOSIDASE VARIANTS**

Suranaree University of Technology has approved this thesis submitted in partial fulfillment of the requirements for the Degree of Doctor of Philosophy.

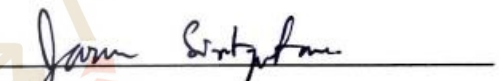
Thesis Examining Committee

  
(Assoc. Prof. Dr. Prachumporn Kongsaree)


Chairperson

  
(Prof. Dr. James R. Ketudat-Cairns)

Member (Thesis Advisor)

  
(Assoc. Prof. Dr. Jarawan Siritapetawee)

Member

  
(Asst. Prof. Dr. Panida Khunkaewla)


Member

  
(Dr. Vincent Blay Roger)

Member

  
(Assoc. Prof. Dr. Chatchai Jothityangkoon)

Vice Rector for Academic Affairs  
and Quality Assurance

  
(Assoc. Prof. Dr. Worawat Meevasana)

Dean of Institute of Science

สุนารี โชคนัด : ปฏิกริยาการย้ายกลูโคสโดยเอนไซม์เบต้ากลูโคซิเดสและเบต้าทรานส์กลูโคซิเดสกลายพันธุ์จากข้าว (TRANSGLYCOSYLATION BY RICE  $\beta$ -GLUCOSIDASES AND  $\beta$ -TRANSGLYCOSIDASE VARIANTS). อาจารย์ที่ปรึกษา : ศาสตราจารย์ ดร.เจมส์ เกตุทัต-คาร์นส์, 141 หน้า.

ปฏิกริยาการไกลโคซิเลชันเป็นกลไกที่สำคัญที่สามารถลดหรือเพิ่มฤทธิ์ทางชีวภาพของสารนั้นได้ เพิ่มความสามารถในการละลายน้ำ และเพิ่มส่วนยึดจับกับตัวรับสัญญาณ (receptor binding sites) ไกลโคไซด์ถูกสร้างได้โดยเอนไซม์ไกลโคซิลทรานส์เฟอเรส โดยการย้ายน้ำตาลจากน้ำตาลนิวคลีโอไทด์ (nucleotide sugars) หรือไกลโคไซด์ไฮโดรเลส โดยผ่านปฏิกริยาทรานส์ไกลโคซิเลชันหรือปฏิกริยาไฮโดรไลซิสแบบย้อนกลับ เอนไซม์คล้ายคลึงไกลโคไซด์ไฮโดรเลส (glycoside hydrolase homologues) บางชนิดเลือกย้ายน้ำตาลจากอนุพันธ์ของคาร์โบไฮเดรทให้กับนิวคลีโอไฟล์มากกว่าให้น้ำ เรียกว่า เอนไซม์ทรานส์กลูโคซิเดส

เอนไซม์ไกลโคไซด์ไฮโดรเลสตระกูลที่ 1 เป็นเอนไซม์ที่พบเป็นวงกว้าง ทำหน้าที่ตัดพันธะโอ-ไกลโคซิดิก ระหว่างส่วนที่เป็นน้ำตาล ที่ต่อกับส่วนที่ไม่ใช่น้ำตาล เอนไซม์ Os9BGlu31 ทรานส์กลูโคซิเดส จากรายงานก่อนหน้านี้พบว่า มีความสามารถเร่งปฏิกริยาการเคลื่อนย้ายกลูโคสในพืชเพื่อสร้างอนุพันธ์ของคาร์โบไฮเดรท และ Os9BGlu31 ในรูปกลายพันธุ์ W243L และ W243N ถูกรายงานว่ามีประสิทธิภาพสูงในการเคลื่อนย้ายกลูโคสให้กับตัวรับที่หลากหลายมากกว่า Os9BGlu31 ดั้งเดิม

ในที่นี้เราได้ทำการศึกษาการย้ายกลูโคสให้กับยาปฏิชีวนะและยาเคมีบำบัด โดย Os9BGlu31 กลายพันธุ์ W243L และ W243N และวิเคราะห์ปฏิกริยาโดยวิธี UPLC จากการศึกษาพบว่ามี 6 ตัวอย่างที่สามารถรับกลูโคสได้แก่ (1) คลอแรมเฟนิคอล (2) ไนโบไมซิน (3) ยาแอมพิซิลลิน (4) อะมอกซิซิลลิน (5) เตตราไซคลิน และ (6) ดอกโซรูบิซิน นอกจากนี้ได้มีการผลิตคลอแรมเฟนิคอลไกลโคไซด์โดย Os9BGlu31W243N และพิสูจน์โครงสร้างทางเคมีด้วยวิธี NMRพบว่า เบต้า-ดี-กลูโคส เชื่อมกับแอลกอฮอล์ปฐมภูมิของคลอแรมเฟนิคอล

เอนไซม์ไกลโคไซด์ไฮโดรเลสตระกูลที่ 3 เอกโซกลูคาเนส ทำหน้าที่ตัดเบต้ากลูแคนในพืช OsExo1 มีการแสดงออกหลากหลายใน *P. pastoris* โดยในขั้นตอนการทำบริสุทธิ์ พบว่า OsExo1 ถูกเติมน้ำตาลในระดับที่ต่างกัน และน้ำตาลเหล่านั้นสามารถถูกตัดได้ด้วยเอนไซม์ Endo-glycosidase H



เอนไซม์ OsExo1 ที่ถูกเติมน้ำตาล (glycosylated) ในระดับสูงมีค่ากิจกรรมจำเพาะ (specific activity) สูงสุดคือ  $17.8 \text{ U}\cdot\text{mg}^{-1}$  ระดับปานกลางคือ  $9.76 \text{ U}\cdot\text{mg}^{-1}$  ระดับต่ำคือ  $4.02 \text{ U}\cdot\text{mg}^{-1}$  ในขณะที่เอนไซม์ที่ถูกตัดน้ำตาลออก (deglycosylated) มีค่ากิจกรรมจำเพาะอยู่ที่  $9.47 \text{ U}\cdot\text{mg}^{-1}$  และดูเหมือนว่าการที่เอนไซม์ถูกเติมน้ำตาลนั้น ไม่มีผลต่อความเสถียรของเอนไซม์ ค่าประสิทธิภาพการเร่งปฏิกิริยาของเอนไซม์ที่ถูกเติมน้ำตาล และเอนไซม์ที่ถูกตัดน้ำตาล ต่อ *p*NPGlc ( $k_{\text{cat}}/K_M$  113 และ  $157 \text{ mM}^{-1}\text{s}^{-1}$ ) ลามินาไรโบส ( $k_{\text{cat}}/K_M$  446 และ  $546 \text{ mM}^{-1}\text{s}^{-1}$ ) และลามินาริน ( $k_{\text{cat}}/K_M$  438 และ  $602 \text{ mM}^{-1}\text{s}^{-1}$ ) พบว่า เอนไซม์ที่ถูกเติมน้ำตาลมีค่าต่ำกว่าเอนไซม์ที่ถูกตัดน้ำตาลออก อย่างไม่มีนัยสำคัญ ส่วนของ OsExo2 ถูกโคลนในพลาสมิด *p*ET32a/DEST และถูกผลิตใน *E. coli* ในขั้นตอนการทำบริสุทธิ์ด้วยวิธี HIC พบว่าเมื่อชะล้างด้วยเอทิลีนไกลคอลที่ความเข้มข้นสูงขึ้นการทำงานของ OsExo2 เพิ่มขึ้นตาม เนื่องจากความสามารถของ OsExo2 ที่เคลื่อนย้ายกลูโคสไปให้กับเอทิลีนไกลคอล การเคลื่อนย้ายกลูโคสโดยเอนไซม์ OsExo1 และ OsExo2 ถูกทดสอบโดยใช้ *p*NPGlc ทำหน้าที่เป็นตัวให้กลูโคสให้กับแอลกอฮอล์ชนิดต่างๆ ที่ทำหน้าที่เป็นตัวรับกลูโคส การทดสอบนี้พบว่า OsExo1 และ OsExo2 สามารถย้ายกลูโคสไปให้กับแอลกอฮอล์สายสั้นที่มีหมู่ไฮดรอกซิลที่เป็นแอลกอฮอล์ชนิดปฐมภูมิผลิตภัณฑ์กลูโคไซด์ของแอลกอฮอล์กลุ่มนี้ได้รับการยืนยัน โครงสร้างทางเคมีด้วยวิธี NMR ได้แก่ (1) methyl- $\beta$ -D-glucoside (2) ethyl- $\beta$ -D-glucoside (3) *n*-propyl- $\beta$ -D-glucoside (4) 1-butyl- $\beta$ -D-glucoside (5) 3-methyl-1-butyl- $\beta$ -D-glucoside (6) propargyl- $\beta$ -D-glucoside (7) 4-hydroxybenzyl- $\beta$ -D-glucoside และ (8) Ethylene-disulfide- $\beta$ -D-glucoside ในขณะที่ *p*NPGlc สามารถทำหน้าที่เป็นได้ทั้งตัวให้และตัวรับกลูโคสในเวลาเดียวกัน ผลิตภัณฑ์ที่ได้จากปฏิกิริยาของ *p*NPGlc สามารถแยกได้ 4 ตัวอย่าง และถูกพิสูจน์โครงสร้างทางเคมีด้วยวิธี NMR ได้แก่ (1) *p*NP-gentiotriose (2) *p*NP-gentiobiose (3) *p*NP-cellobiose และ (4) *p*NP-laminaribiose นอกจากนี้เซลโล-โอลิโกแซ็กคาไรด์ (C2-C5) ลามินาไรโบ-โอลิโกแซ็กคาไรด์ (L2-L5) พอลิแซ็กคาไรด์ ได้แก่ ลามินาริน บาร์เลย์-กลูแคน และลิซิแนน ยังสามารถเป็นตัวให้กลูโคสสำหรับ OsExo1 และ OsExo2 ได้ด้วยเช่นกัน ผลการทดลองเหล่านี้แสดงให้เห็นถึงแนวทางที่มีประสิทธิภาพในการผลิตอนุพันธ์ของคาร์โบไฮเดรตที่เป็นประโยชน์ต่อไป

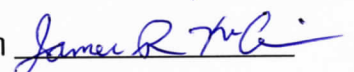
สาขาวิชาเคมี

ปีการศึกษา 2563

ลายมือชื่อนักศึกษา



ลายมือชื่ออาจารย์ที่ปรึกษา



SUNAREE CHOKNUD : TRANSGLYCOSYLATION BY RICE

$\beta$ -GLUCOSIDASES AND  $\beta$ -TRANSGLYCOSIDASE VARIANTS.

THESIS ADVISOR : PROF. JAMES R. KETUDAT-CAIRNS, Ph.D. 141 PP.

$\beta$ -GLYCOSIDE HYDROLASE/  $\beta$ -TRANSGLYCOSIDASE/  $\beta$ -EXOGLUCANASE/  
TRANSGLYCOSYLATION/ ALKYL GLUCOSIDE/ ANTIBIOTIC

Glycosylation is an important mechanism to restrict or increase bioactivity, increase water solubility and provide receptor binding sites. Glycosides can be produced by glycosyltransferases that transfer sugars from nucleotide sugars or glycoside hydrolases via transglycosylation or reverse hydrolysis. Some glycoside hydrolase homologues prefer to transfer sugars from glycoconjugates to nucleophiles other than water and are designated transglycosidases.

oside hydrolase family 1 are a widespread group of enzymes that hydrolyze the O-glycosidic bond between a sugar portion, which can be one or more monosaccharides, linked to a non-sugar moiety. Os9BGlu31 transglycosidase has been recognized to catalyze transglycosylation in production of glycoconjugates in plants from previous reports. Os9BGlu31 variants W243L and W243N were previously shown to have high activity and transglycosylate more substrates than wild-type enzyme. The transglycosylation of medicinal compounds by Os9BGlu31 variants W243L and W243N and assessed by reaction and ultra-high performance liquid chromatography (UPLC). Among the tested acceptor substrates, six acceptors resulted in glycosylated products, including chloramphenicol, nybomycin, ampicillin, amoxicillin, tetracycline, and doxorubicin. Chloramphenicol glucoside was produced

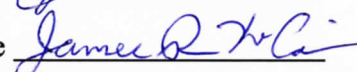
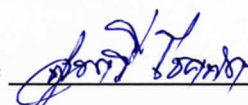
of this carbohydrate was removed by Endoglycosidase H. The high glycosylation form was found to have highest specific activity at  $17.8 \text{ U}\cdot\text{mg}^{-1}$ , the form with medium glycosylation had  $9.76 \text{ U}\cdot\text{mg}^{-1}$ , and the low glycosylation form had  $4.02 \text{ U}\cdot\text{mg}^{-1}$ , while the deglycosylated form had a specific activity of  $9.47 \text{ U}\cdot\text{mg}^{-1}$ . Glycosylation did not seem to be critical for the stability of OsExo1. The catalytic efficiency values of the OsExo1 glycosylated form were lower than the deglycosylated form for *p*NPGlc ( $k_{\text{cat}}/K_M$  113 and  $157 \text{ mM}^{-1}\text{s}^{-1}$ ), laminaribiose ( $k_{\text{cat}}/K_M$  446 and  $546 \text{ mM}^{-1}\text{s}^{-1}$ ), and laminarin ( $k_{\text{cat}}/K_M$  438 and  $602 \text{ mM}^{-1}\text{s}^{-1}$ ). When OsExo2 in pET32a/DEST was produced in *E. coli*, it was found to have transglucosylation activity toward ethylene glycol during HIC purification, evidenced by its activity increasing with increasing ethylene glycol concentration. The transglucosylation activity of OsExo1 and OsExo2 was assessed in reactions using *p*NPGlc as a glucosyl donor substrate and various alcohols as acceptors. OsExo1 and OsExo2 could apparently only transfer glucose to primary alcohols of short-chain molecules. The structures of short-chain alcohols were confirmed by NMR including methyl- $\beta$ -D-glucoside, ethyl- $\beta$ -D-glucoside, *n*-propyl- $\beta$ -D-glucoside, 1-butyl- $\beta$ -D-glucoside, 3-methyl-1-butyl- $\beta$ -D-glucoside, propargyl- $\beta$ -D-glucoside, 4-hydroxybenzyl- $\beta$ -D-glucoside, and  $\beta$ -mercaptoethyl- $\beta$ -D-glucoside. The *p*NPGlc can act as both, glucosyl donor and acceptor substrate at the same time. Four *p*NP-oligosaccharide products were identified from the transglucosylation reaction toward *p*NPGlc including *p*NP-gentiotrioside, *p*NP-gentiobioside, *p*NP-cellobioside, and *p*NP-laminaribiose. Cello-oligosaccharides (C2-C5), laminari-oligosaccharides (L2-L5), and the polysaccharides laminarin, barley glucan, and lichenan could serve as glucosyl donors for OsExo1 and OsExo2. These results suggest efficient enzyme-catalyzed routes to produce useful glycoconjugates.

School of Chemistry

Academic Year 2020

Student's Signature

Advisor's Signature



## ACKNOWLEDGEMENTS

First and foremost, I would like to thank my thesis advisor, Prof. Dr. James R. Ketudat-Cairns, for the opportunity to study towards my Ph.D. degree in Biochemistry and his kind supervision, encouragement, and support during my time at SUT, which allowed me to successfully complete my thesis program.

I sincerely thank Assoc. Prof. Dr. Prachumporn Kongsaree, Assoc. Prof. Dr. Jaruwan Siritapetawee, Asst. Prof. Dr. Panida Khunkaewla, and Dr. Vincent Blay Roger for patiently reading this dissertation and providing helpful comments.

Special thanks are extended to all JKC's Lab members for their help and cheering me up.

I would like to express my deepest gratitude to my family. They were always supporting me and encouraging me with their best wishes.

Finally, I would like to thank School of Chemistry, Center for Protein Structure, Function and Application, Institute of Science, and Institute of Research and Development, Suranaree University of Technology.

Sunaree Choknud



# CONTENTS

	<b>Page</b>
ABSTRACT IN THAI .....	I
ABSTRACT IN ENGLISH.....	III
ACKNOWLEDGEMENTS .....	V
CONTENTS.....	VI
LIST OF TABLES .....	XI
LIST OF FIGURES .....	XII
LIST OF ABBREVIATIONS.....	XVIII
<b>CHAPTER</b>	
<b>I INTRODUCTION .....</b>	<b>1</b>
1.1 General introduction .....	1
1.2 Research objectives.....	3
1.3 Research scope.....	4
<b>II LITERATURE REVIEW .....</b>	<b>5</b>
2.1 Glycoside hydrolases .....	5
2.2 Glycoside hydrolase mechanisms .....	6
2.3 $\beta$ -Glucosidases .....	9
2.4 Glycoside hydrolase family 1 .....	11
2.5 Glycoside hydrolase family 3 .....	12
2.6 Glycosylation .....	16

## CONTENTS (Continued)

	<b>Page</b>
2.7 Chemical glycosylation.....	17
2.8 Enzymatic glycosylation.....	18
2.8.1 Glycoside hydrolases (GH).....	19
2.8.2 Transglycosylase (TG).....	20
2.8.3 Leloir glycosyltransferases (GT).....	23
2.8.4 Glycoside phosphorylases (GP).....	25
<b>III MATERIALS AND METHODS.....</b>	<b>26</b>
3.1 Materials.....	26
3.1.1 Plasmids, bacterial and yeast stains .....	26
3.1.2 Chemicals and reagents.....	27
3.2 General methods .....	29
3.2.1 Preparation of <i>E. coli</i> competent cells.....	29
3.2.2 Transformation of plasmids into competent cells .....	29
3.2.3 Plasmid isolation by alkaline lysis method .....	30
3.2.4 Protein analysis by sodium dodecyl sulfate polyacrylamide gel electrophoresis.....	31
3.3 Site-directed mutagenesis .....	32
3.4 Expression and Purification of Os9BGlu31 and variants .....	34
3.4.1 Expression of Os9BGlu31 and variants .....	34
3.4.2 Purification of Os9BGlu31 and variants .....	34

## CONTENTS (Continued)

	<b>Page</b>
3.5 Transglycosylation of Os9BGlu31 and variants .....	35
3.6 Analytical chromatography.....	36
3.7 Chloramphenicol glucoside purification.....	36
3.8 Expression and purification of OsExo1 .....	37
3.8.1 Expression of OsExo1.....	37
3.8.2 Purification of OsExo1.....	37
3.9 Expression and purification of OsExo2 .....	38
3.9.1 Expression of OsExo2.....	38
3.9.2 Purification of OsExo2.....	38
3.10 Determination of the optimal pH and temperature and temperature stability for OsExo1 .....	39
3.11 Enzyme kinetics parameter determination of OsExo1 .....	40
3.12 Transglycosylation activity of OsExo1 and OsExo2 .....	40
3.13 Purification of OsExo2 transglycosylation products .....	41
3.14 Transglycosylation product structural confirmation .....	43
<b>IV RESULTS AND DISCUSSION.....</b>	<b>44</b>
4.1 Molecular docking of Os9BGlu31W243L mutation analysis by AutoDock Vina .....	44
4.2 Site-directed mutagenesis of Os9BGlu31W243L.....	46
4.3 Expression and purification of Os9BGlu31 and variants.....	46



## CONTENTS (Continued)

	<b>Page</b>
4.4 The activity of Os9BGlu31 variants on <i>p</i> NPGLc, cellobiose, and cellotriose .....	48
4.5 Transglucosylation of antibiotics and anticancer by Os9BGlu31 and variants .....	50
4.5.1 Chloramphenicol glucoside purification .....	58
4.5.2 Chloramphenicol glucoside structural confirmation .....	59
4.6 Sequence analysis of OsExo1 and OsExo2.....	61
4.7 Expression and purification of OsExo1 .....	64
4.8 Expression and purification of OsExo2 .....	65
4.9 Effect of the optimal pH and temperature and temperature stability for OsExo1 N-deglycosylated form .....	67
4.10 Kinetic parameters of OsExo1 .....	69
4.11 Transglucosylation activity of OsExo1 and OsExo2 .....	70
4.12 Purification of transglycosylation products of OsExo2 .....	78
4.13 Transglycosylation product structural confirmation .....	80
4.13.1 <i>p</i> NP-β-D-gentiotriose .....	81
4.13.2 <i>p</i> NP-β-D-gentiobioside .....	83
4.13.3 <i>p</i> NP-β-D-cellobioside.....	84
4.13.4 <i>p</i> NP-β-D-laminaribioside .....	86
4.13.5 Methyl-β-D-glucoside .....	87

## CONTENTS (Continued)

	<b>Page</b>
4.13.6 Ethyl- $\beta$ -D-glucoside .....	88
4.13.7 Propyl- $\beta$ -D-glucoside .....	88
4.13.8 <i>n</i> -Butyl- $\beta$ -D-glucoside.....	89
4.13.9 3-Methyl-1-butyl- $\beta$ -D-glucoside .....	90
4.13.10 2-Hydroxyethyl- $\beta$ -D-glucoside .....	91
4.13.11 Propargyl- $\beta$ -D-glucoside .....	92
4.13.12 Ethylene-disulfide- $\beta$ -D-glucoside .....	92
4.13.13 4-(Hydroxymethyl) benzyl- $\beta$ -D-glucoside.....	93
4.14 Summary and future directions .....	94
<b>V CONCLUSION.....</b>	<b>96</b>
REFERENCES.....	100
APPENDICES .....	113
APPENDIX A PROTEIN PURIFICATIONS.....	114
APPENDIX B NMR SPECTRA .....	121
APPENDIX C PUBLICATIONS.....	139
CURRICULUM VITAE.....	141

## LIST OF TABLES

Table	Page
3.1 Oligonucleotide primers for site-directed mutagenesis of Os9BGlu31 .....	33
3.2 Solvent system for purification of transglycosylation products by silica gel chromatography .....	43
4.1 Scoring functions molecular docking of Os9BGlu 31W243L mutation analysis by AutoDock Vina .....	45
4.2 Enzyme yields during purification of OsExo1 .....	64
4.3 Enzyme yields during purification of OsExo2 .....	66
4.4 Kinetic parameters for OsExoI hydrolysis of <i>p</i> NPGlc, laminaribiose, and laminarin substrates .....	69

## LIST OF FIGURES

Figure	Page
2.1 Glycoside hydrolase activity .....	6
2.2 Endo/exo-acting glycoside hydrolases .....	6
2.3 General mechanisms of inverting and retaining glycosidases .....	7
2.4 The distance of catalytic residues in the active sites .....	8
2.5 Structures of $\beta$ -glucosidases from different GH families .....	10
2.6 Phylogenetic tree of plant family 3 glycoside hydrolases .....	13
2.7 Relative activities of OsExo1 and OsExo2 on <i>p</i> NP-glycosides, oligo- saccharides and polysaccharides .....	14
2.8 The mechanism of substrate-product assisted processive catalysis by HvExo1 .....	15
2.9 General strategy of glycosylation via a chemical method .....	18
2.10 Glycosylation reactions catalyzed by the four types of enzymes .....	19
2.11 Structural comparison of Ptt-XET16-34 and Tm-NXG1 .....	20
2.12 Superposition of a homology model of Os9BGlu31 transglucosidase on the X-ray crystal structure of the Os3BGlu6 $\beta$ -glucosidase covalent intermediate with 2-fluoro- $\alpha$ -D-glucoside (PDB: 3GNR) .....	21
2.13 Heatmap of the <i>p</i> NP release catalyzed by 21 Os9BGlu31 variants when glycosylating 22 different acceptors .....	22
2.14 Reaction mechanism of glycosyltransferases and glycoside phosphorylases .....	24

## LIST OF FIGURES (Continued)

Figure	Page
3.1	Construct of the protein-coding sequence of recombinant pET32a(+)/ DEST with the <i>Os9bglu31</i> ..... 27
3.2	Construct of the protein-coding sequence of recombinant pET32a(+)/ DEST with the <i>OsExo2</i> ..... 27
3.3	Construct of the protein-coding sequence of recombinant pPICZ $\alpha$ BNH8 with the <i>OsExo1</i> ..... 27
4.1	Locations of mutation points predicted on Os9BGlu31W243L ..... 46
4.2	Coomassie blue SDS-PAGE analysis of Os9BGlu31 variants H123E/W243L, Y313H/W243L, Y313Q/W243L, Y313S/W243L, E441T/W243L, and E441H/W243L with N-terminal thioredoxin/ His <sub>6</sub> -tagged fusion protein after 1 <sup>st</sup> IMAC ..... 47
4.3	Coomassie blue-stained SDS-PAGE analysis of Os9BGlu31 wild type and its variants W243L and W243N throughout purification ..... 48
4.4	Polar interactions in active site of the complex of the BGlu1 E176Q mutant with cellopentaose..... 49
4.5	Superposition of X-ray crystal structure of Os9BGlu31W243L on the X-ray crystal structure of the BGlu1 E386G-Y341A with cellotetraose (PDB: 3SCW) ..... 49
4.6	UPLC chromatograms of reaction of Os9BGlu31 wild type and its W243H, W243K, W243N, and W243R variants with chloramphenicol..... 51

## LIST OF FIGURES (Continued)

<b>Figure</b>	<b>Page</b>
4.7	Chemical structure of chloramphenicol glucoside.....51
4.8	UPLC chromatograms of reaction of Os9BGlu31 wild type and its W243L and W243N variants with nybomycin .....52
4.9	Plausible structure of nybomycin glucoside .....52
4.10	UPLC chromatograms of reaction of Os9BGlu31 wild type and its W243L and W243N variants with ampicillin .....53
4.11	Plausible structure of ampicillin glucoside .....53
4.12	UPLC chromatograms of reaction of Os9BGlu31 wild type and its W243L variants with amoxicillin .....54
4.13	Plausible structure of amoxicillin glucoside .....55
4.14	UPLC chromatograms of reaction of Os9BGlu31 wild type and its W243L and W243N variants with tetracycline .....56
4.15	Plausible structure of tetracycline glucoside.....56
4.16	UPLC chromatograms of reaction of Os9BGlu31 wild type and its W243L and W243N variants with doxorubicin.....57
4.17	Plausible structure of doxorubicin glucoside.....58
4.18	TLC analysis of chloramphenicol glucoside purification by reverse phase chromatography on C18 resin.....58
4.19	<sup>1</sup> H-NMR spectrum of chloramphenicol glucoside.....60
4.20	<sup>13</sup> C-NMR spectrum of chloramphenicol glucoside.....60

## LIST OF FIGURES (Continued)

<b>Figure</b>	<b>Page</b>
4.21 Alignment of HvExo1 with HvExo2, ZmExo3, OsExo1, OsExo2, and OsExo3 .....	62
4.22 Superposition of a homology model of OsExo1 on the X-ray crystal structure of the HvExo1 (PDB: 3WLK) .....	63
4.23 Superposition of a homology model of OsExo1 on the X-ray crystal structure of the HvExo2 (PDB: 3WLK) .....	63
4.24 Coomassie blue SDS-PAGE analysis of OsExo1 purification .....	65
4.25 Coomassie blue SDS-PAGE analysis of OsExo2 purification .....	66
4.26 Optimal pH profiles of glycosylated and deglycosylated OsExo1 forms .....	68
4.27 Optimal temperature profiles of glycosylated and deglycosylated OsExo1 .....	68
4.28 Thermostability profile of OsExo1 glycosylated and deglycosylated forms .....	68
4.29 TLC analysis of the transglucosylation of pNPGlc by OsExo1 .....	71
4.30 TLC analysis of the transglucosylation of pNPGlc by OsExo2 .....	72
4.31 TLC analysis of the transglucosylation by OsExo1 from pNPGlc to alcohols .....	73
4.32 TLC analysis of the transglucosylation by OsExo2 from pNPGlc to alcohols .....	74
4.33 TLC analysis of the transglucosylation of alcohols by OsExo2 with pNPGlc and cellobiose donors .....	75
4.34 TLC analysis of the transglucosylation from oligosaccharides to methanol by OsExo1 .....	75



## LIST OF FIGURES (Continued)

Figure	Page
4.35	TLC analysis of the transglucosylation from oligosaccharides to methanol by OsExo2..... 75
4.36	TLC analysis of the transglucosylation from polysaccharides to methanol by OsExo1..... 76
4.37	TLC analysis of the transglucosylation from polysaccharides to methanol by OsExo2..... 77
4.38	TLC analysis of purification of transglucosylation products of <i>p</i> NP-Glc generated by OsExo2 ..... 79
4.39	TLC analysis of purification of transglucosylation products of alcohols generated by OsExo2 ..... 80
4.40	Chemical structure of <i>p</i> NP- $\beta$ -D-gentiotrioside ..... 82
4.41	Chemical structure of <i>p</i> NP- $\beta$ -D-gentiobioside..... 83
4.42	Superimposed $^1\text{H-NMR}$ spectra of <i>p</i> NP- $\beta$ -D-cellobioside standard and <i>p</i> NP- $\beta$ -D-cellobioside isolated sample ..... 85
4.43	Chemical structure of <i>p</i> NP- $\beta$ -D-cellobioside ..... 85
4.44	Chemical structure of <i>p</i> NP- $\beta$ -D-laminaribioside..... 87
4.45	Chemical structure of methyl- $\beta$ -D-glucoside ..... 87
4.46	Chemical structure of ethyl- $\beta$ -D-glucopyranoside ..... 88
4.47	Chemical structure of <i>n</i> -propyl- $\beta$ -D-glucopyranoside ..... 89
4.48	Chemical structure of <i>n</i> -butyl- $\beta$ -D-glucopyranoside..... 90
4.49	Chemical structure of 3-methyl-1-butyl- $\beta$ -D-glucopyranoside..... 91

**LIST OF FIGURES (Continued)**

<b>Figure</b>		<b>Page</b>
4.50	Chemical structure of 2-hydroxyethyl- $\beta$ -D-glucofyranoside .....	91
4.51	Chemical structure of propargyl- $\beta$ -D-glucofyranoside.....	92
4.52	Chemical structure of ethylene-disulfide- $\beta$ -D-glucofyranoside .....	93
4.53	Chemical structure of 4-hydroxy-benzyl- $\beta$ -D-glucofyranoside .....	94



## LIST OF ABBREVIATIONS

ABTS	2,2'-azinobis-3-ethylbenthaiazolinesulfonic acid
AIM	Auto-induction media
APS	Ammonium persulfate
bis-acrylamide	N, N-methylene-bis-acrylamide
4HMBA	4-(Hydroxymethyl)benzoic acid
BME	$\beta$ -mercaptoethanol
BMGY	Buffered glycerol complex medium
BMMY	Buffered methanol complex medium
bp	Base pairs
BuOH	Butanol
3-meBu	3 methyl butanol
C2	Cellobiose
C3	Cellotriose
C4	Cellotetraose
C5	Cellopentaose
cDNA	Complementary deoxynucleic acid
CV	Column volume
DMSO	Dimethyl sulfoxide
DNA	Deoxyribonucleic acid
DNase	Deoxyribonuclease

**LIST OF ABBREVIATIONS (Continued)**

DP	Degree of polymerization
EDTA	Ethylenediamine tetraacetate
ETG	Ethylene glycol
EtOH	Ethanol
EtOAc	Ethyl acetate
GH	Glycoside hydrolase
GH1	Glycoside hydrolase family 1
GH3	Glycoside hydrolase family 3
Glc	Glucose
HCl	Hydrochloric acid
HIC	Hydrophobic interaction chromatography
HMBC	Heteronuclear Multiple Bond Correlation
HSQC	Heteronuclear Single Quantum Coherence
IMAC	Immobilized metal affinity chromatography
IPTG	Isopropyl thiol- $\beta$ -D-galactoside
kDa	Kilo Dalton(s)
LB	Luria-Bertani lysogeny broth
L2	Laminaribiose
L3	Laminaritriose
L4	Laminaritetraose
L5	Laminaripentaose

**LIST OF ABBREVIATIONS (Continued)**

(m, $\mu$ )g	(milli, micro) Gram
(m, $\mu$ )l	(milli, micro) Liter
(m, $\mu$ )M	(milli, micro) Molar
( $\mu$ )mol	(micro) Mole
MeOH	Methanol
MW	Molecular weight
MWCO	Molecular weight cut off
NaOAc	Sodium acetate
nm	Nanometer
NMR	Nuclear Magnetic Resonance
OD	Optical density
PCR	Polymerase chain reaction
PEG	Polyethylene glycol
PGO	peroxidase-glucose oxidase
PMSF	Phenylmethylsulphonyl fluoride
<i>p</i> NP	<i>para</i> -nitrophenyl
<i>p</i> NP <sub>Glc</sub>	<i>p</i> NP- $\beta$ -D-glucopyranoside
<i>p</i> NP <sub>C2</sub>	<i>p</i> NP- $\beta$ -D-cellobioside
PrOH	Propanol
PropynOH	Propargyl alcohol
rpm	Rotations per minute

**LIST OF ABBREVIATIONS (Continued)**

SEC	Size exclusion chromatography
SDS	Sodium dodecyl sulfate
SDS-PAGE	Polyacrylamide gel electrophoresis with SDS
TB	Terrific broth
TEMED	Tetramethylenediamine
Tris	Tris-(hydroxymethyl)-aminoethane
UPLC	Ultra high-performance liquid chromatography
UV	Ultraviolet
v/v	volume per volume
w/v	weight per volume
YNB	Yeast nitrogen base
YPDS	Yeast extract peptone dextrose medium with sorbitol

# CHAPTER I

## INTRODUCTION

### 1.1 General introduction

Glycoside hydrolases are involved in many biological processes of living organisms. These include biomass conversion in microorganisms, breakdown of glycolipids and exogenous glucosides and cellular communication in animals (Ketudat Cairns and Esen, 2010; Clark et al., 1996), and chemical defense (Morant et al., 2008), lignification (Escamilla-Trevino et al., 2006), cell wall modification (Hrmova and Fincher, 2001), and phytohormone conjugate activation in plants (Lee et al., 2006). Usually, glycoside hydrolases catalyze break-down of glycosidic bonds. However, the enzymes can also catalyze the glycosylation reaction by the thermodynamically controlled reverse hydrolysis or transglycosylation (Desmet et al., 2012; Tran et al., 2019, Thenchartanan et al., 2020).

A glycoconjugate is a compound that comprises a sugar portion (glycon), which can be one or more monosaccharides, linked to a non-sugar moiety (aglycon) via a glycosidic bond. The glycosidic bond can be an O-, N-, S-, or C- linkage to the glycon anomeric carbon, which can exist as  $\alpha$ - or  $\beta$ - diastereoisomers, with the  $\beta$ -forms being most common (Bartnik and Facey, 2017; Mestrom et al., 2019). Many small molecule drugs, such as antibiotics and anticancer therapeutic agents, are glycosides. Glycoconjugates are also found in cosmetic ingredients and food (Nishimura et al., 1995;



Sua et al., 2016). The glycosidic residues significantly improve the solubility, stability, emulsifying properties, and bioactivity of the molecules (Pandey et al., 2014; Kren and Rezanka, 2008).

Although chemical synthesis can be used to generate glycoconjugates, the unique and complex structures of glycoconjugates, which usually require numerous protection, deprotection and activation steps to achieve specific synthesis, make them very difficult and costly to generate by chemical synthesis (Rather and Mishra, 2013). Enzymatic glycosylation can form a specific glycosidic bond in one step and under environmentally friendly conditions. There are three categories of carbohydrate-active enzymes that can catalyze the synthesis of glycoconjugates: glycosyltransferases, glycosidases (glycoside hydrolases), and transglycosidases (Song et al., 2006). The glycosyltransferases can provide high recovery yield with high selectivity of donor and acceptor specificity. Although they are very efficient enzymes, their requirement for expensive activated donors is the major constriction in their application for the commercial production of glycoconjugates (Lim et al., 2005). Glycosidases are attractive enzymes for glycoconjugate production due to their natural abundance, robustness and ability to allow a variety of acceptors and cheaper glycosyl donor substrates. Reverse hydrolysis or transglycosylation by glycosidases can be used for synthetic purposes. Nevertheless, application of glycoside hydrolases in glycosylation suffers from their hydrolytic activity, decreasing their use for glycosylation. Retaining glycosidase homologues are sometimes found to have much higher activity for transglycosylation than hydrolysis, and such enzymes are called transglycosidases. Transglycosidase performance makes them very interesting for application (Luang et al., 2013; Komvongsa et al., 2015; Adari et al., 2016; Nam et al., 2017; Tran et al., 2019).

Engineering of glycoside hydrolases and transglycosidases can be done to achieve better glycosylation of compounds of interest (Teze et al., 2014; Bissaro et al., 2015; Tran et al., 2019, Thenchartanan et al., 2020). Molecular docking programs, such as AutoDock Vina, can be used to predict noncovalent bound conformations and free energies of binding for ligands to proteins in order to efficiently obtain substitutions of amino acids leading to the desired properties by site-directed mutagenesis (Trott and Olson, 2010).

Here, the study aimed to investigate the effects of various substitution mutations of Os9BGlu31 to improve use of different donor and acceptor substrates, as well as use of GH3 exoglucanases for transglycosylation, allowing purification and structural confirmation of the product glycosides. This information could allow the efficient catalytic routes to produce novel and useful glycoconjugates.

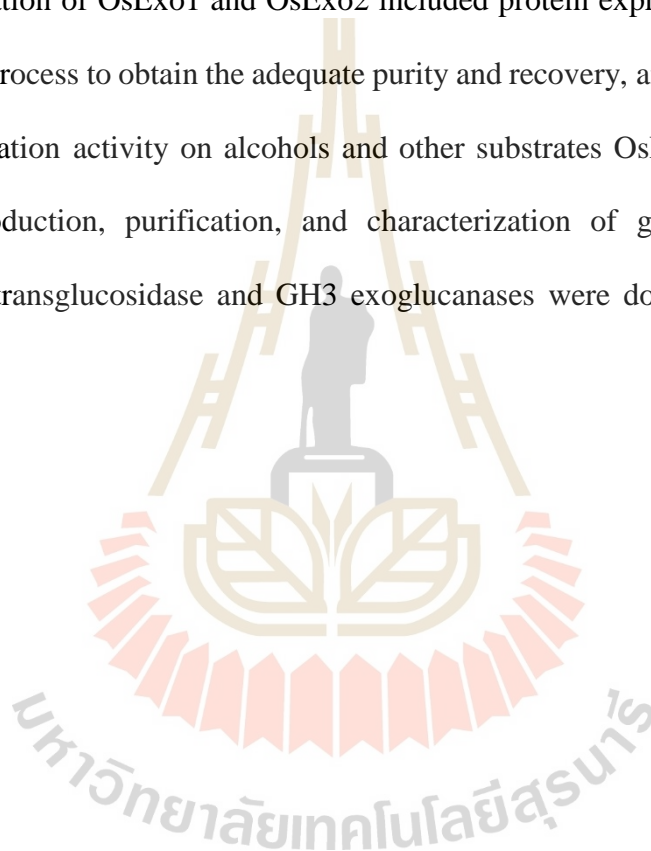
## **1.2 Research objectives**

The objectives of this study include:

1. To engineer the transglycosylation selectivity of Os9BGlu31 by site directed mutagenesis to improve use of different glucosyl donor and acceptor substrates.
2. To investigate the transglycosylation activity of OsExo1 and OsExo2 on alcohols and other substrates.
3. To produce, purify and characterize the transglycosylation products of Os9BGlu31, OsExo1 and OsExo2.

### 1.3 Research scope

The research scope of the project includes investigation of the transglycosylation properties of Os9BGlu31 active site cleft variants, OsExo1, and OsExo2. This study was focused on the selectivity for different donor and acceptor substrates for mutations of Os9BGlu31 transglucosidase designed to improve use of different donor substrates. The investigation of OsExo1 and OsExo2 included protein expression, improving the purification process to obtain the adequate purity and recovery, and investigation of the transglycosylation activity on alcohols and other substrates OsExo1 and OsExo2. In addition, production, purification, and characterization of glycoside products of Os9BGlu31 transglucosidase and GH3 exoglucanases were done to determine their structures.



## CHAPTER II

### LITERATURE REVIEW

#### 2.1 Glycoside hydrolases

Glycoside hydrolases (EC 3.2.-.-) are present in essentially all living organisms, performing different functions, and are also referred to as glycosidases and glycosyl hydrolases. These enzymes are widespread and hydrolyze  $\alpha$ - or  $\beta$ -glycosidic bonds between two carbohydrates or between carbohydrate and non-carbohydrate moieties (O-, N- and S-linked glycosides), leading to the formation of a sugar hemiacetal or hemiketal and the corresponding free aglycon (Figure 2.1) (Stick and Williams, 2009). A classification of glycoside hydrolases in families based on amino acid sequence similarity has been generated (Henrissat, 1991). The classification based on sequence similarity has led to assignment of more than 170 families ([www.cazy.org](http://www.cazy.org); Lombard et al., 2014). The CAZy (Carbohydrate-Active enzymes) database provides a reliable prediction of mechanism (retaining/inverting), active site residues and possible substrates. Based on 3D structural similarity and conservation of catalytic amino acids, the sequence-based families with related structures have been classified into clans (Henrissat and Bairoch, 1996).

Glycoside hydrolases also can be classified into endo- or exo-glycoside hydrolases (Figure 2.2), based on whether the enzyme cleaves an internal glycosidic bond in the internal part of a chain (endo) or at the end of a chain (exo). The endo- or

exo-acting activity does not have a relationship to the mechanism utilized, for example, endoglucanases (cellulases) can be retaining or inverting enzymes (Stick and Williams, 2009).

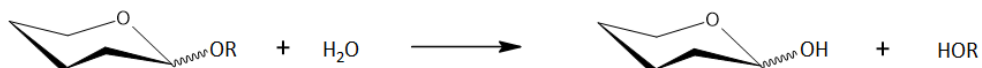


**Figure 2.1** Glycoside hydrolase activity (Stick and Williams, 2009).

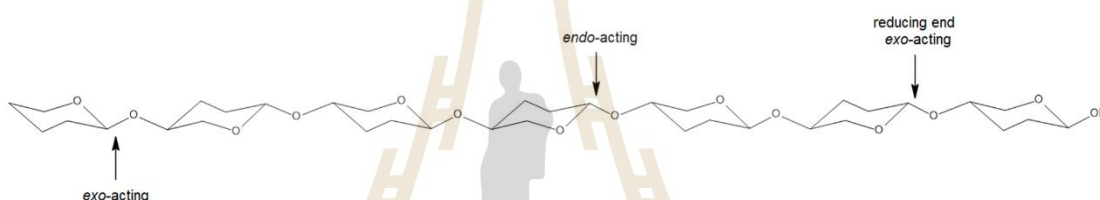


**Figure 2.2** Endo/exo-acting glycoside hydrolases (Stick and Williams, 2009).

## 2.2 Glycoside hydrolase mechanisms

The enzymatic hydrolysis of the glycosidic bond usually utilizes two acidic catalytic residues in the active site that act as a general acid or proton donor and a general base or nucleophile for hydrolysis (Koshland, 1953). This hydrolysis can occur by two major mechanisms, inversion and retention, which differ in whether the anomeric configuration of the product changes from that of the substrate or not (McCarter and Withers, 1994).

The inverting mechanism is a single displacement mechanism (Koshland, 1953), in that bond breaking and forming both proceed in a single step (Davies et al., 2003;

Sinnott, 1990). The hydrolysis starts with a general acid catalyst protonating the glycosidic oxygen, following by water, taking the role of a nucleophile, attacking on the anomeric carbon. The water is activated by extraction of a proton by a carboxylate base leading to inversion of the anomeric conformation (Figure 2.3 top).

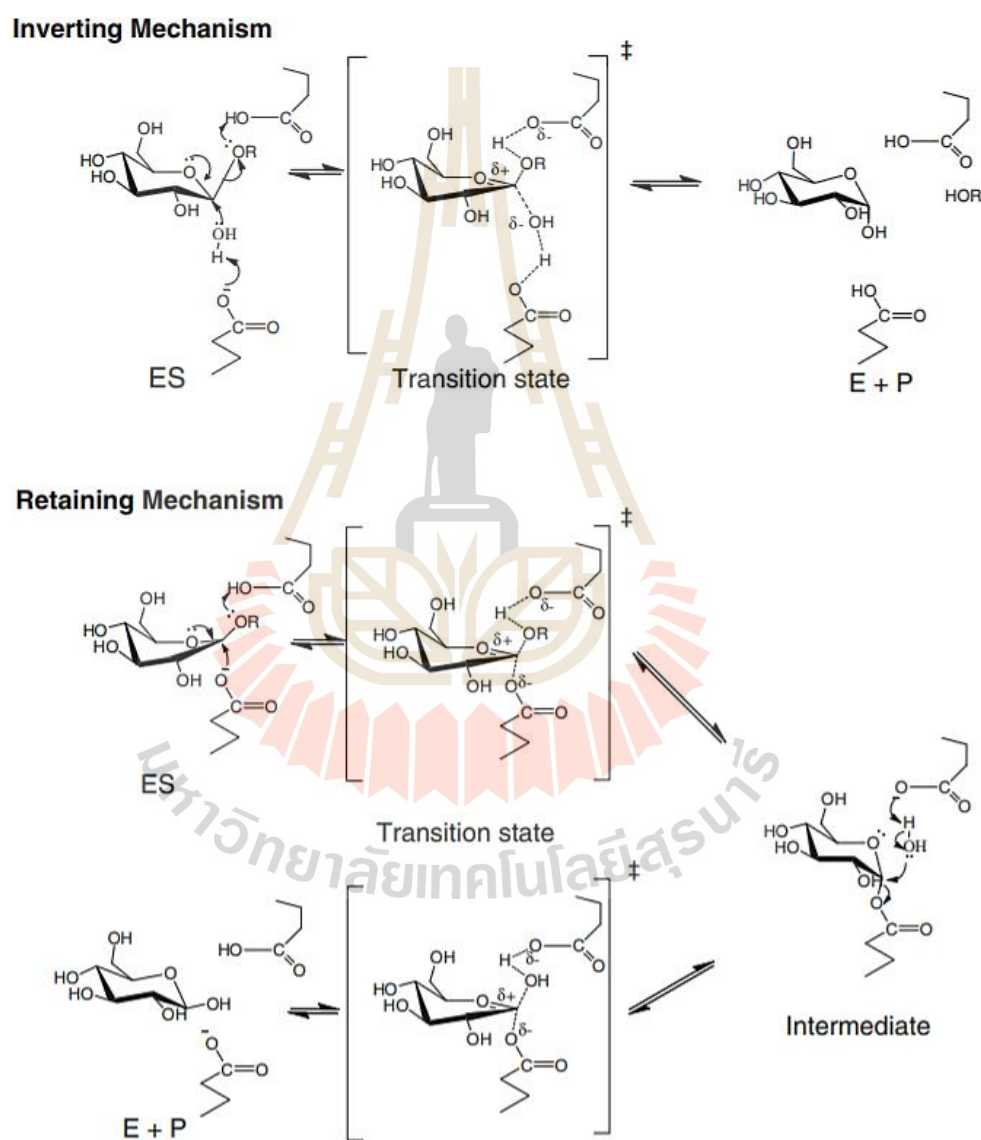


**Figure 2.3** General mechanisms of inverting and retaining  $\beta$ -glycoside hydrolases (Ketudat-Cairns, and Esen, 2010).

The retaining mechanism is a double displacement mechanism, consisting of two steps (Figure 2.3 bottom). This mechanism uses two essential residues (generally Asp or Glu) that are usually located  $\sim 5.5$  Å apart in the active site of the enzyme, which is closer together than the catalytic residues of the inverting mechanism ( $\sim 10$  Å, Figure 4) (Zechel and Withers, 2000). In the first step, an acid/base catalyst protonates the glycosidic oxygen, while a general nucleophile residue attacks the anomeric carbon to form a covalent glycosyl-enzyme intermediate (Figure 2.3). In the second step, the general acid/base residue deprotonates a water molecule, which generates a nucleophilic species to attack at the anomeric carbon and displace the free sugar, which has the same anomeric configuration as the substrate.

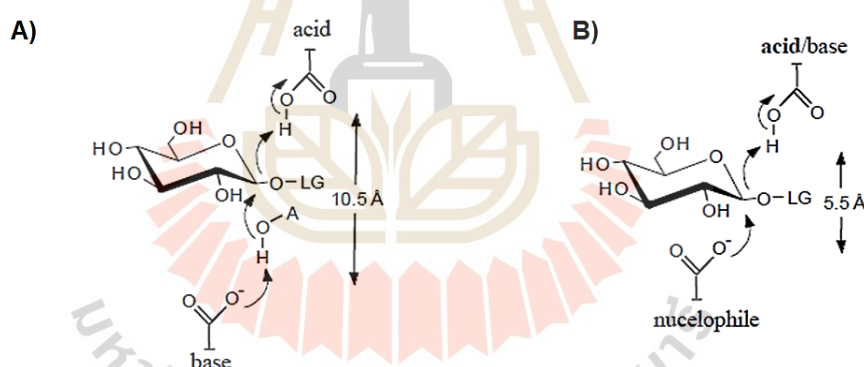


**Figure 2.4** The distance of catalytic residues in the active sites of (A) an inverting  $\beta$ -glucosidase and (B) a retaining  $\beta$ -glucosidase. In A, the general acid and nucleophile are located on opposite sides of the glycosidic bond at least 10 Å apart, and in B, two general acid-base are located on different sides of the glycosidic bond approximately 5.5 Å apart (Zechel and Withers, 2000; Lundemo, 2015).



## 2.3 $\beta$ -Glucosidases

$\beta$ -Glucosidases (EC. 3.2.1.21) are hydrolases that catalyze the hydrolysis of  $\beta$ -glycosidic bonds to release nonreducing terminal glucosyl residues from glycosides and oligosaccharides (Ketudat Cairns and Esen, 2010). These enzymes are universally found in living organisms, including animals, plants, fungi, protists, bacteria, and archaea. They play important roles in many biological processes, such as biomass conversion in microorganisms, breakdown of glycolipids and exogenous glucosides in animals (Ketudat Cairns and Esen, 2010), and chemical defense (Morant et al., 2008), lignification (Escamilla-Trevino et al., 2006), cell wall modification (Hrmova and Fincher, 2001) and phytohormone conjugate activation (Lee et al., 2006) in plants.

$\beta$ -Glucosidases are found in at least 9 families of GH and they have various structures, depending on of which GH family they are a member ([www.cazy.org](http://www.cazy.org)).  $\beta$ -Glucosidases are grouped into GH families 1, 2, 3, 5, 9, 16, 30, 39 and, 116 and most plant  $\beta$ -glucosidases that have been characterized fall in GH1 (Ketudat Cairns and Esen, 2010). The families GH1, GH5, and GH30 belong to the Clan GH-A, the members of which have similar  $(\beta/\alpha)_8$  barrel domains that contain their active site. In contrast the family GH 9 and GH116 catalytic domains have  $(\alpha/\alpha)_6$  solenoid structures (Cantarel et al., 2009; Ketudat Cairns and Esen, 2010; Charoenwattanasatien et al., 2016). GH3 enzymes use the cooperation of two domains, the first one being a  $(\beta/\alpha)_8$  barrel or triose phosphate isomerase (TIM) barrel domain and the other being a  $(\beta/\alpha)_6$  sandwich domain, for their active sites (Figure 2.5) (Hrmova et al., 2001; Hrmova et al., 2002).

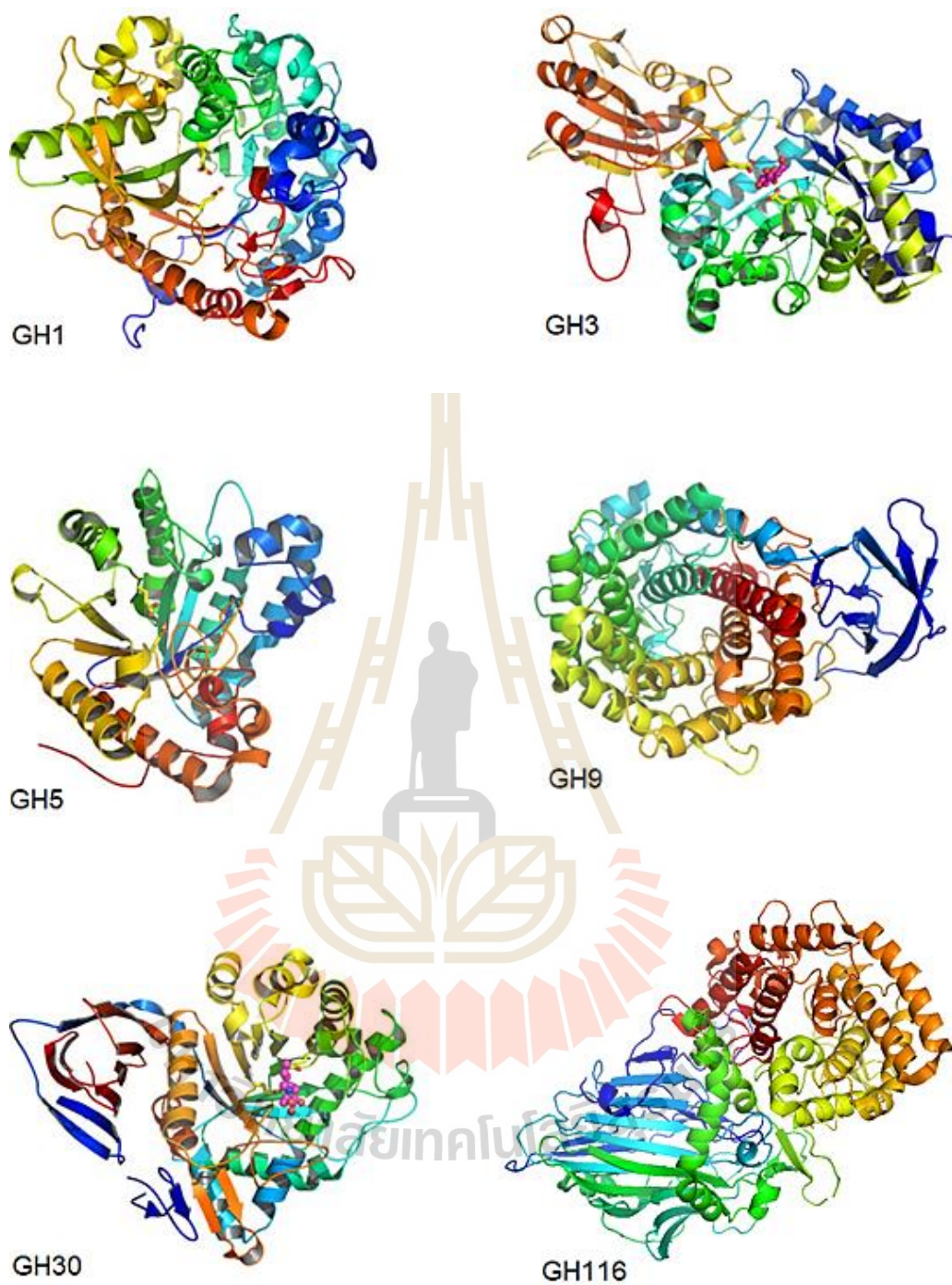


**Figure 2.5** Structures of  $\beta$ -glucosidases from different GH families (Ketudat-Cairns and Esen, 2010; Charoenwattanasatien et al., 2016).

## 2.4 Glycoside hydrolase family 1

Glycoside hydrolase family 1 (GH1) includes enzymes that hydrolyze O-glycosidic bonds at the nonreducing end of carbohydrates to release  $\beta$ -D-glucose,  $\beta$ -D-galactose,  $\beta$ -D-mannose,  $\beta$ -D-fucose, phospho- $\beta$ -D-galactose, 1,6-linked disaccharides, modified  $\beta$ -D-glucose residues from a carbohydrate or lipid and also hydrolyze a variety of glycosides, including aryl- and alkyl- $\beta$ -D-glycosides (<http://www.cazy.org>). For example, rice BGlu1 (which was renamed Os3BGlu7 in a systematic designation, Opassiri et al., 2006) can hydrolyze  $\beta$ -1,3- and  $\beta$ -1,4-linked oligosaccharides and pyridoxine 5'-O- $\beta$ -D-glucoside, and also has high transglucosylation activity with pyridoxine acceptor (vitamin B6) to synthesize pyridoxine 5'-O- $\beta$ -D-glucoside (Opassiri et al., 2004). The transglucosylation activity of BGlu1 predominantly adds  $\beta$ -1,4-linked glucosyl residues and the E414G glycosynthase mutant of BGlu1 is able to synthesize long  $\beta$ -1,4-linked gluco-oligosaccharides of at least 11 glucosyl residues (Homalai et al., 2007).

Rice Os9BGlu31 is a GH1 enzyme catalyzes transglucosylation that functions in production of glycoconjugates in plants (Luang et al., 2013). A few other related transglucosidases have been described. Two enzymes in GH1 from carnation and delphinium transfer glucosyl moieties from phenolic glucosyl esters, such as feruloyl glucose and 1-O- $\beta$ -D-vanillyl glucose, to the anthocyanin cyanidin 3-O-glucoside (Matsuba et al., 2010). The galactolipid: galactolipid galactosyltransferase was found to correspond to the GH1 enzyme SFR2 (Sensitive to Freezing 2), and transfers the galactosyl residues from one monogalactosyl diacyl glyceride to another to produce  $\beta$ -

linked di-galactosyl diacyl glycerol and oligogalactosyl diacyl glycerides (Moellering et al., 2010).

GH1 members catalyze their reactions with a molecular mechanism leading to overall retention of the anomeric configuration, which involves the formation and breakdown of a covalent glycosyl enzyme intermediate (Figure 2.3). Almost all GH1 enzymes contain two conserved catalytic glutamate residues located at the C-terminal ends of  $\beta$ -strands 4 and 7 (Jenkins et al., 1995).

## 2.5 Glycoside hydrolase family 3

Glycoside hydrolase family 3 enzymes include over 25,000 entries in the CAZY database. The sequence similarity relationships between enzymes that have been identified within GH3 in higher plant enzymes can be described by a phylogenetic tree with two distinct groups. One group contains the  $\beta$ -D-glucan exo-glucohydrolases-like enzymes, while the second group contains  $\beta$ -D-xylosidase-like enzymes (Hrmova et al., 2002) (Figure 2.6). The GH3 glucan  $\beta$ -D-glucosidases from barley are broad specificity exo-hydrolases that remove single glucosyl residues from the non-reducing ends of a range of  $\beta$ -D-glucans,  $\beta$ -D-glucosyl-oligosaccharides and aryl  $\beta$ -D-glucosides, including (1,3)- $\beta$ -D-glucans, (1,4)- $\beta$ -D-glucans, (1,3;1,4)- $\beta$ -D-glucans and (1,6)- $\beta$ -D-glucans, *p*-nitrophenyl- $\beta$ -D-glucoside, certain cyanogenic  $\beta$ -D-glucosides and some  $\beta$ -D-oligo xyloglucosides (Hrmova and Fincher, 1998). In rice OsExo1 and OsExo2 also show broad specificity exo-hydrolase activities toward  $\beta$ -D-glucosyl-oligosaccharides and  $\beta$ -D-polysaccharides (Prawisut et al., 2020; Prawisut, 2018) (Figure 2.7). The family GH3 members play important roles in fundamental biological processes, for examples,

recycling and remodeling of cell wall, and the modification of host-pathogen interactions during microbial infection of plants (Cournoyer and Faure, 2003; Hrmova and Fincher, 2001). GH3 is also a phytohormone-responsive family of proteins contributing the biological activity of indole-3-acetic acid (IAA), abscisic acid (ABA), jasmonic acid (JA), and salicylic acid (SA) (Zhang et al., 2018). They affect plant growth and developmental processes, as well as acting in response to some types of stress (Jain et al., 2006).

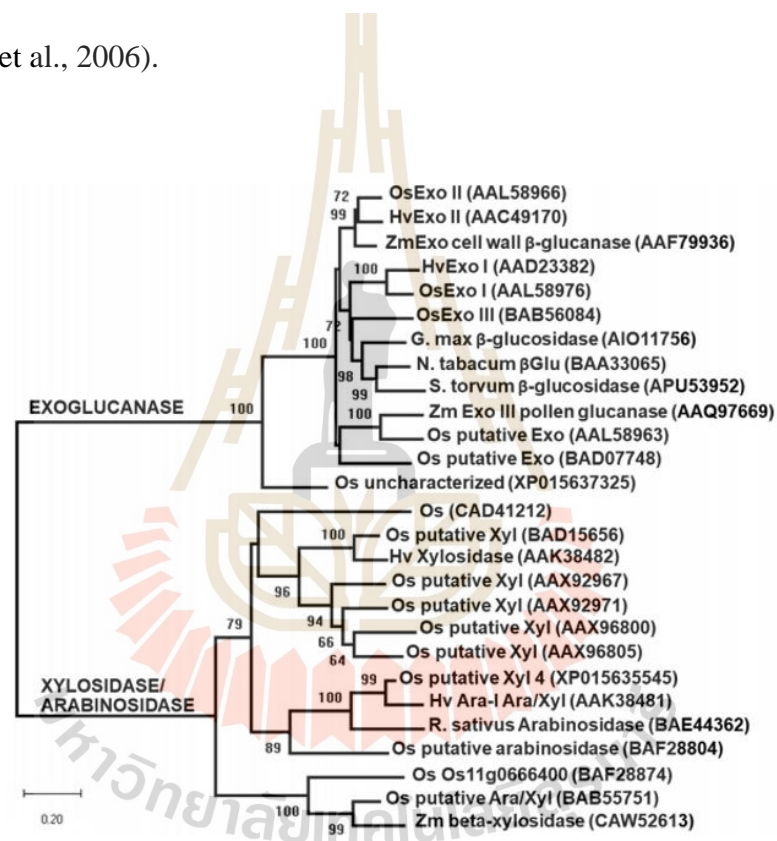


**Figure 2.6** Phylogenetic tree of plant family 3 glycoside hydrolases. Rice proteins are marked Os, barley are marked Hv, and maize are mark Zm, while other proteins have the genus initial and species name. Genbank nr accession numbers are given in parentheses (Prawisut et al., 2020).



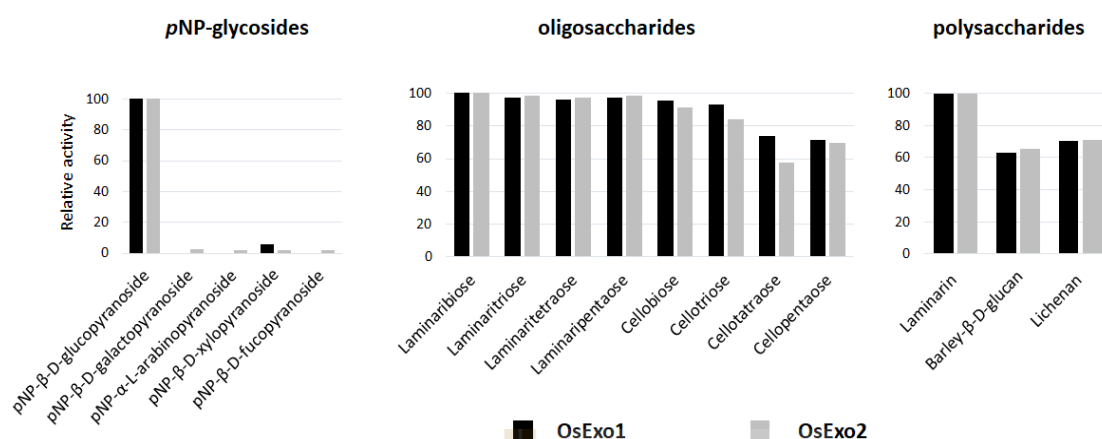


**Figure 2.7** Relative activities of OsExo1 and OsExo2 on *pNP*-glycosides, oligosaccharides and polysaccharides (Prawisut et al., 2020; Prawisut, 2018).

The GH3 enzymes have a retaining catalytic mechanism, which removes single monosaccharide from the non-reducing end of their substrate, with retention of anomeric configuration (Koshland, 1953; Hrmova et al., 1996). This mechanism utilizes two carboxylic acid residues as catalytic acid/base and nucleophile. In barley Exo1, the catalytic nucleophile, Asp285, is located in the N-terminal ( $\beta/\alpha$ )<sub>8</sub> domain in a highly conserved GFVISDW motif in plant family GH3  $\beta$ -D-glycosidases. The catalytic acid is E491, which is conserved in plant family GH3 exoglucanase-like enzymes, but is present only in closely related members of the GH3 family (Harvey et al., 2000; Hrmova et al., 2001).

Recently, Streltsov et al. (2019) examined product and substrate pathways along the catalytic cycle of the plant GH3 exo-hydrolase HvExo1, and how the displacement of the glucose trapped in the active site after the previous round of hydrolysis leads to processive hydrolysis of oligo- and polysaccharide substrates (Figure 2.8).

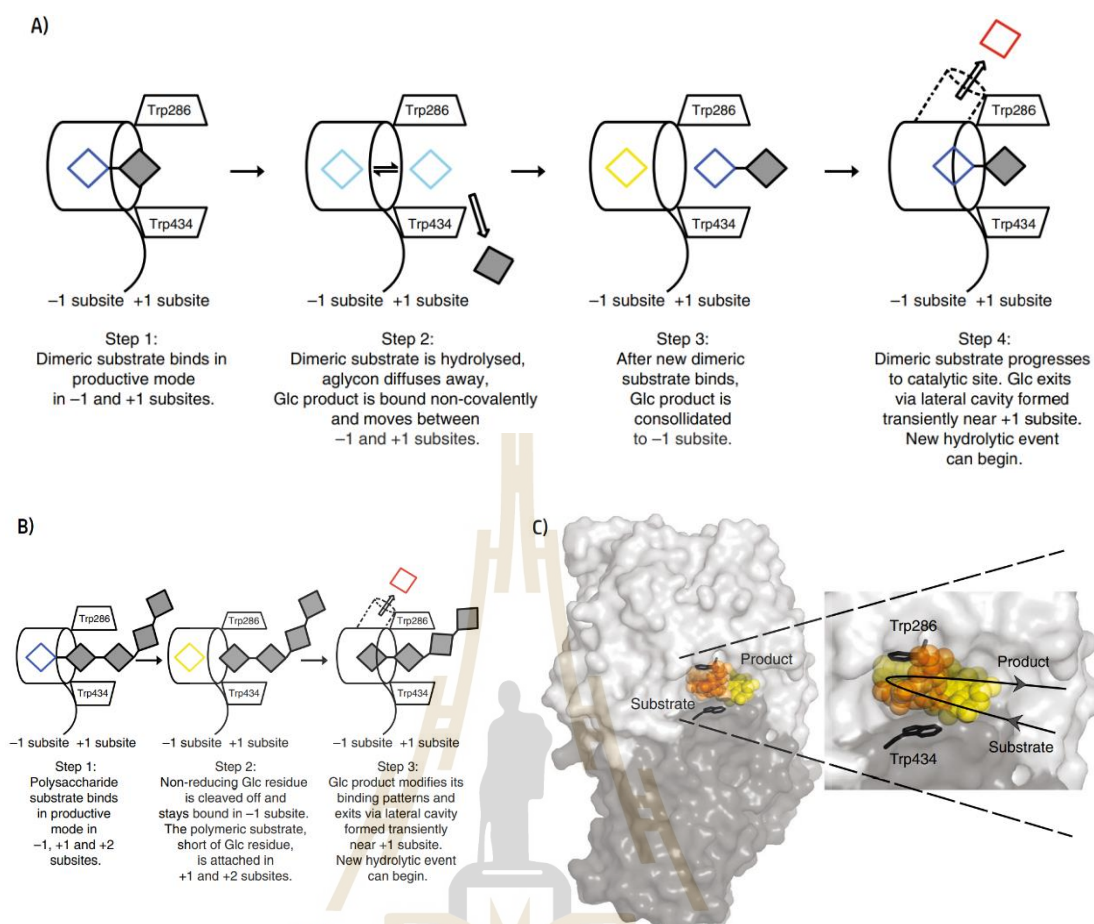


**Figure 2.8** The mechanism of substrate-product assisted processive catalysis by HvExo1. A) Process for hydrolysis of disaccharides, B) Processive hydrolysis of a polysaccharide, C) Image of the active site cleft of Exo1 showing the routes for entrance of the new substrate and exit of the trapped glucose product (Streltsov et al., 2019).

The results revealed the glucose product displacement route and suggested that each hydrolytic event, including glucose release, is precisely coordinated with the incoming substrate association and hydrolysis. The glucose product modifies its binding pattern and thereby causes the transient formation of a lateral cavity, which serves as a route for glucose departure from the active site. This departure allows the



non-reducing glucosyl residue of the substrate to enter for the next catalytic round. This process allows for substrate-product assisted processive catalysis through multiple hydrolytic events without release of the polymer or oligomer substrate from HvExo1.

## 2.6 Glycosylation

Glycoconjugates are carbohydrates that are covalently linked to other biological compounds via a glycosidic bond by the reaction called glycosylation. Such compounds can include proteins (glycoproteins), lipids (glycolipids), other small molecules (glycosides) (Kytidou et al., 2020), and it was recently reported that RNA can also carry glycans on the cell surface (glycoRNA) (Flynn et al., 2021). A glycosidic linkage is a covalent bond that can be an O- (O-glycoside), N- (glycosylamine), S-(thioglycoside), or C- (C-glycoside) glycosidic bond. The configuration of the anomeric carbon of the glycone can exist as  $\alpha$ - (axial) or  $\beta$ -linkage (equatorial) diastereoisomer with the  $\beta$ -forms being most common (Bartnik and Facey, 2017).

Glycosylation of metabolites in plants serves several purposes in many biological processes. Many glycosides occur in secondary metabolites in plants, which store the chemicals in the form of inactive glycosides that can be activated by enzymatic hydrolysis (Bowles, 2005; Ketudat Cairns and Esen, 2010). Examples include the phytohormones abscisic acid (ABA), auxin (indole acetic acid, IAA), cytokinins (CKs), brassinosteroids (BRs), salicylic acid, and gibberellins that regulate growth, development, and responses to environmental stresses (Gachon et al., 2005). Glycosylation enhances water-solubility of hydrophobic metabolites, which improves their bioavailability (Vetter, 2000; Kren and Martinkova, 2001). The position where the

sugar is attached in a glycosylated molecule may support its the stability, for example the ascorbic acid-2-O-glucoside is chemically more stable than ascorbic acid-6-O-glucoside (Jones and Vogt, 2001). Furthermore, it may decrease acute toxicity or harmful effects. For example, endogenous  $\beta$ -glucosidase will hydrolyze cyanogenic glycosides in a plant when the plant is damaged and the enzyme mixes with the substrate, releasing an  $\alpha$ -hydroxy nitrile group from D-glucose so that it can breakdown to cyanide and a ketone (Cressey and Reeve, 2019; Kytidou et al., 2020).

## 2.7 Chemical glycosylation

The chemical synthesis of glycoconjugates is extremely valuable, but requires numerous steps, including protection, activation, glycosylation, and deprotection (Rather and Mishra, 2013). Typically, all hydroxyl groups of sugars are first protected by acetylation with acetic anhydride. Then, an activation step involves exchange of anomeric hydroxyl group with a bromine or chlorine atom, followed by glycosylation using silver or mercury salt catalysts, in this step the formation ratio of  $\alpha$ - and  $\beta$ -glycosidic products is dependent on the thermodynamic stability of the isomers. Finally, deprotection by sodium methoxide in methanol releases the non-anomeric hydroxyl groups (Figure 2.9) (Lundemo, 2015).

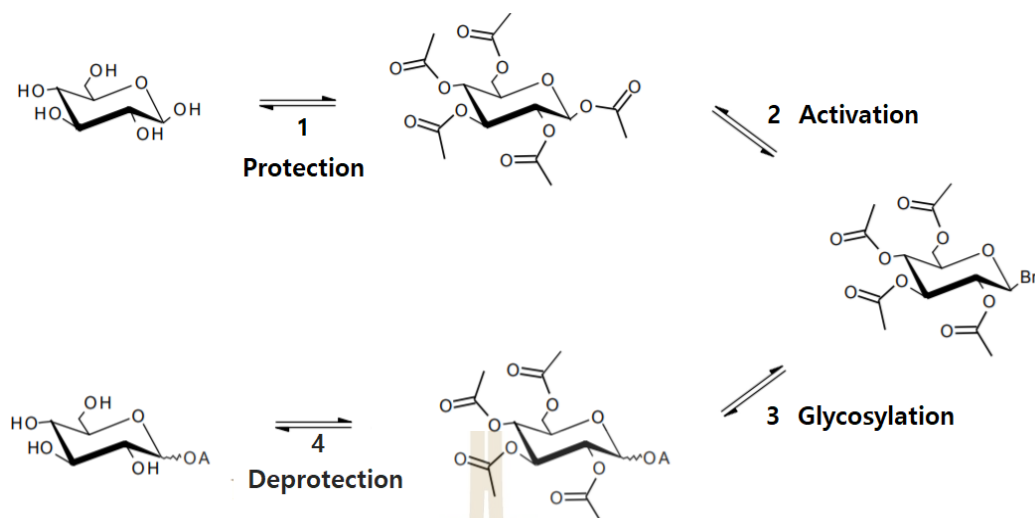


**Figure 2.9** General strategy of glycosylation via a chemical method. A = Acceptor. (Lundemo, 2015).

## 2.8 Enzymatic glycosylation

There are four groups of enzymes capable of catalyzing glycosylation reaction: glycoside hydrolases (GH), transglycosylases (TG), Leloir glycosyltransferases (GT), and glycoside phosphorylases (GP) (Figure 2.10), each of which has its own advantages and disadvantages, as described below.

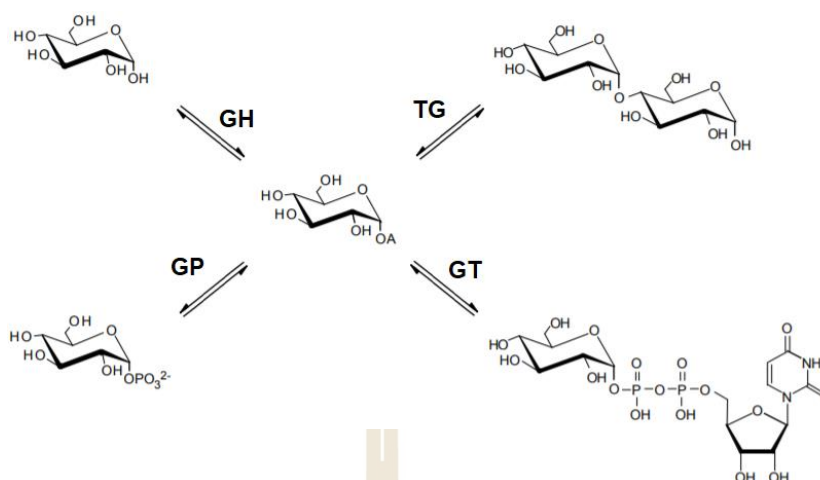


**Figure 2.10** Glycosylation reactions catalyzed by the four types of enzymes; glycoside hydrolases (GH), transglycosylases (TG), glycoside phosphorylases (GP) and Leloir glycosyl transferases (GT). A = Acceptor (Lundemo, 2015).

### 2.8.1 Glycoside hydrolases (GH)

Glycoside hydrolases (GH) are hydrolyzing enzymes, which break the glycosidic bond by inserting water. However, glycosidases can also catalyze the glycosylation reaction by thermodynamically controlled reverse hydrolysis (Rather and Mishra, 2013). GH often have low regioselectivity, which leads to a mixture of products when the acceptor contains more than one hydroxyl group (Lundemo, 2015).

An important parameter of the glycosidase activities which affects the catalyzed synthesis is the water in the reaction (Davies and Henrissat, 1995). In aqueous conditions, GH catalyze breakdown of the glycosidic linkage by hydrolysis activity, but the equilibrium can be shifted by increasing the concentration of glucose or alcohol, or reducing the concentration of water (Ljunger et al., 1994; Thenchartanan et al., 2020).

### 2.8.2 Transglycosylase (TG)

Transglycosylases (TG) are members of retaining glycosidase families that can catalyze the transformation of one glycoside to another (Romero-Télez et al., 2019). A TG works by the same mechanism as retaining glycoside hydrolases (Figure 2.3). TG are found relatively rarely in nature, however, and they all have homologous hydrolytic enzymes. For instance, xyloglucan endo-transglycosylase Ptt-XET16-34 is related to its homologous glycosidase Tm-NXG1 xyloglucan endoglucanase (Baumann et al., 2007). Structural comparison of these enzymes revealed a difference in loops near the active site accounted the specificity difference for hydrolysis or transglycosylation. Figure 2.11 shows the ribbon representation of the superimposition of Ptt-XET16-34 (green) onto Tm-NXG1 (yellow) illustrating the structural differences that appear mainly in loops 1 through 3 and in the C-terminal region.

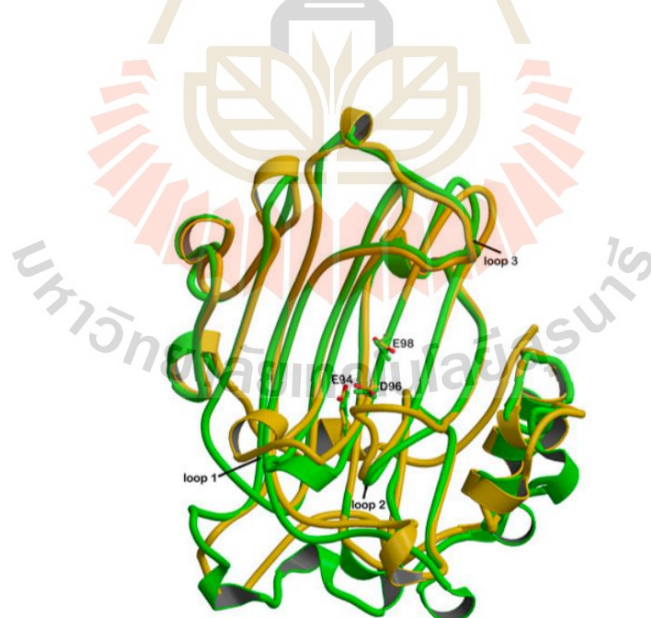


**Figure 2.11** Structural Comparison of Ptt-XET16-34 (green) and Tm-NXG1 (yellow) (Baumann et al., 2007).

Site-directed mutagenesis of Os9BGlu31 by Luang et al., 2013 indicated catalytic functions for the putative catalytic acid/base (Glu169) and nucleophile (Glu387) residues, and showed the unusual His386 residue did not affect the ratio of hydrolysis to transglycosylation. The wild type enzyme displays an unusual lack of inhibition by mechanism-based inhibitors of GH1  $\beta$ -glucosidases that utilize a double displacement retaining mechanism (Luang et al., 2013).

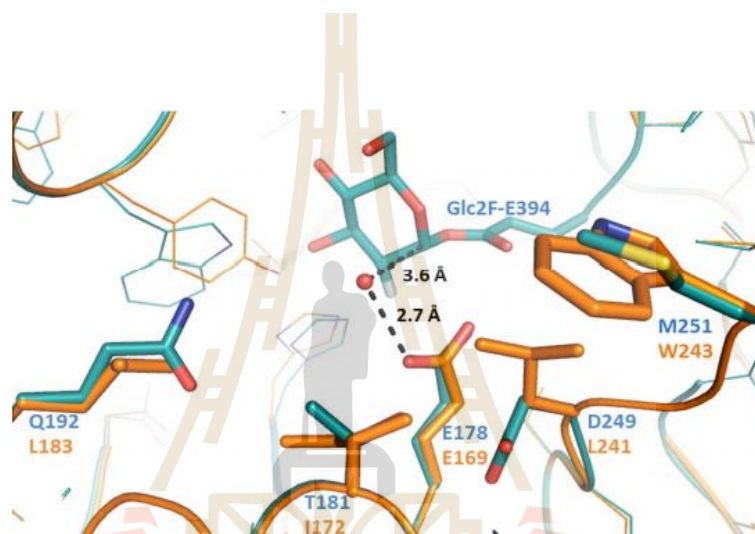


**Figure 2.12** Superposition of a homology model of Os9BGlu31 transglucosidase on the X-ray crystal structure of the Os3BGlu6  $\beta$ -glucosidase covalent intermediate with 2-fluoro- $\alpha$ -D-glucoside (PDB: 3G9R) (Komvongsa et al., 2015).

The Os9BGlu31 W243 residue was found to be critical to the substrate and product specificity of Os9BGlu31 transglucosidase due to the importance of the corresponding residue in the substrate specificities of Os3BGlu6 by superposition between Os3BGlu6 and Os9BGlu31 within 8.7 Å away from acceptor water binding site in the superposition (Figure 2.12) and mutation of this residue allows production



of a range of glucoconjugates, while I172T and L183Q mutations decreased the activity. Different mutations at W243 (A, D, M, N, F and Y) had variable effects, depending on the acceptor substrate (Komvongsa et al., 2015). The mutated Os9BGlu31 transglucosidase variants act to transfer glucose between a broad range of carboxylic and phenolic oxygens. Evaluation of 22 different acceptor substrates with all possible Os9BGlu31 variants at residue 243 showed W243L and W243N exhibited high activity, and the double mutant L241D/W243N showed very high activity on certain substrates and exceptionally high levels of hydrolysis (Tran et al., 2019) (Figure 2.13).

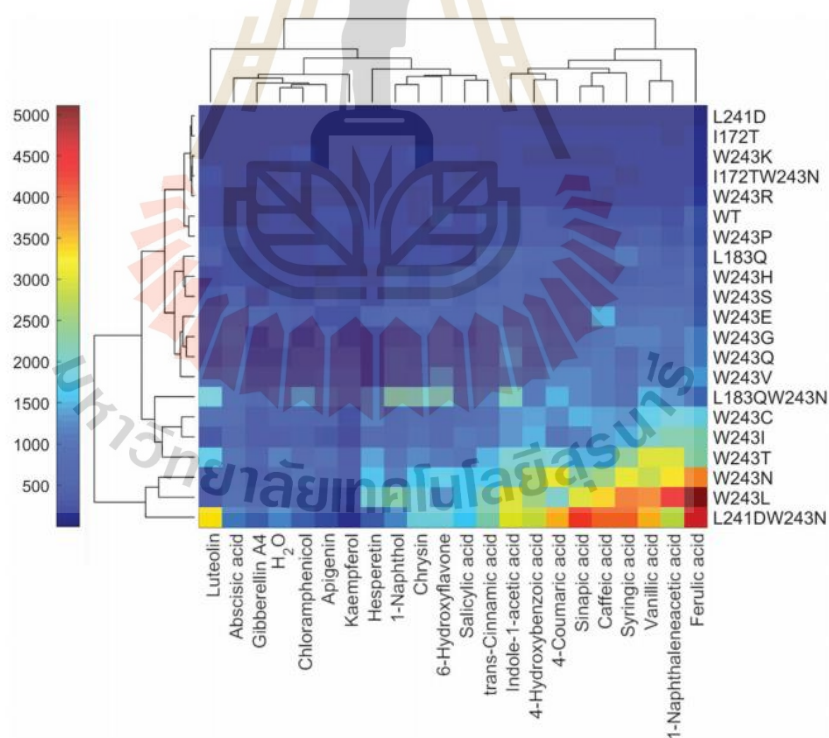


**Figure 2.13** Heatmap of the *p*NP release catalyzed by 21 Os9BGlu31 variants when glycosylating 22 different acceptors (Tran et al., 2019).



### 2.8.3 Leloir glycosyltransferases (GT)

Leloir glycosyltransferases (GT) catalyze the formation of a glycosidic bond between a carbohydrate or aglycon acceptor and the sugar from an activated sugar nucleotide or sugar phospholipid donor (Lairson et al., 2008). The acceptor can also be a lipid, protein, nucleic acid, antibiotic, or other small molecules. The nucleotide-dependent Leloir glycosyltransferases can reach quantitative yields with high selectivity, and exist with a wide range of donor and acceptor specificities, enabling the stereo- and regioselective extension and branching of large glycans and glycoconjugates (Cardini et al., 1950). Although very efficient, industrial implementation is limited due to the high price of nucleotide-activated donors. As with GH, two mechanistic classes can be distinguished based on the stereochemistry upon formation of the glycosidic bond at the anomeric center, which can either be retained or inverted with high selectivity for the  $\alpha$ - or  $\beta$ -anomer (Lim et al., 2005). Inverting GT use general base catalyst that deprotonates the incoming nucleophile of the acceptor, while the sugar forms an oxocarbenium ion-like transition state, facilitating direct displacement by an  $S_N2$  mechanism and the catalytic rate can be increased by using divalent metals (i.e.  $Mn^{2+}$  or  $Mg^{2+}$ ), which are coordinated by the amino acid motif Asp-X-Asp (Mestrom et al., 2019).

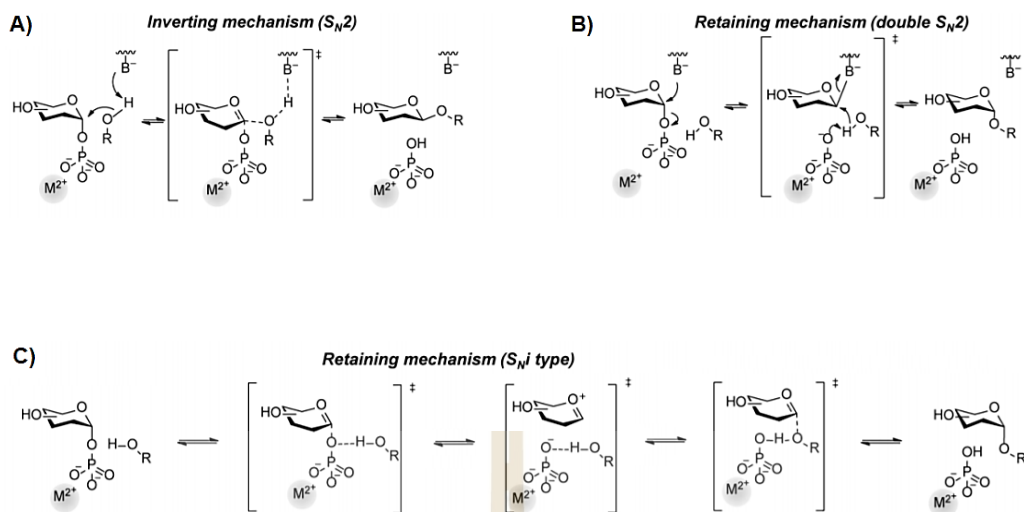


**Figure 2.14** Reaction mechanism of glycosyltransferases and glycoside phosphorylases resulting in inversion (A) or retention (B, C) of the anomeric glycosidic bond (Mestrom et al., 2019).

In GT, retaining transfer can proceed by a double-displacement mechanism involving a covalently bound glycosyl-enzyme intermediate via an  $S_N2$  mechanism, or by a transient ion-pair intermediate via a  $S_Ni$ -type mechanism. The former is similar to the double displacement mechanism described for GH in Figure 2.3. The latter involves the formation of a discrete enzyme-stabilized oxocarbenium ion-like intermediate that is shielded on one side by the enzyme, thereby preventing nucleophilic attack from the opposite side of the reaction center and leading to complete retention of anomeric configuration in the product (Figure 2.14) (Lairson et al., 2008).

#### 2.8.4 Glycoside phosphorylases (GP)

Glycoside phosphorylases (GP) are enzymes that catalyze the reversible phosphorolysis of glycosidic bonds. For example, phosphorolysis of glycogen and amylopectin result in transfer of the non-reducing end terminal glycosyl residue to phosphate to make  $\alpha$ -glucose-1-phosphate (Kitaoka and Hayashi, 2002). Similar to GT, GP also utilize activated sugars glycosyl phosphates as a glycosyl donor. However, the natural function of GP is not glycosylation, but degradation. GP use inorganic phosphate as a glycone acceptor in di- and oligosaccharide degradation processes, to produce  $\alpha$ -glucose-1-phosphate and a saccharide of reduced length (O'Neill and Field, 2015). The high energy of the glycosyl phosphate allows the reversible reaction to be used for synthetic purposes efficiently (Puchart, 2015). The two common mechanisms of GP, as well as their structures, are similar to GH or GT, with the stereochemical outcome resulting in retention or inversion of configuration. These enzymes always occur in an exo-fashion leading to formation of a monosaccharide or disaccharide 1-phosphate (Figure 2.14).

# CHAPTER III

## MATERIALS AND METHODS

### 3.1 Materials

#### 3.1.1 Plasmids, bacterial and yeast stains

The *Os9bglu31* cDNA was previously cloned into the pET32a(+)/DEST expression vector to produce N-terminally thioredoxin-, His<sub>6</sub>- and S-tagged fusion proteins with an enterokinase and TEV protease cleavage sites between the fusion tags and enzyme, as shown in Figure 3.1 (Tran et al., 2019).

The *OsExo2* cDNA was previously cloned into the pET32a(+)/DEST expression vector to produce N-terminally thioredoxin-, His<sub>6</sub>- and S-tagged fusion proteins with an enterokinase cleavage site between the fusion tags and enzyme, as shown in Figure 3.2 and the cDNA optimized for *OsExo1* was previously cloned into the pPICZ $\alpha$ BNH8 expression vector to produce fusion protein with  $\alpha$ -factor in the N-terminus and His<sub>8</sub>-tagged in the C-terminus, as shown in Figure 3.3 (Prawisut et al., 2020; Prawisut, 2018).

The *Escherichia coli* stains DH5 $\alpha$  and XL1-blue were used for cloning and Origami B(DE3) strain was used to express the Os9BGlu31 and the OsExo2. *P. pastoris* strain SMD1168H was used to express the OsExo1 protein.

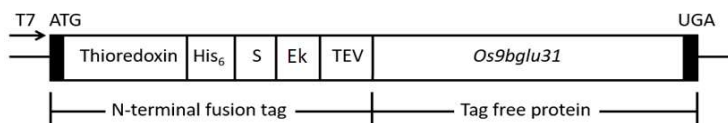


**Figure 3.1** Construct of the protein-coding sequence of recombinant pET32a(+)/DEST with the *Os9bglu31*.

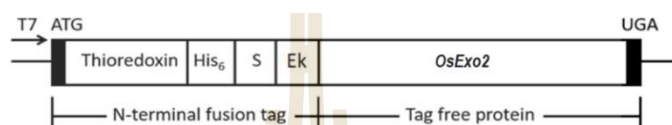


**Figure 3.2** Construct of the protein-coding sequence of recombinant pET32a(+)/DEST with the *OsExo2*.



**Figure 3.3** Construct of the protein-coding sequence of recombinant pPICZαBNH8 with the *OsExo1*.

### 3.1.2 Chemicals and reagents

*Pfu* DNA polymerase was produced in-house with a plasmid generated in the group of Dr. Mariena Ketudat-Cairns (Appendix A). TEV protease was produced in-house by following instruction from Polayes et al., 1998. Oligonucleotide primers, DNase A, RNase I, lysozyme, amoxicillin, ampicillin, kanamycin, and tetracycline were purchased from Bio Basic, Inc. *DpnI*, *EndoH*, and deoxynucleotides (dATP, dTTP, dCTP, and dGTP) were purchased from New England Biolabs, Ltd. Tryptone,

yeast extract, agar, yeast nitrogen base (YNB) were purchased from HiMedia Laboratories Pvt Ltd. Zeocin was purchased from Invitrogen, Co. Nybomycin was purchased from Bio Australis, Co. *p*-Nitrophenol  $\beta$ -D-glucoside (*p*NPGlc) was purchased from Shanghai Laihao Trade Co. Ltd. Polyethylene glycol 6000 (PEG6000), biotin, isopropyl- $\beta$ -D-thiogalactoside (IPTG), *p*-nitrophenol  $\beta$ -D-cellobioside (*p*NPC2), chloramphenicol, streptomycin, cefixime, cefotaxime and doxorubicin were purchased from Sigma-Aldrich Inc. Cello-oligosaccharides and laminari-oligosaccharides with degrees of polymerization 2-5 were purchased from Megazyme, Ltd. Sodium chloride (NaCl), sodium carbonate (Na<sub>2</sub>CO<sub>3</sub>), sodium sulfate (Na<sub>2</sub>SO<sub>4</sub>), acrylamide, sodium hydroxide (NaOH), sodium acetate (NaOAc), sodium citrate (Na<sub>3</sub>C<sub>6</sub>H<sub>5</sub>O<sub>7</sub>), sodium dodecyl sulfate (SDS), sodium dihydrogen phosphate (NaH<sub>2</sub>PO<sub>4</sub>), disodium hydrogen phosphate (Na<sub>2</sub>HPO<sub>4</sub>), potassium dihydrogen phosphate (KH<sub>2</sub>PO<sub>4</sub>), dipotassium hydrogen phosphate (K<sub>2</sub>HPO<sub>4</sub>), potassium acetate (CH<sub>3</sub>COOK), calcium chloride (CaCl<sub>2</sub>), cobalt chloride (CoCl<sub>2</sub>), magnesium sulfate (MgSO<sub>4</sub>), ammonium persulfate (APS), ammonium sulfate (NH<sub>4</sub>)<sub>2</sub>SO<sub>4</sub>, ammonium chloride (NH<sub>4</sub>Cl), Triton X-100, Tris(hydroxymethyl) aminomethane, ethylene diamine tetra acetic acid (EDTA), hydrochloric acid (HCl), N, N', N'', N'''- tetramethyl ethylenediamine (TEMED), glacial acetic acid,  $\beta$ -mercaptoethanol (BME), phenylmethyl-sulfonyl fluoride (PMSF), Coomassie brilliant blue R250, propanol, isopropanol, propargyl alcohol, butanol, 3-methyl butanol, octanol, 4-(hydroxymethyl) benzoic acid, dimethyl sulfoxide (DMSO), glycerol, ethylene glycol, glucose, and  $\alpha$ -lactose were purchased from Carlo Erba Reagents. HPLC-grade water, methanol, ethanol, chloroform, dichloromethane, and ethyl acetate were purchased from RCI Labscan, Ltd. Deuterium oxide (D<sub>2</sub>O) and chloroform-D (CDCl<sub>3</sub>) were purchased from Cambridge Isotope Laboratories, Inc.

## 3.2 General methods

### 3.2.1 Preparation of *E. coli* competent cells

Glycerol stocks of DH5 $\alpha$  and XL1-Blue were streaked on LB plates without antibiotic. Origami (DE3) was streaked on an LB plate containing 15  $\mu$ g/ml kanamycin and 12.5  $\mu$ g/ml tetracycline and incubated at 37 °C for 16-18 hours. A single colony was picked and inoculated into 5 ml of LB broth with shaking at 37 °C, 200 rpm for 16-18 hours. One hundred microliters of starter culture were transferred to 100 ml of LB broth and shaken at 37 °C, 200 rpm until the optical density at 600 nm (OD600) reached 0.4 - 0.6. The cell culture was chilled on ice for 5 minutes in sterile polypropylene tubes and collected at 4,000 rpm at 4 °C for 10 minutes. The cell pellets were resuspended in 10 ml ice-cold sterile 0.1 M CaCl<sub>2</sub> and centrifuged to collect the cell pellets again. Finally, the pellets were resuspended with 1 ml of 0.1 M CaCl<sub>2</sub> containing 15% glycerol and 50  $\mu$ l aliquots were stored at -80 °C.

### 3.2.2 Transformation of plasmids into competent cells

An aliquot of frozen competent cells was thawed 5 minutes on ice, then 1  $\mu$ l of cloning or expression plasmids (20 - 100 ng) or site-directed mutagenesis reactions were mixed with fresh or thawed competent cells. The reaction was incubated on ice for 30 minutes. The plasmid was transformed by heat shocking the cells at 42 °C for 45 seconds and quickly chilled on ice for 5 minutes. Two hundred microliters of LB broth was added to the transformed competent cells, which were then incubated at 37 °C for 1 hour. The transformed cells were spread on LB agar containing appropriate antibiotics and incubated at 37 °C overnight.



### 3.2.3 Plasmid isolation by alkaline lysis method

A single colony of transformed recombinant bacteria was picked into 5 ml of LB broth and incubated at 37 °C with shaking at 200 rpm for 16 - 18 hours. The cultured cells were collected by centrifugation at 10,000xg, 1 minute. The supernatant was removed and the cells were resuspended in 100 µl of lysis buffer I (50 mM glucose, 10 mM EDTA, 50 mM Tris-HCl, pH 8.0). Then, 200 µl of freshly prepared lysis buffer II (0.2 N NaOH, 1% (w/v) SDS) was added and the tube was inverted 4 - 6 times. After that, 150 µl of ice-cold lysis buffer III (3 M potassium acetate, pH 4.8) was added and the tube was mixed by inverting 4 - 6 times. The alkaline lysis reaction was incubated on ice for 5 minutes and the clear solution containing the plasmids was separated from the cell debris by centrifugation at 13,000xg, 10 minutes. The supernatant was transferred to a new tube and the DNA was precipitated with 2 volumes of absolute ethanol for 10 minutes at 4 °C. The precipitated DNA was collected by centrifugation at 13,000xg for 10 minutes. After removing the supernatant, the pellet was washed with 500 µl of 70% ethanol and centrifugation was repeated, followed by removal of the ethanol. The left-over solution was removed by speed vacuum. Then, the DNA pellet was resuspended in 100 µl TE buffer containing 2 µg RNase A and incubated at 37 °C for 10 minutes. The RNase A-treated plasmids were further purified by adding 70 µl of ice-cold precipitation solution (20% PEG 6000, 2.5 M NaCl) and chilled on ice for 1 hour. The precipitated DNA was collected by centrifugation at 13,000xg for 10 minutes. The supernatant was removed and the pellet was washed by adding 0.5 ml of 70% ethanol and inverting the tube twice, after which the ethanol solution was removed and the tube dried by speed vacuum. Finally, the DNA was re-dissolved with 30 µl of TE buffer or sterile water.

### **3.2.4 Protein analysis by sodium dodecyl sulfate polyacrylamide gel electrophoresis**

The protein profile and the apparent molecular weights of proteins in various fractions were determined by sodium dodecyl sulfate polyacrylamide gel electrophoresis (SDS-PAGE), as described by Laemmli (1970). The 12% SDS-PAGE separating gel consisted of 12% (w/v) acrylamide (11.2%)/bis-acrylamide (0.8%), 375 mM Tris-HCl, pH 8.8, 0.1% SDS, 0.05% ammonium persulfate and 0.05% TEMED, while the 4% stacking gel consisted of 4% (w/v) acrylamide, 125 mM Tris-HCl, pH 6.8, 0.1% SDS, 0.05% ammonium persulfate and 0.05% TEMED. Protein samples were mixed 5:1 with 6X loading buffer (50 mM Tris-HCl, pH 6.8, 10% SDS, 0.2 mg/ml bromophenol blue, 50% glycerol, 20%  $\beta$ -mercaptoethanol) and boiled for 5 minutes to denature proteins. Twenty microliters of protein samples were loaded into sample wells, and electrophoresed through the polymerized gel at 170 V with Tris-glycine electrode buffers (50 mM Tris base, 125 mM glycine and 0.1% SDS, pH 8.3) until the dye front reached the bottom of the gel plate. The gels were subsequently stained in staining solution containing 0.1% (w/v) Coomassie Brilliant Blue R250, 40% (v/v) methanol, and 10% (v/v) acetic acid in water for 30 minutes, then destained with de-staining solution (40% (v/v) methanol and 10% (v/v) acetic acid) for 1 - 2 hours. The molecular masses of protein bands were determined by comparing to standard low molecular weight protein markers (GE Healthcare, Uppsala, Sweden), which consist of phosphorylase (97.4 kDa), bovine serum albumin (66 kDa), ovalbumin (45 kDa), bovine carbonic anhydrase (31 kDa), trypsin inhibitor (21.5 kDa), and bovine  $\alpha$ -lactalbumin (14 kDa).

### 3.3 Site-directed mutagenesis

To generate a more effective model for Os9BGlu31 interactions with substrates, the structure of Os9BGlu31W243L was solved in collaboration with Linh Tran and Robert C. Robinson. This structure was submitted to docking studies to predict which amino acids should be changed to explore using cellobiose and cellotriose as a donor substrate and improve interactions with acceptor substrates (Vincent Blay, unpublished). The mutations causing the desired amino acid substitutions were introduced into the Os9BGlu31 coding sequence by mutagenesis with the primers listed in Table 3.1. The pET32a/DEST-TEV/Os9BGlu31 plasmid was used as a template for a full-length plasmid strand amplification from two complementary oligonucleotide primers containing the desired mutation point. *Pfu* DNA polymerase was used to synthesize the mutated plasmid DNA during the temperature cycling, which includes step 1, 95 °C 30 seconds; step 2, 95 °C 30 seconds; step 3, 55 °C 1 minute and step 4, 68 °C 10 minutes, with steps 2 to 4 repeated for 15 cycles. The PCR product was treated with *DpnI* endonuclease for 3 hours at 37 °C to eliminate methylated and hemi-methylated DNA of the parental DNA template. Cyclization and repair of the dsDNA products were accomplished by transforming the DNA into competent XL-1 Blue *E. coli* cells. The transformants were selected on agar plates containing ampicillin. All mutations were confirmed by DNA sequencing (Macrogen, Seoul, Korea).

**Table 3.1** Oligonucleotide primers for site-directed mutagenesis of Os9BGlu31.

Mutant		Oligonucleotides	T <sub>m</sub> (°C)	Length
H123E	Fwd	5'-cacgtaacgatatatgaaatcgaatttcctcaggc-3'	74.3	35
	Rev	5'-gctgaggaaaatcgaaatcctatatacgttacgtg-3'	74.3	35
I172T	Fwd	5'-gtcaatgagcctaaccaccgagccgattggcgg-3'	83.5	32
	Rev	5'-ccgccaatcggctcgggtgtaggctcattgac-3'	83.5	32
L183Y	Fwd	5'-gatacgatcaaggaatctaccgccacggcgatg-3'	81.2	34
	Rev	5'-catcgccgtggcggatagattccttgatcgtatc-3'	81.2	34
L241E-	Fwd	5'-gggctcacattggaggtaattggtacgagc-3'	76.3	31
W243N	Rev	5'-gctcgtaccaattaccctcaatgtgagccc-3'	76.3	31
L241T-	Fwd	5'-gggctcacattgaccgtaattggtacgagc-3'	78.5	31
W243N	Rev	5'-gctcgtaccaattaccggtcaatgtgagccc-3'	78.5	31
L241V -	Fwd	5'-gggctcacattgctcggtaattggtacgagc-3'	78.5	31
W243N	Rev	5'-gctcgtaccaattaccgaccaatgtgagccc-3'	78.5	31
L241Y -	Fwd	5'-gggctcacattgtaccgtaattggtacgagc-3'	75.5	31
W243N	Rev	5'-gctcgtaccaattaccgtacaatgtgagccc-3'	75.5	31
Y313H	Fwd	5'-gtcggatttaaccaccatgctgcgccattttgtgag-3'	79.6	35
	Rev	5'-ctcacaaaaatggcgacatggtggttaaatccgac-3'	79.6	35
Y313Q	Fwd	5'-gtcggatttaaccaccaggtcgcgccattttgtgag-3'	80.2	35
	Rev	5'-ctcacaaaaatggcgacctggtggttaaatccgac-3'	80.2	35
Y313S	Fwd	5'-gtcggatttaaccactctgctgcgccattttgtgag-3'	78.1	35
	Rev	5'-ctcacaaaaatggcgacagagtggttaaatccgac-3'	78.1	35

**Table 3.1** Oligonucleotide primers for site-directed mutagenesis of Os9BGlu31 (continued).

Mutant		Oligonucleotides	T <sub>m</sub> (°C)	Length
W434E	Fwd	5'-gcagggtacttcgtg <b>gag</b> tcgttcctggacgtg-3'	83.6	34
	Rev	5'-cacgtccaggaacga <b>ctc</b> cacgaagtagccctgc-3'	83.6	34
E441H	Fwd	5'-cctggacgtgttc <b>cat</b> tacctgttcggctacc-3'	79.0	32
	Rev	5'-ggtagccgaacaggtat <b>atg</b> gaacacgtccagg-3'	79.0	32
E441Q	Fwd	5'-cctggacgtgttc <b>cag</b> tacctgttcggctacc-3'	79.4	32
	Rev	5'-ggtagccgaacaggtat <b>ctg</b> gaacacgtccagg-3'	79.4	32
E441T	Fwd	5'-cctggacgtgttc <b>act</b> tacctgttcggctacc-3'	80.0	32
	Rev	5'-ggtagccgaacaggtat <b>cgt</b> gaacacgtccagg-3'	80.0	32

### 3.4 Expression and Purification of Os9BGlu31 and variants

#### 3.4.1 Expression of Os9BGlu31 and variants

The pET32a/DEST/TEV/Os9BGlu31 plasmid, which encodes an N-terminally thioredoxin and His<sub>6</sub>-tagged Os9BGlu31 fusion protein, were transformed into *E. coli* Origami B(DE3) cells. The cells were cultured in LB media containing 50 µg/ml ampicillin, 15 µg/ml kanamycin, and 12.5 µg/ml tetracycline at 37 °C, while shaking at 200 rpm, until the culture reached an optical density at 600 nm of around 0.4 - 0.5. The expression of protein was induced by 0.4 mM IPTG, at 20 °C for 18 hours.

#### 3.4.2 Purification of Os9BGlu31 and variants

The recombinant Os9BGlu31 and variants containing the thioredoxin and 6x histidine-tag at their N-termini were purified by Immobilized Metal Affinity

Chromatography (IMAC). The cell pellets were harvested by centrifugation and resuspended in extraction buffer (50 mM Tris-HCl, pH 8.0, 150 mM sodium chloride, 200 µg/ml lysozyme, 1% (v/v) Triton-X, 0.1 mg/ml trypsin inhibitor from soybean, 1 mM PMSF, 4 µg/ml DNase I), then the suspended cells were incubated at 30 °C for 30 minutes and clarified by centrifugation at 12,000 rpm for 30 minutes. The supernatant was applied to IMAC (Co<sup>2+</sup>) resin. The resin was washed with the equilibration buffer (150 mM NaCl, 50 mM Tris-HCl, pH 8.0), followed by 20 mM imidazole in the equilibration buffer, and eluted with 250 mM imidazole in the equilibration buffer. The IMAC fractions were analyzed by SDS-PAGE, evaluating the predicted size of the fusion protein at approximately 70 kDa. In order to produce a highly purified protein, the N-terminal fusion tag was removed by cleavage with 1 mg TEV protease per 50 mg of the fusion protein at 4 °C for 16 hours. Then, the digested proteins were loaded onto the second IMAC to remove the cleaved tag and other IMAC-binding contaminant proteins.

### **3.5 Transglycosylation of Os9BGlu31 and variants**

The transglycosylation activity with various glucose acceptor substrates were assayed with 5 mM antibiotic acceptor substrates (ampicillin, amoxicillin, cefixime, cefotaxime kanamycin, chloramphenicol, streptomycin, and tetracycline) or 0.5 mM (nybomycin, doxorubicin, and paclitaxel), 5 mM or 1 mM *p*NPGlc as donor substrate, and 1 µg of the selected variant enzyme in 50 mM citrate, pH 4.5, and 5% DMSO. The reactions were incubated at 30 °C for 12 hours and then stopped by heating at 90 °C for 5 minutes.

### 3.6 Analytical chromatography

The residual substrates and the reaction products were analyzed by thin-layer chromatography (TLC) and ultra-high-performance liquid chromatography (UPLC). The TLC analysis (Silica gel 60 F254) were developed with mobile phase and carbohydrates detected by painting with 10% sulfuric acid in ethanol for staining and heating to visualize the spots. The UPLC analysis used a ZORBAX SB-C18 (1.8  $\mu\text{m}$ , 2.1 x 150 mm) column on an Agilent 1290 UPLC, the column equilibrated in 95% solvent A (water) and 5% solvent B (acetonitrile). The compounds were eluted by a linear gradient from 5% to 50% B (v/v) for 13 min, 50% to 70% B (v/v) for 1 min, and 70% to 5% B (v/v) for 2 min, at a flow rate of 0.3 ml min<sup>-1</sup>, the absorbance was measured by UV/visible absorbance at wavelengths between 220, 360, and 540 nm, monitored by a Diode-Array Detector (DAD) (Tran et al., 2019).

### 3.7 Chloramphenicol glucoside production and purification

Transglucosylation of chloramphenicol was performed by using Os9BGlu31W243N with 5 mM substrates in 50 mM citrate pH 4.5, and 5% (v/v) DMSO. The reaction was incubated at 30 °C for 12 hours. The reaction was evaporated the aqueous solution by rotary evaporator and then applied to silica gel column chromatography with a solvent system of CHCl<sub>3</sub>: MeOH. A mixture of *p*NPGlc and chloramphenicol glucoside was eluted by 10% MeOH. The mixture was evaporated then re-dissolved in water and further purified over a C18 silica column (Sep-pak cartridges) with a solvent system of H<sub>2</sub>O: MeOH, monitored by silica gel TLC. The fractions showing a single spot on TLC were pooled, collected and dried by speed vacuum centrifuge.



## 3.8 Expression and purification of OsExo1

### 3.8.1 Expression of OsExo1

Glycerol stock of pPICZ $\alpha$ BNH8/*OsExo1* in *P. pastoris* SMD1168H from previous work by Prawisut, 2018 was spreaded on 250  $\mu$ g/ml zeocin YPD plate. A single colony that had been selected was inoculated into 100 ml of buffered glycerol-complex medium (BMGY) with 25  $\mu$ g/ml zeocin and grown in a shaking incubator (200 rpm) at 28 °C overnight, 10% of the starter culture were inoculated in 1000 ml of BMGY until the cell culture OD<sub>600</sub> reached 2-3. The cells were harvested by centrifugation at 3000xg for 10 minutes at 20 °C and resuspended in 1000 ml of buffered methanol-complex medium (BMMY) medium. The protein expression was induced by adding methanol to 1% (v/v) final concentration every 24 hours for 3 days at 20 °C.

### 3.8.2 Purification of OsExo1

The protein was purified from the culture broth after removal of the cells by centrifugation at 4000xg at 4 °C for 10 minutes. The pH of the culture broth with secreted protein was adjusted to 8.0 with 1 M Na<sub>2</sub>CO<sub>3</sub> and it was loaded onto a 5 ml IMAC column charged with Ni<sup>2+</sup>, and the column was washed with 5 column volumes of 250 mM Tris-HCl, pH 8.0, then the protein was eluted with gradient of 0 to 250 mM imidazole, 150 mM NaCl in 20 mM Tris-HCl, pH 8.0. The fractions with  $\beta$ -glucosidase activity were pooled, concentrated and the imidazole removed by centrifugation in a 50 kDa molecular-weight cutoff ultrafiltration membrane at 3000xg at 4 °C for 10 minutes. The protein was separated into 2 parts, one was purified by size exclusion chromatography over a Superdex S200 10/300 GL column in 20 mM Tris-HCl, pH 8.0, and 150 mM NaCl, run at a flow rate of 0.3 ml/min, and the fractions containing activity

were analyzed on SDS-PAGE and pooled as appropriate. The other half of the preparation was digested by endoglycosidase H and purified over the Superdex S200 10/300 GL column.

### **3.9 Expression and Purification of OsExo2**

#### **3.9.1 Expression of OsExo2**

The recombinant pET32a/DEST/OsExo2 in *E. coli* Origami B(DE3) was inoculated into LB broth containing 15 µg/ml kanamycin, 12.5 µg/ml tetracycline and 50 µg/ml ampicillin at 37 °C overnight. The starter culture was added to 5% to 4 liters auto-induction medium (AIM) containing the same antibiotics and grown continuously at 37 °C with shaking at 200 rpm until the OD600 reached 0.8 - 1.0. The flasks were then transferred to 15 °C for 24 hours. The cells were collected by centrifugation at 4000×g at 4 °C for 10 minutes.

#### **3.9.2 Purification of OsExo2**

The cell pellets were resuspended with extraction buffer (20 mM Tris-HCl, pH 8.0, 200 µg/ml lysozyme, 1% Triton-X100, 1 mM PMSF, and 0.25 mg/ml DNase I, sonicated and incubated at room temperature for 30 minutes. Soluble protein was separated from cell debris by centrifugation at 12,000×g for 20 minutes at 4 °C. The recombinant protein was purified with 3 steps. First, crude protein was immediately loaded into IMAC resin equilibrated with nickel (II) sulfate followed by equilibration buffer (20 mM Tris-HCl, pH 8.0, and 150 mM NaCl) and the recombinant protein was eluted with a gradient of 0-260 mM imidazole in equilibration buffer. The fractions were assayed for hydrolysis of 1 mM pNPGlc in 50 mM sodium acetate, pH 5, and

those with activity were pooled. The pool of active fractions was concentrated in a 50 kDa MWCO ultrafiltration membrane by centrifugation at 3500xg. Then, 0.5 ml of concentrated protein was loaded onto a Superdex 200 gel filtration column in 20 mM Tris-HCl, pH 8.0, 500 mM NaCl, and 1 mM EDTA, run at a flow rate of 0.3 ml/min. Next, the protein was loaded onto a phenyl sepharose column (5 ml), equilibrated with 2 M NaCl in 50 mM Tris-HCl, pH 8, and eluted with gradient of 2 to 0 M NaCl, followed by a gradient of 0 - 20% ethylene glycol in 50 mM Tris-HCl, pH 8, at a flow rate of 0.5 ml/min. Finally, protein fractions containing *p*NPGlc hydrolysis activity were assessed by SDS-PAGE and apparently pure fractions were pooled, and the buffer changed to equilibration buffer in a 50 kDa MWCO ultrafiltration membrane.

### **3.10 Determination of the optimal pH and temperature and temperature stability for OsExo1**

The optimum pH of OsExo1 was determined in a 140  $\mu$ l reaction containing 1 mM *p*NPGlc substrate in 50 mM buffers with pH in the range between 2.5 and 9.0 (universal citrate phosphate buffer). The reactions were incubated at 30 °C for 15 minutes and then 70  $\mu$ l of 2 M sodium carbonate was added to stop the reaction. Enzyme activity was measured as *p*NP released, based on the absorbance at 405 nm. The optimum temperature was assessed in reactions at temperatures from 10 °C to 80 °C in 5 °C increments. The enzyme activity was assayed against 1 mM *p*NPGlc in 50 mM sodium acetate, pH 5.0, for 15 minutes. Then reaction was stopped by adding 70  $\mu$ l of 2 M sodium carbonate and the *p*NP released was measured by absorbance at 405 nm. The temperature stability was determined by incubating the enzyme in 50 mM sodium

acetate, pH 5.0, for 15 minutes, at temperatures from 0 °C to 80 °C in 10 °C increments. The activity of the enzyme was assayed against 1 mM *p*NPGlc at 30 °C for 15 minutes, then 70 µl of 2 M sodium carbonate was added to stop the reaction and the absorbance of the *p*NP released was measured at 405 nm.

### 3.11 Enzyme kinetics parameter determination of OsExo1

The kinetic parameters of the purified protein were determined in triplicate reactions for hydrolysis of *p*NPGlc, laminaribiose, and laminarin. Initially, a time course was run for each substrate and condition to determine the amount of enzyme and time that gave a linear time course, indicating initial velocity. The substrate concentrations used covered a from one third to three times the apparent  $K_M$  or a broader range. The  $K_M$  and  $V_{max}$  values were calculated by fitting the rate of product formation and substrate concentrations from non-linear regression analysis of Michaelis-Menten plots with Grafit 5.0 (Erithacus Software, Horley, Surrey, U.K.). The apparent catalytic rate constant ( $k_{cat}$ ) values are calculated by dividing the maximum velocity ( $V_{max}$ ) by the total amount of enzyme protein in the reaction.

### 3.12 Transglycosylation activity of OsExo1 and OsExo2

The varieties of glucosyl donors tested in transglucosylation reactions were *p*NPGlc, oligosaccharides, and polysaccharides, while an alcohol series of potential glucosyl acceptors were tested. The transglycosylation activity with *p*NPGlc was assessed in 100 µl reactions with 5 units of the enzyme in 50 mM sodium acetate, pH 5.0, at 30 °C for 0 min, 5 min, 30 min, 1 hr, 3 hr, 6 hr, and 12 hr (1 unit of enzyme is

defined by the amount of enzyme required for the production of 1  $\mu\text{mol}$  of *p*NP from 1 mM *p*NPGlc per minute at 30 °C in 50 mM sodium acetate, pH 5.0). The glucosyl donors cellobiose (C2), cellotriose (C3), cellotetraose (C4), laminaribiose (L2), laminaritriose (L3), laminaritetraose (L4), laminaripentaose (L5), laminarin, barley glucan, and lichenan were tested with methanol as acceptor. The reactions were carried out in 100  $\mu\text{l}$  with 1 unit of the enzyme, 1 mM oligosaccharide or 0.5% (w/v) polysaccharide and 5% (v/v) methanol as a glucosyl acceptor, in 50 mM sodium acetate, pH 5.0, at 30 °C for 24 hours. The glucosyl acceptors tested included ethylene glycol, methanol, ethanol, propanol, butanol, and 3-methyl-1-butanol. The reaction was carried out in 100  $\mu\text{l}$  with 1 unit of the enzyme, 5% (v/v) alcohol and 1 mM *p*NPGlc as a glucosyl donor, in 50 mM sodium acetate, pH 5.0, at 30 °C overnight. The reactions were stopped by heating at 90 °C 5 min, then the reactions and standards were spotted onto silica gel TLC plates, which were developed in butanol: acetic acid: water (2:1:1 v/v) and stained with 10% sulfuric acid in ethanol, followed by heating at 120 °C until the color of carbohydrate-containing spots developed.

### 3.13 Purification of OsExo2 transglycosylation products

The transglycosylation reactions by OsExo2 were carried out in 10 mM *p*NPGlc, 100 ml with 1 unit of the enzyme in 50 mM sodium acetate, pH 5.0, at 30 °C for 12 hours. The reaction was evaporated in a rotary evaporator and then applied to silica gel chromatography with a solvent system of  $\text{CHCl}_3$ : MeOH. A mixture of *p*NPGlc and *p*NP-oligosaccharides was collected together. The mixture was evaporated in a rotary evaporator then re-dissolved in water and further purified by reverse phase chromatography over a C18 column with a solvent system of  $\text{H}_2\text{O}$ : MeOH. A mixture

of *p*NP-oligosaccharides was collected from the C18 column, then further purified by TLC with a solvent of butanol: acetic acid: water (2:1:1 v/v), the single products identified under UV were scraped out from TLC, then dissolved by 50% MeOH in CHCl<sub>3</sub>. The solvents were separated from silica gel by centrifugation at 10,000xg for 10 minutes, and the extraction was repeated for three times. The samples were dried by SpeedVac vacuum concentrator at 40 °C, until dried.

The transglycosylation product of alcohols, including methanol, ethanol, propanol, butanol, 3-methyl-1-butanol, and ethylene glycol as glucosyl acceptor were produced in 100 ml reactions with 5% (v/v) alcohol, 5 mM *p*NPGlc (glucosyl donor), and 2 units of the enzyme in 50 mM sodium acetate, pH 5.0, at 30 °C for 48 hours. The reaction was evaporated by rotary evaporator and then applied to silica gel column chromatography with a solvent system of EtOAc: MeOH by slowly increasing MeOH in increments of 2% (Table 3.2).

Cellobiose was used as a glucosyl donor substrate in the reaction of propargyl alcohol,  $\beta$ -mercaptoethanol, and 4-hydroxymethyl benzyl alcohol. The reactions were carried out in 100 ml with 2% (v/v) propargyl alcohol or mercaptoethanol or 5 mM 4-hydroxymethyl benzyl alcohol (dissolved in acetone), 5 mM cellobiose served as a glucosyl donor, and 2 units of the enzyme in 50 mM sodium acetate, pH 5.0, at 30 °C for 48 hours. The aqueous solution was evaporated from the reaction mixture by rotary evaporator and then remaining material applied to silica gel with system of CH<sub>2</sub>Cl<sub>2</sub>: MeOH by slowly increasing MeOH in increments of 2% (Table 3.2).

**Table 3.2** Solvent system for purification of transglycosylation products by silica gel chromatography.

Substrate	Solvent system	Elution (%MeOH)
Methanol	EtOAc: MeOH	10
Ethanol	EtOAc: MeOH	6
<i>n</i> -Propanol	EtOAc: MeOH	4
1-Butanol	EtOAc: MeOH	2
3-Methyl-1-butanol	EtOAc: MeOH	2
Propargyl alcohol	CH <sub>2</sub> Cl <sub>2</sub> : MeOH	2
4-Hydroxymethyl benzyl alcohol	CH <sub>2</sub> Cl <sub>2</sub> : MeOH	4
$\beta$ -Mercaptoethanol	CH <sub>2</sub> Cl <sub>2</sub> : MeOH	8

### 3.14 Transglycosylation product structural confirmation

The transglycosylation product structures were confirmed by NMR spectrometry on a 500 MHz NMR spectrometer (Bruker AVANCE III). Deuterated water (D<sub>2</sub>O) and deuterated chloroform (CDCl<sub>3</sub>), were used as solvents, depending on the solubility of compound. The anomeric protons and anomeric carbons were identified by <sup>1</sup>H and <sup>13</sup>C NMR. The glycosidic linkages in di and tri-saccharides were analyzed by 2D NMR, the -CH<sub>2</sub> protons using C-H correlations were identified from HSQC spectra and the key glycosidic linkages present in tri and di-saccharides using two and three C-H bond correlations were identified from HMBC spectra.



## **CHAPTER IV**

### **RESULTS AND DISCUSSIONS**

#### **4.1 Molecular docking of Os9BGlu31W243L mutation analysis by AutoDock Vina**

One of the objectives of this work is to engineer Os9BGlu31 by site-directed mutagenesis to enable the use of different glucosyl donor substrates. To guide this engineering, we evaluated different possible variants of Os9BGlu31 *in silico*, using a molecular docking strategy. Molecular docking allows ranking glucose donors on different mutants by predicting their relative binding affinities. Os9BGlu31W243L was used as the enzyme, since it can be crystallized and also shows high activity (Tran et al., 2019; unpublished). Cellobiose and cellotriose were used as ligands. The mutants were prepared by virtual point mutagenesis using the software FoldX. The docking software AutoDock Vina was then used, which approximates the potential energy for any conformation of the ligand onto the protein model using an empirical scoring function. The conformation that minimizes this scoring function is found by using an optimization algorithm. The resulting conformation may approximate the bound pose of the ligand that one would observe experimentally, and the value of the scoring function (i.e., the score of the pose), may provide a relative indication of its enthalpy of binding. The results of the docking simulations are shown in the Table 4.1 and the

locations of those mutation were around the active site of the protein as shown in Figure 4.1

**Table 4.1** Scoring functions molecular docking of Os9BGlu 31W243L mutation analysis by AutoDock Vina.

mutant	Difference of Scoring function to parent (higher is better)	
	cellobiose	cellotriose
Parent	0	0
H123E	0	0.4
I172T	0	0.8
L183Y	0.3	0.2
L241E	0.4	0.5
L241V	0.3	0.2
L241T	-0.3	0.4
L241Y	0.2	0.2
Y313H	0.4	0.1
Y313Q	0.2	-0.1
Y313S	0.7	0.1
W434E	0	0.5
E441H	0.3	0.5
E441Q	0.1	0.5
E441T	-0.3	0.4

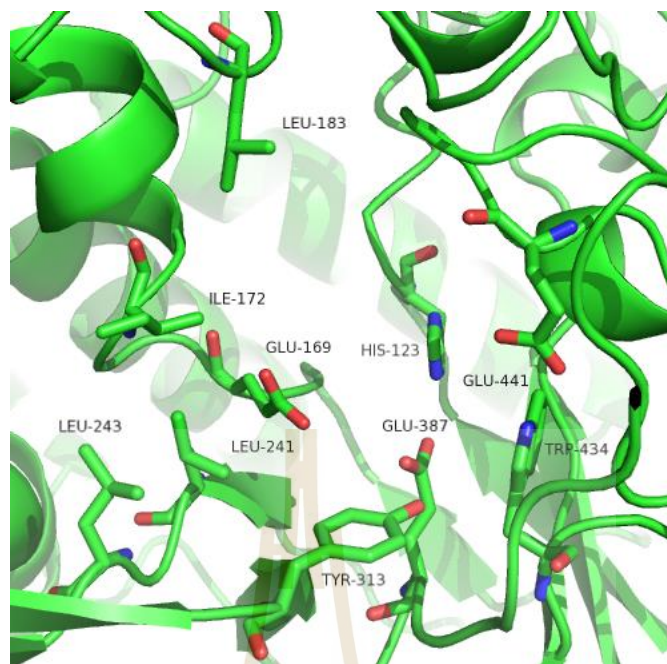


**Figure 4.1** Locations of mutation points predicted on Os9BGlu31W243L.

## 4.2 Site-directed mutagenesis of Os9BGlu31W243L

The mutations to generate the desired amino acid substitutions were introduced into the Os9BGlu31 coding sequence by mutagenesis with the primers designed base on the molecular docking results (Table 4.1). All mutations were confirmed by DNA sequencing (Macrogen, Seoul, Korea) and 6 samples were successful in the cloning step, including variants H123E/W243L, Y313H/W243L, Y313Q/W243L, Y313S/W243L, E441T/W243L, and E441H/W243L.

## 4.3 Expression and purification of Os9BGlu31 and variants

The Os9BGlu31 wild type, W243N, and W243L were previously cloned into the pET32a(+)/DEST expression vector to produce an N-terminally thioredoxin-, His<sub>6</sub>- and

S-tagged Os9BGlu31 fusion protein with an enterokinase and TEV protease cleavage site (Luang et al., 2013; Komvongsa et al., 2015; Tran et al., 2019). The mutation of Os9BGlu31 based on W243L including variant H123E/W243L, Y313H/W243L, Y313Q/W243L, Y313S/W243L, E441T/W243L, and E441H/W243L were made in the same construct to give similar properties. The fusion proteins were expressed in *E. coli* strain Origami B(DE3). In the initial step, the fusion proteins were purified by IMAC. The 70 kDa thioredoxin and histidine-tagged Os9BGlu31 fusion proteins were eluted by imidazole and the eluents contained many impurities after the purification (1<sup>st</sup> IMAC, Figure 4.2). To remove impurity proteins, the proteins from 1<sup>st</sup> IMAC were then cleaved by TEV protease and the 50 kDa tag-free protein were further purified by a 2<sup>nd</sup> IMAC. The purity of the protein increased to greater than 95% for Os9BGlu31 wild type, W243L and W243N, as show in Figure 4.3.

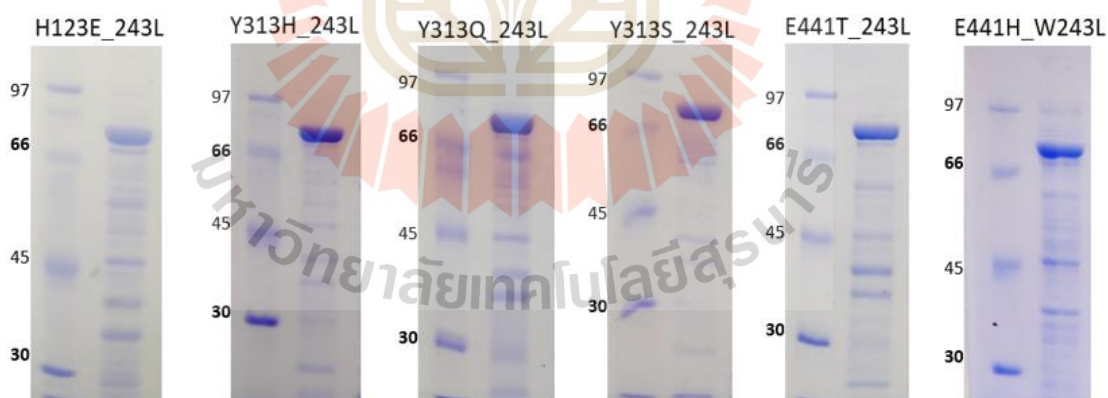


**Figure 4.2** Coomassie blue SDS-PAGE analysis of Os9BGlu31 variants H123E/W243L, Y313H/W243L, Y313Q/W243L, Y313S/W243L, E441T/W243L, and E441H/W243L with N-terminal thioredoxin/His6-tagged fusion protein after 1<sup>st</sup> IMAC.

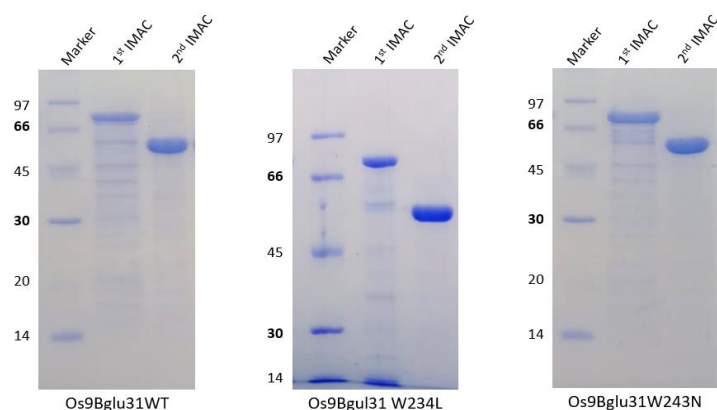


**Figure 4.3** Coomassie blue SDS-PAGE analysis of Os9BGlu31 wild type and its variants W243L and W243N throughout purification including marker, the N-terminal thioredoxin/His6-tagged fusion protein after 1<sup>st</sup> IMAC, and the purified protein after cleavage the tag with TEV protease with a 2<sup>nd</sup> IMAC.

#### 4.4 The activity of Os9BGlu31 variants on *p*NPGlc, cellobiose, and cellotriose

The hydrolysis and transglucosylation activities of Os9BGlu31 variants H123E/W243L, Y313H/W243L, Y313Q/W243L, Y313S/W243L, E441T/W243L, and E441H/W243L were tested on *p*NPGlc, cellobiose, and cellotriose as a glucosyl donor and ferulic acid as a glucosyl acceptor. Unfortunately, no activity could be detected in the reactions.

The previous studies had reported that rice BGlu1 residues H130, Y315, and E440 involve in binding with the nonreducing residue in the subsite -1 of cellotetraose and cellopentaose (Chuenchor et al., 2011; Pengthaisong et al., 2012), those residues correspond to Os9BGlu31 H123, Y313, and E441, respectively (Figure 4.4 and 4.5).

This suggested that the mutation of positions H123, Y313, and E441 may significantly impede binding with the substrates.

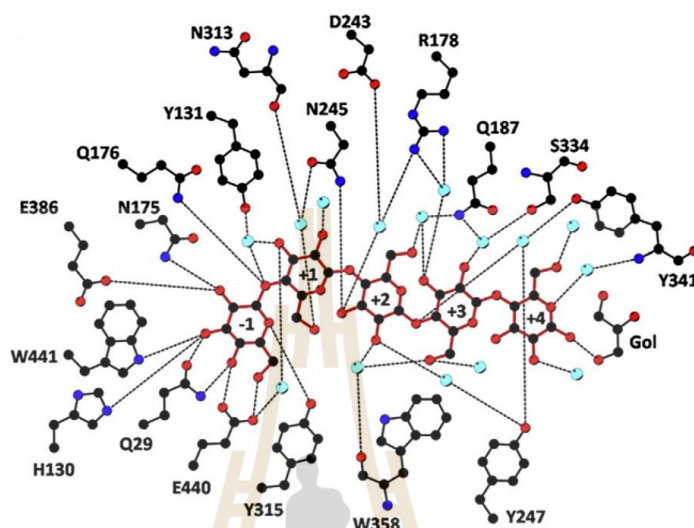


**Figure 4.4** Polar interactions in active site of the complex of the rice BGlucanase E176Q mutant with cellopentaose (Chuenchor et al., 2011).

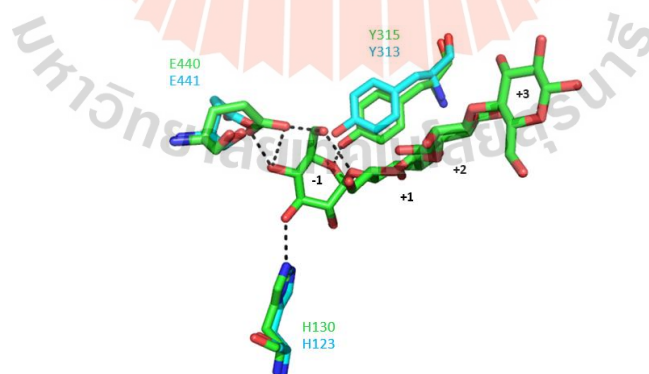


**Figure 4.5** Superposition of X-ray crystal structure of Os9BGlucanase31W243L on the X-ray crystal structure of the BGlucanase E386G-Y341A with cellopentaose (PDB: 3SCW). Os9BGlucanase31W243L is shown in cyan, while the BGlucanase E386G/Y341A is shown in green.



## 4.5 Transglucosylation of antibiotics and anticancer drugs by Os9BGlu31 variants

The transglucosylation activity of Os9BGlu31 variants were previously characterized for transferring the glucosyl molecule from the donor substrate *p*NPGlc to various acceptors, such as phenolic compounds and carboxylic acids (Luang et al., 2013; Komvongsa et al., 2015; Tran et al., 2019). Here we studied the transglucosylation by Os9BGlu31 and its variants with antibiotics, i.e. ampicillin, amoxicillin, cefixime, cefotaxime, chloramphenicol, kanamycin, streptomycin, tetracycline, and nybomycin, and the anticancer drugs doxorubicin and paclitaxel. The reactions of these medicinal compounds with Os9BGlu31 and its variants were qualified by UPLC. Among the tested acceptor substrates, only six acceptors were detected to be glycosylated, including chloramphenicol, nybomycin, ampicillin, amoxicillin, tetracycline, and anticancer doxorubicin.

The reaction mixture of chloramphenicol with *p*NPGlc catalyzed by Os9BGlu31 wild type and its variants W243H, W243K, W243N, and W243R were subjected to UPLC and the absorption was measure at 360 nm. The UPLC chromatograms are shown in Figure 4.6. Based on the chromatograms, Os9BGlu31 W243N exhibited the highest activity. Chloramphenicol contains one primary and one secondary alcohol that can be glycosylated, but the primary hydroxyl is most amenable to glycosylation. Because the primary alcohol is more potent as a nucleophile than the secondary alcohol when considering steric hindrance, since the bulk of methyl groups on secondary alcohols effectively blocks the way of attack by the nucleophilic oxygen, as shown in Figure 4.7. Chloramphenicol glucoside was produced, purified, and characterized using NMR analysis, as described in Section 4.5.1.



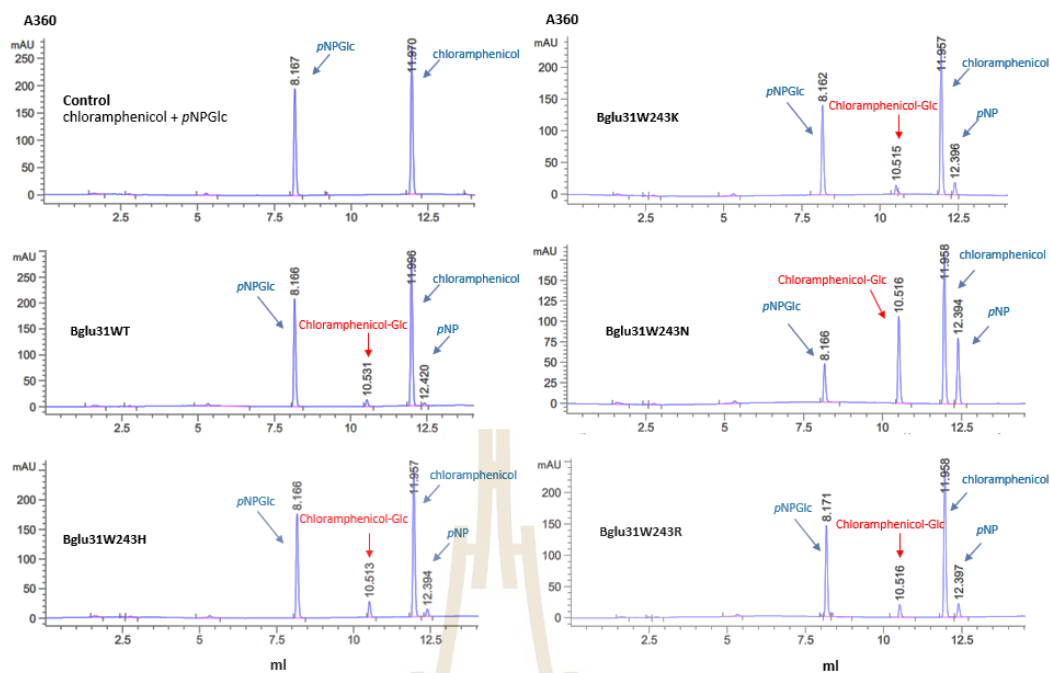


**Figure 4.6** UPLC Chromatograms of reaction of Os9BGlu31 wild type and its W243H, W243K, W243N, and W243R variants with chloramphenicol acceptor monitored at 360 nm.

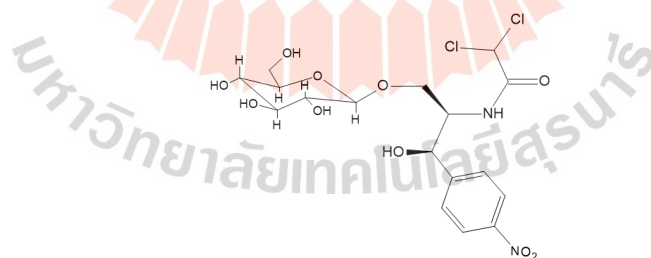


**Figure 4.7** Chemical structure of chloramphenicol glucoside.

A reaction mixture of a nybomycin with *p*NPGlc catalyzed by Os9BGlu31 wild type and its variants W243L and W243N were subjected to UHPLC and the absorption was measured at 360 nm. The UPLC chromatograms are shown below in Figure 4.8.

Based on the chromatograms, Os9BGlu31 W243N exhibited highest activity. The product was not completely characterized using NMR but the product was tentatively identified as nybomycin glucoside based on the UPLC results and based on the structure of nybomycin, there is only one -OH, which is a primary alcohol, that can be glycosylated, as shown in Figure 4.9.

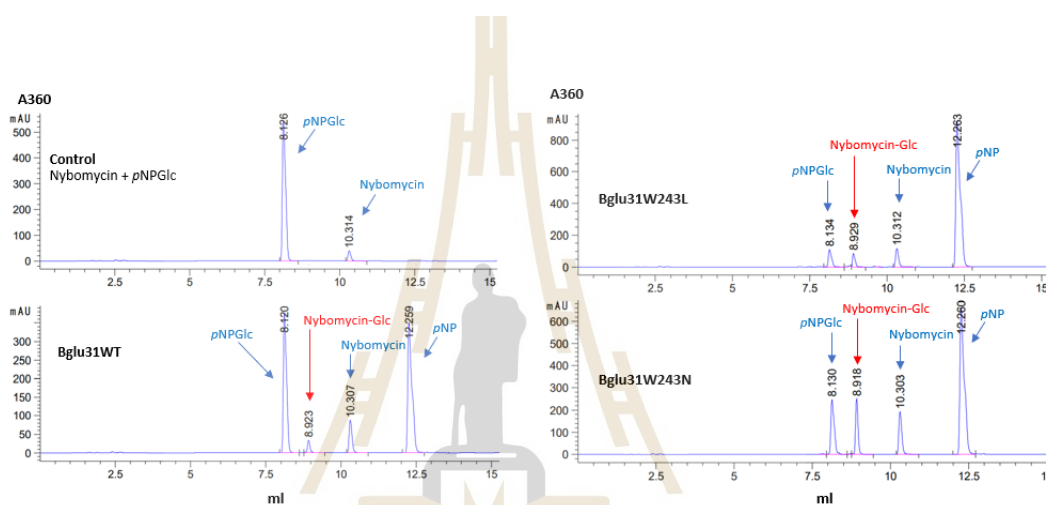


**Figure 4.8** UPLC Chromatograms of transglycosylation reaction of nybomycin catalyzed by Os9BGlu31 wild type and its W243L and W243N variants.

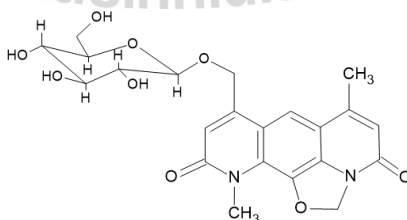


**Figure 4.9** Plausible structure of nybomycin glucoside.

The mixtures from reactions of ampicillin with *p*NPGlc catalyzed by Os9BGlu31 wild type and its variants W243L and W243N were subjected to UPLC and the absorption was measured at 360 nm. The UPLC chromatograms are shown below in Figure 4.10. Based on the chromatograms, there is no significantly different activity between wild type and variant enzyme. The product was not completely characterized using NMR, but the product was tentatively identified as ampicillin glucoside based on the UPLC results and based on the structure of ampicillin, which has only one carboxyl group that can be glycosylated, as shown in Figure 4.11.

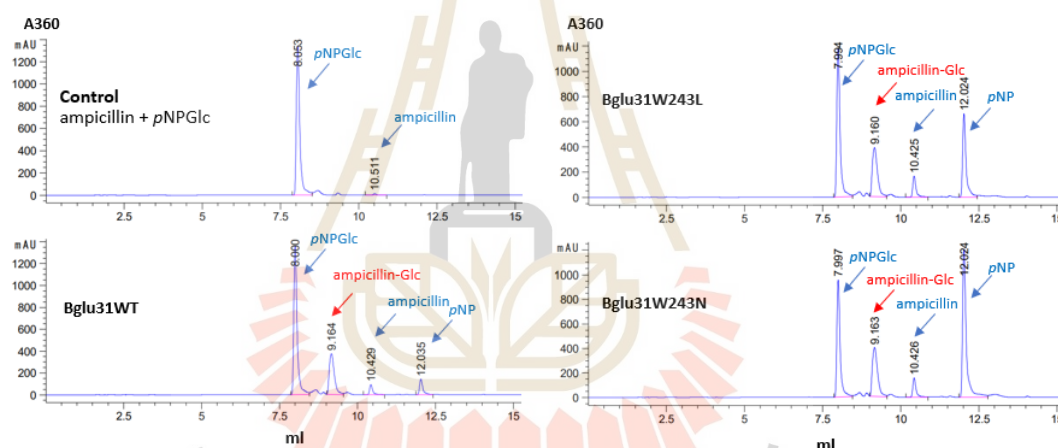


**Figure 4.10** UPLC Chromatograms of transglycosylation reactions of ampicillin catalyzed by Os9BGlu31 wild type and its W243L and W243N variants.

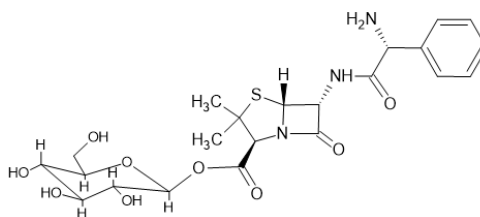


**Figure 4.11** Plausible structure of ampicillin glucoside.

The mixtures from reaction of amoxicillin with *p*NPGlc catalyzed by Os9BGlu31 wild type and its W243L variant were subjected to UPLC and the absorption was measured at 360 nm. The UPLC chromatograms are shown below in Figure 4.12. Based on the chromatograms, the W243L variant showed higher activity than wild type enzyme. Unusually, the new peak of glycoside product had a longer retention time than the amoxicillin peak. The product was not characterized but the product was tentatively identified as amoxicillin glucoside. From the structure of ampicillin, there are two positions that could be glycosylated either the carboxyl group, as shown in Figure 4.13A, or the phenol group hydroxyl, as shown in Figure 4.13B.

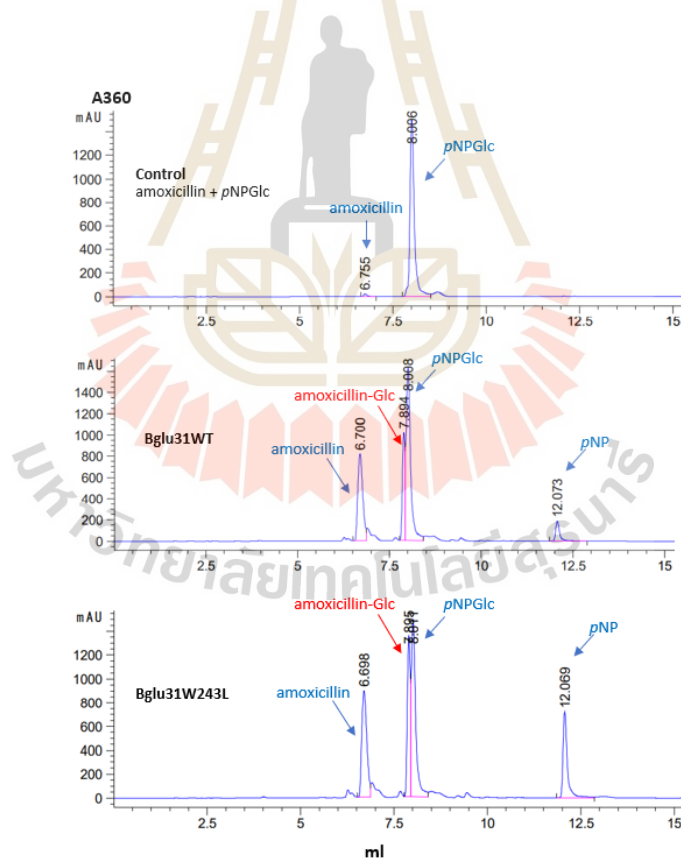


**Figure 4.12** UPLC Chromatograms of reaction of Os9BGlu31 wild type and its W243L variants with amoxicillin.

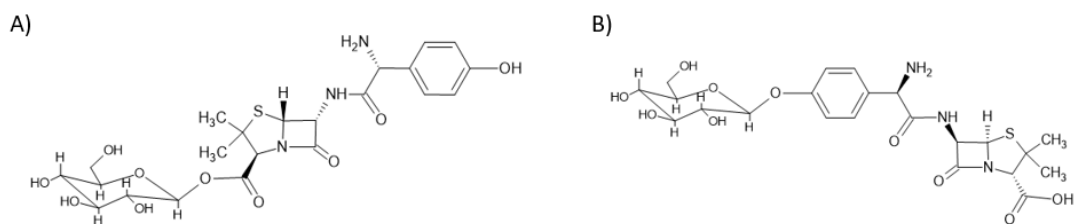


**Figure 4.13** Plausible structures of amoxicillin glucoside. A) Glucose ester; B) Phenolic glucoside.

The product mixtures from reactions of tetracycline with *p*NPGlc by Os9BGlu31 wild type and its variants W243L and W243N were subjected to UPLC and the absorption was measured at 360 nm. The UPLC chromatograms are shown below in Figure 4.14. Based on the chromatograms, there is no significantly different activity between wild type and variant enzymes. The product was not completely characterized using NMR but the product was tentatively identified as tetracycline glucoside based on UHPLC results. The structure of tetracycline has several -OH groups, but the position at the phenol group -OH is most likely to be glycosylated, since it looks less crowded, so that it can more easily get into the active site of the enzyme, as shown in Figure 4.15.

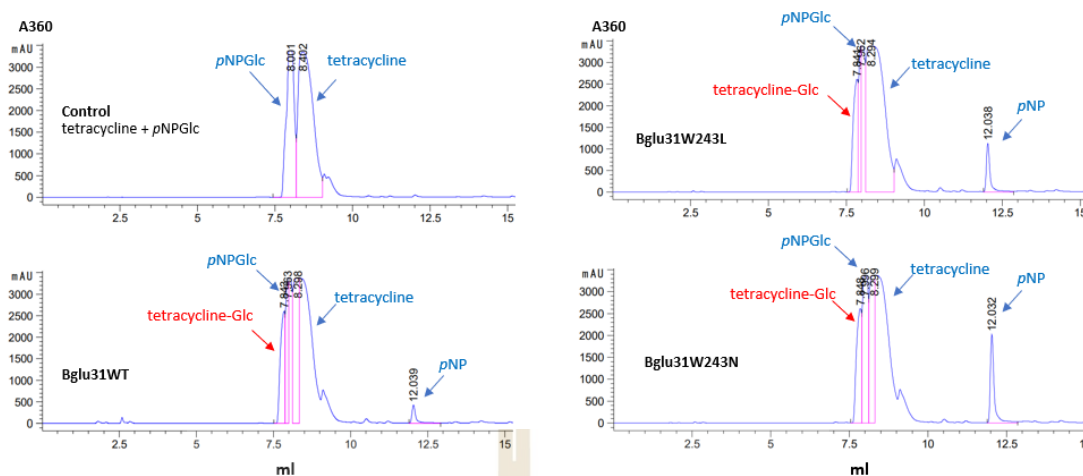


**Figure 4.14** UPLC Chromatograms of transglycosylation reaction of tetracycline catalyzed by Os9BGlu31 wild type and its W243L and W243N variants.

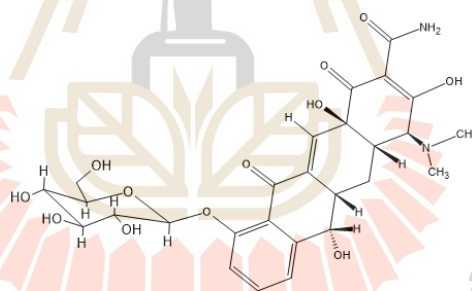


**Figure 4.15** Plausible structure of tetracycline glucoside

The mixtures from reaction of doxorubicin with *p*NPGlc catalyzed by Os9BGlu31 wild type and its variants W243L and W243N were subjected to UPLC with detection by absorption at 360 and 540 nm. The UPLC chromatograms are shown below in Figure 4.16. Based on the chromatograms, Os9BGlu31 W243N exhibited highest activity. The product was not completely characterized by NMR, but the product was

tentatively identified as doxorubicin glucoside, based on UPLC results and the structure of doxorubicin, it is likely that the primary alcohol could be glycosylated, as shown in Figure 4.17.

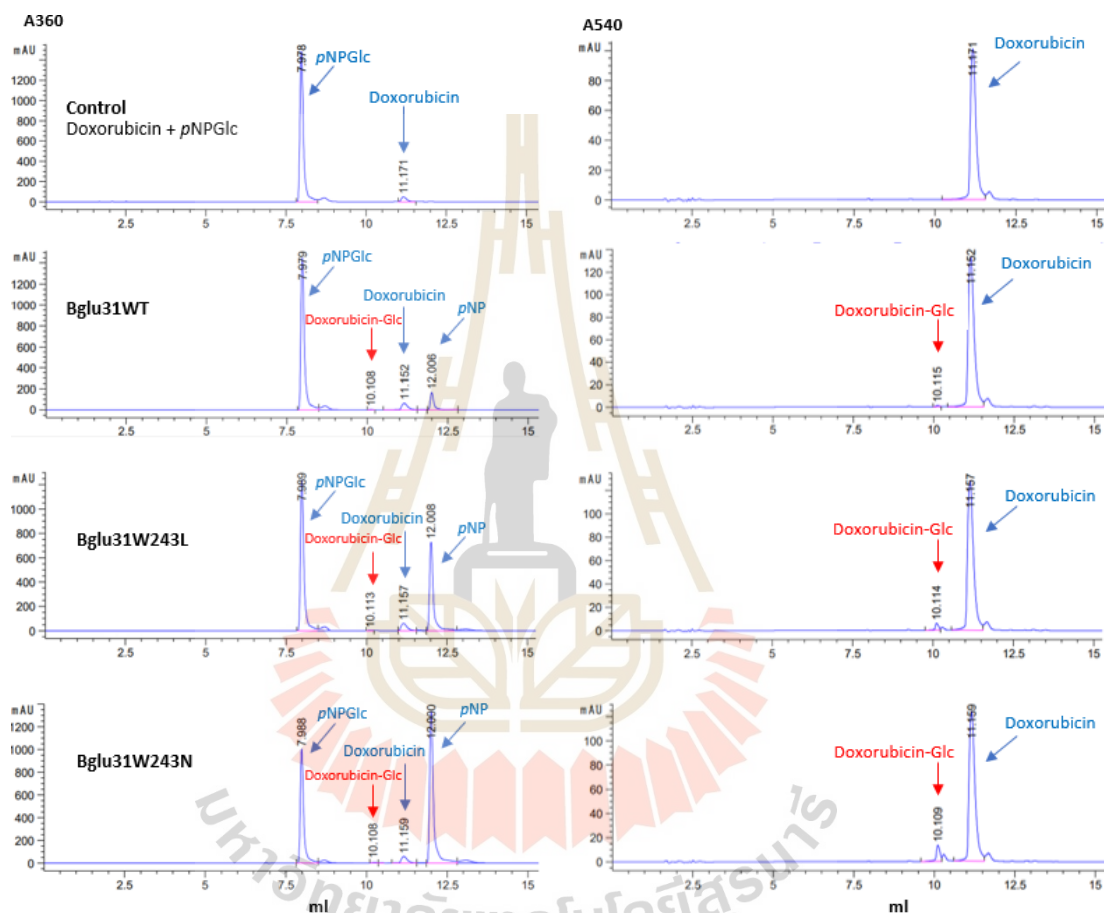


**Figure 4.16** UPLC Chromatograms of reactions of Os9BGlu31 wild type and its W243L and W243N variants with doxorubicin and pNPGlc.



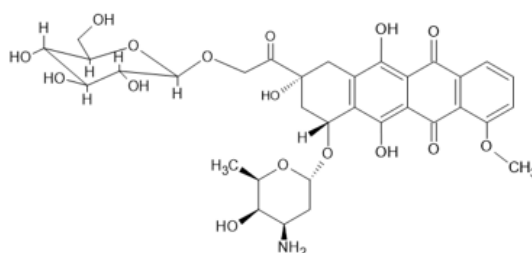


**Figure 4.17** Plausible structure of doxorubicin glucoside.

#### 4.5.1 Chloramphenicol glucoside purification

The transglucosylation of chloramphenicol was performed with Os9BGlu31 W243N as catalyst. The first step of the purification was silica gel column chromatography to eliminate *p*-nitrophenol and glucose. The mixture of *p*NPGlc and chloramphenicol glucoside was collected together, since the polarities of both glycosides are very close. The mixture was further purified by C18 reverse phase chromatography, which is able to separate the two glucosides (Figure 4.18).

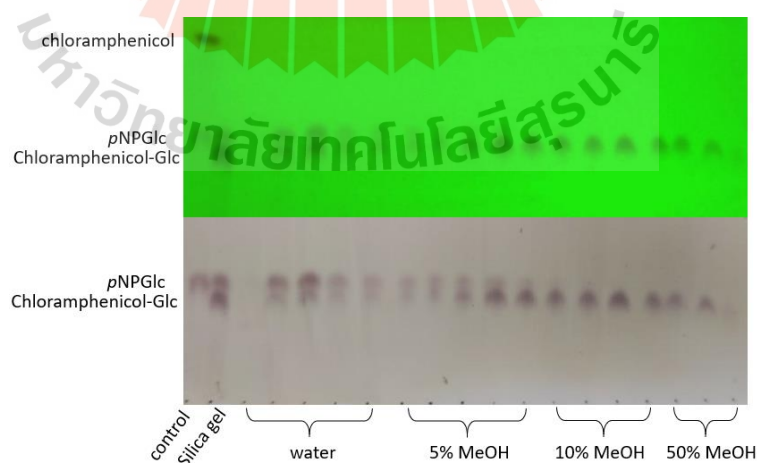


**Figure 4.18** TLC analysis of chloramphenicol glucoside purification by reverse phase chromatography on C18 resin. Fractions are marked by the solvents in which they eluted.

#### 4.5.2 Chloramphenicol glucoside structural confirmation

The purified chloramphenicol glucoside had a  $R_f = 0.45$  (silica gel TLC with  $\text{CHCl}_3$ : MeOH 4:1 v/v as solvent). The NMR spectra showed the following peaks:  $^1\text{H}$  NMR ( $\text{D}_2\text{O}$ , 500 MHz):  $\delta$  8.23 (d,  $J = 8.5\text{Hz}$ , 2H), 7.63 (d,  $J = 8.5\text{Hz}$ , 2H), 6.22 (s, 1H), 5.21 (d,  $J = 3.5\text{Hz}$ , 1H), 4.45 (d,  $J = 8\text{Hz}$ , 1H), 4.40-4.37 (m, 1H), 4.15 (dd,  $J = 5.5, 11\text{Hz}$ , 1H), 3.90 (dd,  $J = 2, 12.5\text{Hz}$ , 1H), 3.80 (dd,  $J = 7.5, 11\text{Hz}$ , 1H), 3.67 (dd,  $J = 6, 12.5\text{Hz}$ , 1H), 3.49-3.42 (m, 2H), 3.36 (appt,  $J = 9.5\text{Hz}$ , 1H), 3.28 (appt,  $J = 8.5\text{Hz}$ , 1H);  $^{13}\text{C}$  NMR ( $\text{D}_2\text{O}$ , 125 MHz)  $\delta$  166.8, 148.3, 147.1, 127.1, 123.6, 102.8, 75.9, 75.5, 72.9, 70.9, 69.6, 68.9, 65.9, 60.7, and 55.4 ppm.

The anomeric protons coupling constant value was 8 Hz at a chemical shift of 4.45 ppm (Figure 4.19), and anomeric carbon had a chemical shift of 102.8 ppm (Figure 4.20), which suggest the anomeric glycosidic linkage displays the expected  $\beta$ -configuration as the chemical structure of chloramphenicol glucoside shown in Figure 4.19 and 4.20.

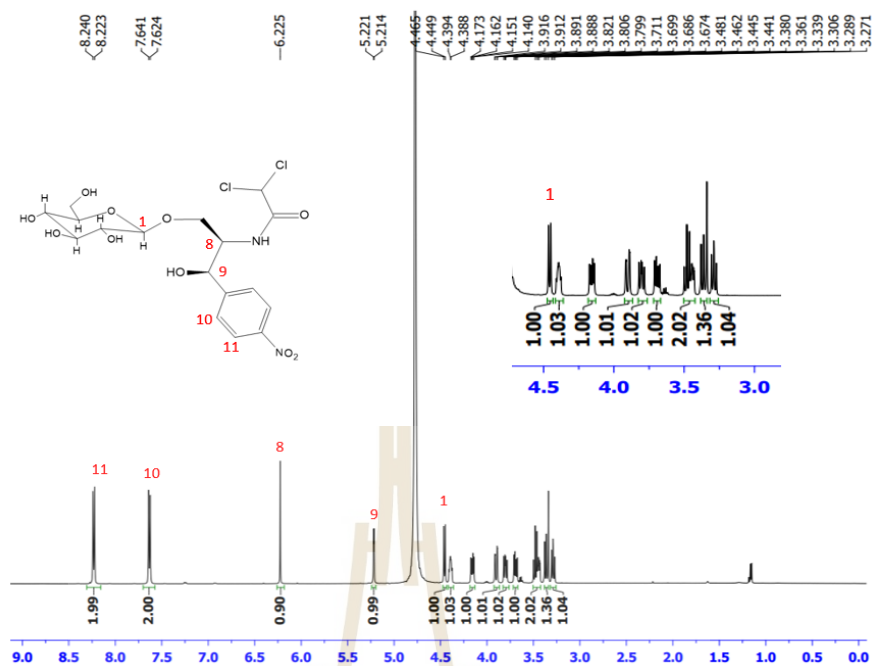


**Figure 4.19** <sup>1</sup>H-NMR spectrum of chloramphenicol glucoside.

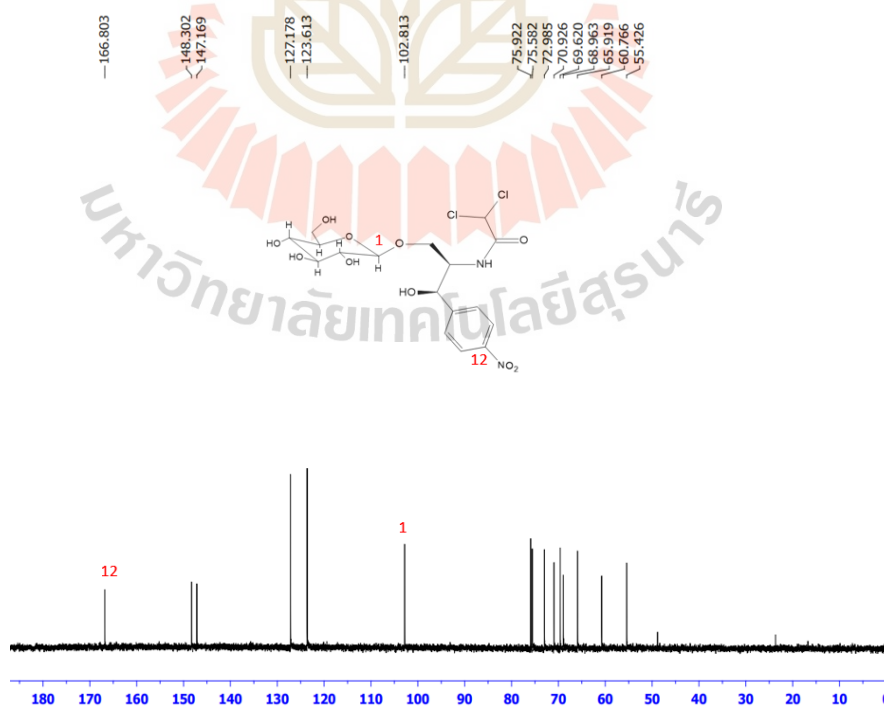


**Figure 4.20** <sup>13</sup>C-NMR spectrum of chloramphenicol glucoside.

## 4.6 Sequence analysis of OsExo1 and OsExo2

The protein-sequence-similarity based phylogenetic tree of higher plant GH3 enzymes shows a topology with two distinct groups (Figure 2.6). One group contains the  $\beta$ -D-glucan glucohydrolases-like enzymes, while the second group contains  $\beta$ -D-xylosidase-like enzymes, which also include enzymes with  $\alpha$ -L-arabinosidase or combined  $\beta$ -D-xylosidase and  $\alpha$ -L-arabinosidase activities (Lee et al., 2003). Six proteins encoded by rice GH3 genes are located in the  $\beta$ -D-glucan glucohydrolases-like enzymes group that includes *H. vulgare* exoglucanase 1 (HvExo1) and exoglucanase 2 (HvExo2). The sequence most similar to HvExo1 was designated OsExo1, while that most similar to HvExo2 was named OsExo2 (Prawisut et al., 2021). A third enzyme more similar to a *Z. mays* exoglucanase was designated OsExo3.

The alignment of OsExoI, OsExoII, barley HvExoI and HvExoII, along with the characterized maize GH3 enzyme are shown in Figure 4.21. As can be seen, the enzyme sequences are highly conserved within this group of plant enzymes and the catalytic nucleophile and acid/base (indicated by triangles) can clearly be identified based on their characterization in HvExoI. Glycosylation sites in OsExoI were predicted by NetNGlyc (Blom et al., 2004), with predicted to be glycosylated at Asn210, Asn322 and Asn520.

Homology model structures of OsExo1 and OsExo2 were predicted by SWISS-MODEL (Waterhouse et al., 2018), based on the X-ray crystal structure of the HvExo1 in complex with 4-deoxy-glucose (PDB: 3WLK). The protein models shown high similarity of overall structure and location of catalytic residues as shown in Figure 4.22 and 4.23.

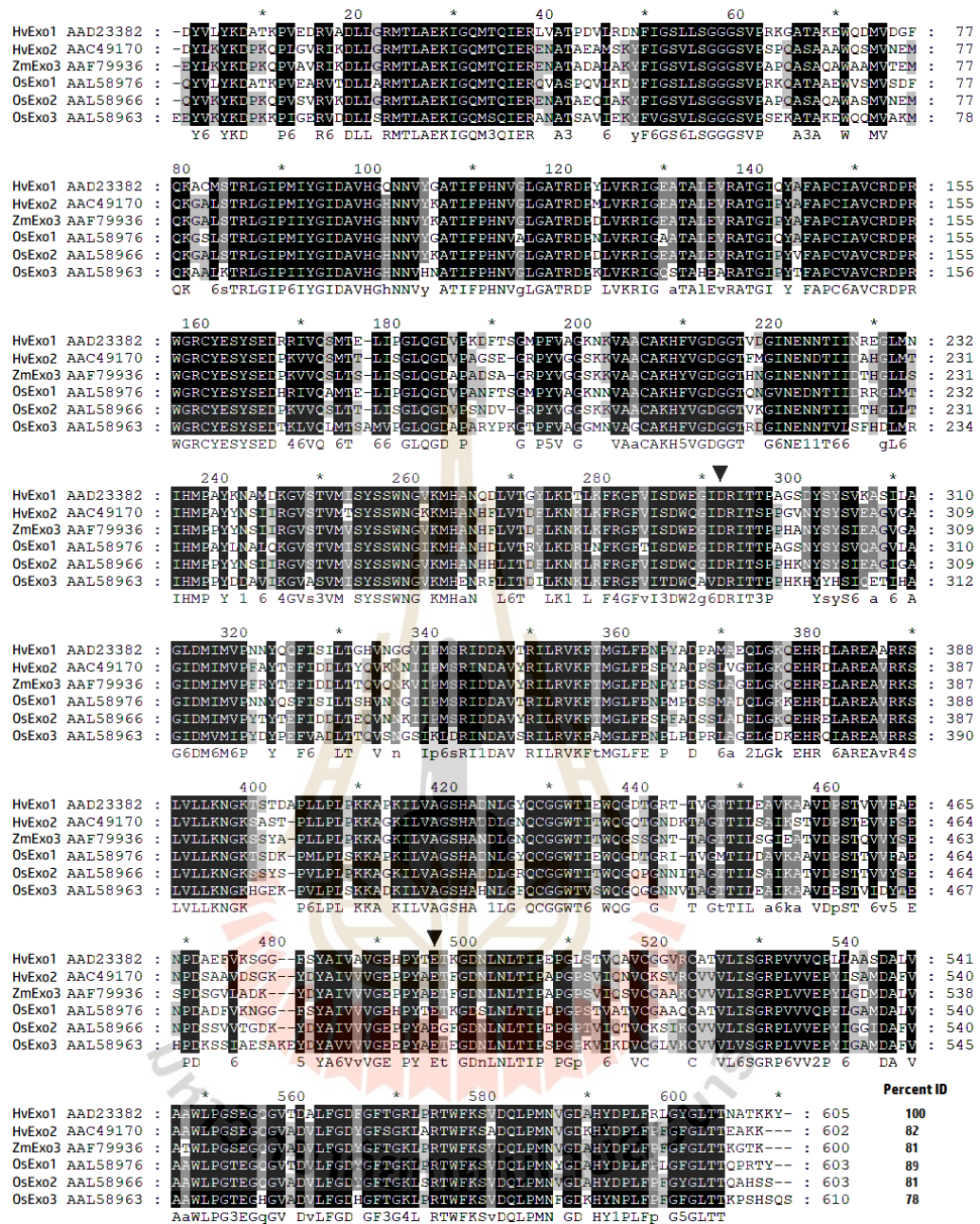


**Figure 4.21** Alignment of HvExo1 with HvExo2, ZmExo3, OsExo1, OsExo2, and OsExo3. The mature protein sequences, shown with their NCBI Genbank accession numbers, Conserved residues are shaded, with black background for completely conserved sites. The consensus sequence is displayed below each section, and overall percent identity with HvExo1 is shown at the end. Triangles mark the positions of the catalytic nucleophile, D285 in HvExo1, D313 in OsExo1, and D311 in OsExo2 and acid/base, E491 in HvExo1, E513 in OsExo1, and E512 in OsExo2.



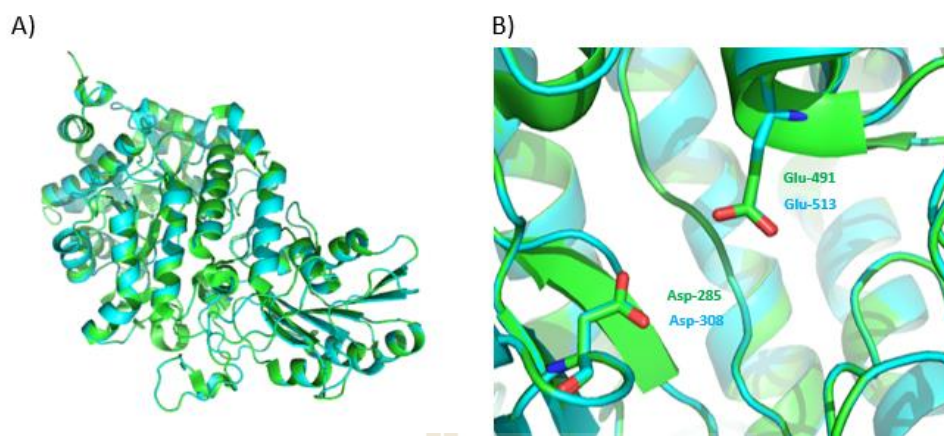


**Figure 4.22** Superposition of a homology model of OsExo1 on the X-ray crystal structure of the HvExo1 (PDB: 3WLK). OsExo1 is shown in cyan, while the HvExo1 is shown in green. A) Cartoon representation of the overall structure, B) active site with the catalytic nucleophile and acid/base side chains represented as sticks.

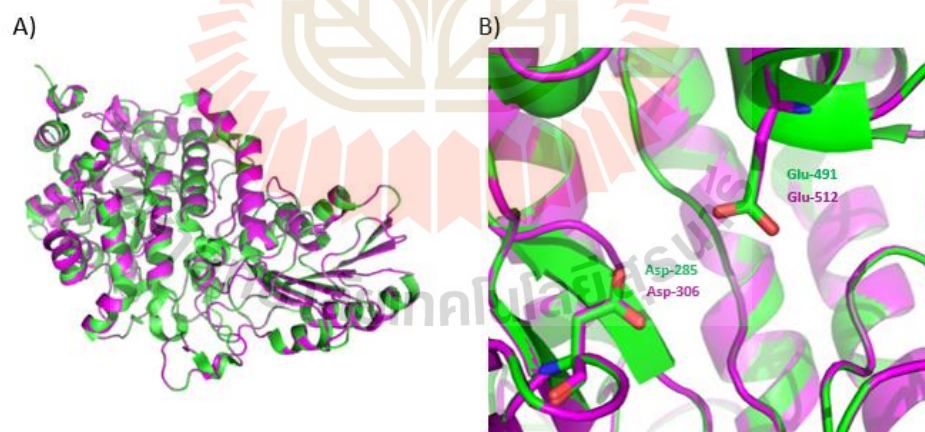


**Figure 4.23** Superposition of a homology model of OsExo2 on the X-ray crystal structure of the HvExo1 (PDB: 3WLK). OsExo2 is shown in purple, while the HvExo1 is shown in green. A) Cartoon representation of the overall structure, B) active site with the catalytic nucleophile and acid/base side chains represented as sticks.

## 4.7 Expression and purification of OsExo1

OsExo1 was expressed in *P. pastoris* SMD1168H and purified from the culture broth by IMAC on resin charged with Ni<sup>2+</sup>. The protein was separated into 2 portions, one was purified by SEC. Another was digested by endoglycosidase H before purified by SEC. From SEC result, the OsExoI was found to be glycosylated at different levels (Appendix A, Figure A.1 and A.2), and most of the carbohydrate could be removed by digestion with endoglycosidase H (Appendix A, Figure A.3) (Figure 4.24). The high glycosylation form was found to have highest specific activity at 17.81 units mg<sup>-1</sup> (Table 4.2), while the deglycosylated form had a specific activity of 9.47 units mg<sup>-1</sup>, equivalent to that of the medium glycosylation pool of enzyme.

**Table 4.2** Enzyme yields during purification of OsExo1.

Purification step	Yield		Specific activity	Purification factor	Recovery (%)
	Protein	Activity			
	(mg)	(units)	(units mg <sup>-1</sup> )	(fold)	
Crude protein	19200	84.5	0.004	1	100.00
IMAC	1.60	8.87	5.55	1260	10.50
SEC					
- high glycosylated	0.14	2.56	17.81	4047	3.04
- medium glycosylated	0.40	3.90	9.76	2218	4.62
- low glycosylated	0.40	1.61	4.02	913	1.9



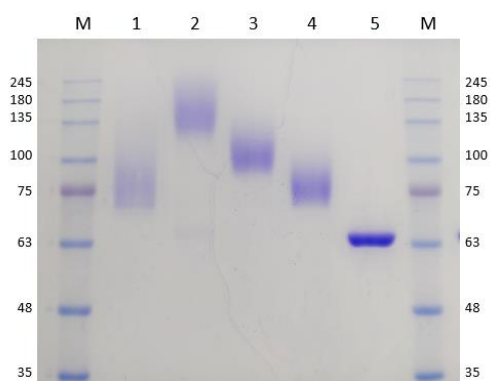


**Figure 4.24** Coomassie blue SDS-PAGE analysis of OsExo1 purification. Lane M, protein marker; Lane 1, purified protein by IMAC; Lane 2, - 4, purified protein after SEC; Lane 5, purified protein after deglycosylation with endoglycosidase H and SEC.

#### 4.8 Expression and purification of OsExo2

The recombinant OsExo2 was expressed in *E. coli* Origami B(DE3) by auto-induction medium (AIM) (Prawisut et al., 2020). The protein was purified with 3 steps. First, crude protein was immediately loaded into IMAC with  $\text{Ni}^{2+}$ . The fractions were assayed for hydrolysis of *p*NPGlc (Appendix A, Figure A.4 and A.5). The pool of active fractions was concentrated and then purified further by SEC (Appendix A, Figure A.6 and A.7). Next, the protein was loaded onto a phenyl Sepharose column (HIC) and the protein was separated into 2 fractions eluted by low ethylene glycol concentration (HIC1) and high ethylene glycol concentration (HIC2). Finally, protein fractions containing *p*NPGlc hydrolysis activity were assessed by SDS-PAGE (Figure 4.25). During the purification of OsExo2, it was apparent that the activity dropped when ethylene glycol from the HIC purification was removed. Therefore, we tested the effect of ethylene glycol on the enzymatic activity, the activity increased with increasing ethylene glycol concentration (Appendix A, Figure A.8 and A.9).

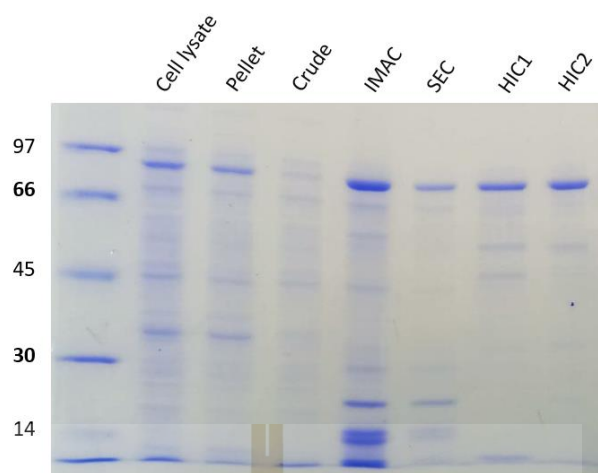


**Figure 4.25** Coomassie blue SDS-PAGE analysis of OsExo2 purification. Lane M, protein markers; Pellet is the insoluble fraction of the bacterial cells from the expression, Crude is the soluble fraction extracted from those cells, IMAC, HIC and SEC.

**Table 4.3** Enzyme yields during purification of OsExo2.

Purification step	Yield		Specific activity (units mg <sup>-1</sup> )	Purification factor (fold)	Recovery (%)
	Protein (mg)	Activity (units)			
Crude protein	8096	7.51	0.000927	1	100.00
IMAC Flow through	7200	2.54	0.000352	0.380	33.80
IMAC elution	12.0	1.29	0.107	116	17.10
SEC	2.92	0.417	0.143	154	5.55
HIC1	0.176	0.119	0.679	732	1.59
HIC2	0.0406	0.0805	1.980	2140	1.07

#### **4.9 Effect of the optimal pH and temperature and temperature stability for OsExo1 N-deglycosylated form**

The pH optimum and activity profile of the N-deglycosylated OsExo1 form (Figure 4.26) was similar to that of the glycosylated OsExo1 for, OsExo2 expressed in *E. coli*, and rHvExo1 (glycosylated and N-deglycosylated forms) (Luang et al., 2010), which showed bell-shaped activity versus pH curves, and highest activities detected at pH 5.0. The temperature optimum for the glycosylated OsExo1 enzyme was 45 °C (Figure 4.27), but >80% maximal activity was seen from 35-50 °C. The temperature optimum at 45 °C may indicate the stability of the substrate-enzyme and energy of the transition state complex, rather than the stability of the enzyme itself. The temperature stability of OsExo1 N-deglycosylated was similar to that of glycosylated OsExo1, OsExo2 and the N-deglycosylated rHvExo1 (Prawisut et al., 2020; Prawisut, 2018; and Luang et al., 2010), which were stable in the range between 0 and 40 °C (Figure 4.28), while the temperature stability of glycosylated rHvExo1 was stable only at the temperature range between 10 and 20 °C. These results of the deglycosylated OsExo1 were different from the report of *Aspergillus kawachii*  $\alpha$ -L-arabinosidase, for which the N-glycosylation of asparagine in the catalytic domain increased the thermostability of the enzyme (Koseki et al., 2006). Since OsExo1 (glycosylated and N-deglycosylated forms) and OsExo2 were stable at 0 - 40 °C for 15 minutes, glycosylation does not seem to be critical for stability of the rice isoenzymes.

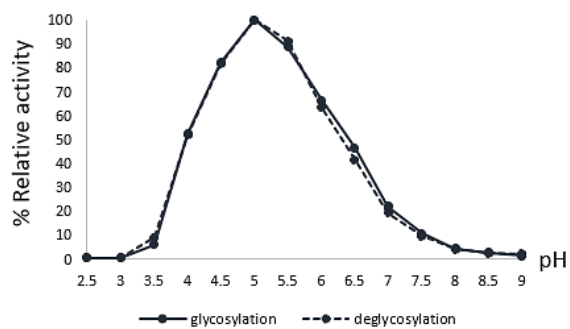


**Figure 4.26** Optimal pH profiles of glycosylated and deglycosylated OsExo1 forms.

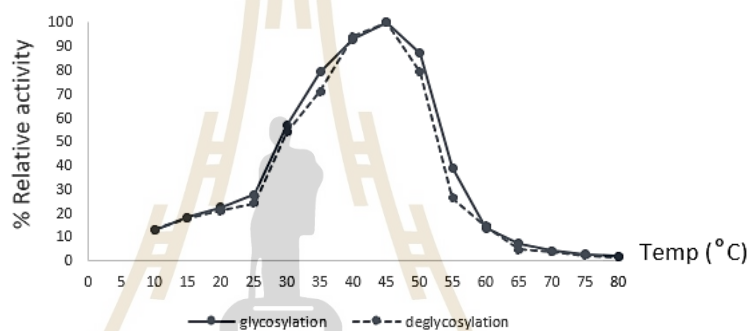


**Figure 4.27** Optimal temperature profiles of glycosylated and deglycosylated OsExo1.

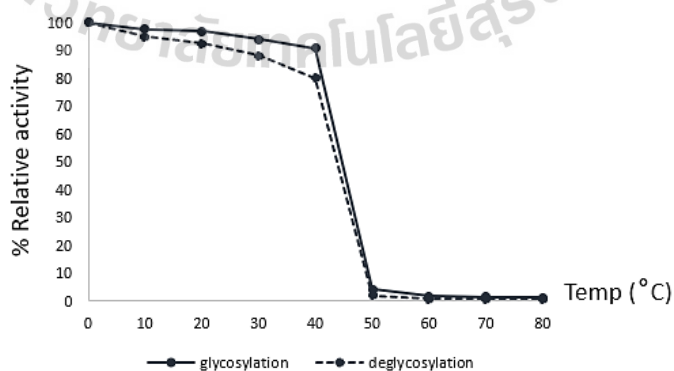


**Figure 4.28** Thermostability profile of OsExo1 glycosylated and deglycosylated forms.

#### 4.10 Kinetic parameters of OsExo1

The kinetic parameters for hydrolysis of *p*NPGlc, laminaribiose, and laminarin were determined for both glycosylated and N-deglycosylated forms (Table 4.4). Both forms were highly active on laminaribiose, and laminarin, for which the specificity constants ( $k_{\text{cat}}/K_M$ ) were about 4-fold higher than that for *p*NPGlc.

**Table 4.4** Kinetic parameters for OsExoI hydrolysis of *p*NPGlc, laminaribiose, and laminarin substrates.

Substrate	Glycosylation	Deglycosylation
<b><i>p</i>NPGlc</b>		
$K_M$ (mM)	0.66±0.018	0.62±0.016
$k_{\text{cat}}$ (s <sup>-1</sup> )	74.77±0.46	97.86±0.58
$k_{\text{cat}}/K_M$ (mM <sup>-1</sup> s <sup>-1</sup> )	113	157
<b>Laminaribiose</b>		
$K_M$ (mM)	0.156±0.018	0.156±0.014
$k_{\text{cat}}$ (s <sup>-1</sup> )	69.67±2.26	87.20±2.19
$k_{\text{cat}}/K_M$ (mM <sup>-1</sup> s <sup>-1</sup> )	446	546
<b>Laminarin</b>		
$K_M$ (mM)	0.124±0.01	0.125±0.01
$k_{\text{cat}}$ (s <sup>-1</sup> )	54.2±1.3	74.99±0.29
$k_{\text{cat}}/K_M$ (mM <sup>-1</sup> s <sup>-1</sup> )	438	602

#### 4.11 Transglucosylation activity of OsExo1 and OsExo2

The transglucosylation activities of OsExo1 and OsExo2 were tested with *p*NP<sub>Glc</sub>, oligosaccharides, and polysaccharides as glucosyl donors and a series of alcohols as glucosyl acceptors.

The transglucosylation activities toward *p*NP<sub>Glc</sub> by OsExo1 (glycosylated and N-deglycosylated forms) and OsExo2 were observed at various times. During the initial stages of the reaction at 5 min, a small amount of glucose was observed, in addition to 3 products of *p*NP-oligosaccharides. As the reaction progressed, in 30 minutes - 6 hours reaction, the transient transglucosylation products *p*NP-oligosaccharides and oligosaccharides were detected. By 12 hours, the *p*NP-oligosaccharides and oligosaccharides were hydrolyzed, and only the major hydrolytic product glucose was observable (Figure 4.29 and Figure 4.30). This transient production of transglucosylation products is similar to previous work from Luang et al., 2010 on HvExo1.

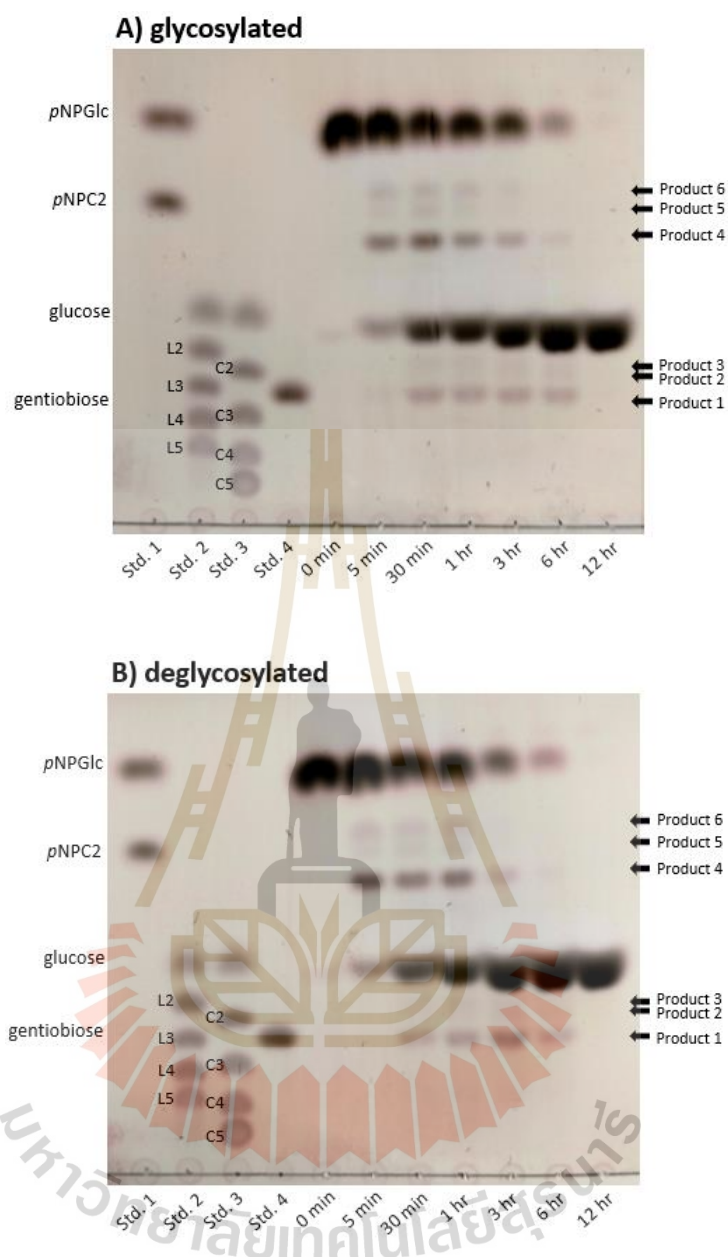


**Figure 4.29** TLC analysis of the transglucosylation of *pNPGlc* by *OsExo1*. A) glycosylated, B) deglycosylated enzyme. Standards contain *pNPGlc* and *pNP*-cellobiose (std. 1), glucose and L2-L5 (std. 2), glucose and C2-C5 (std. 3), and gentiobiose (std. 4). The presence of reaction products with unknown structures are indicated as Product 1–6. The reaction times are indicated in hours below the lanes.



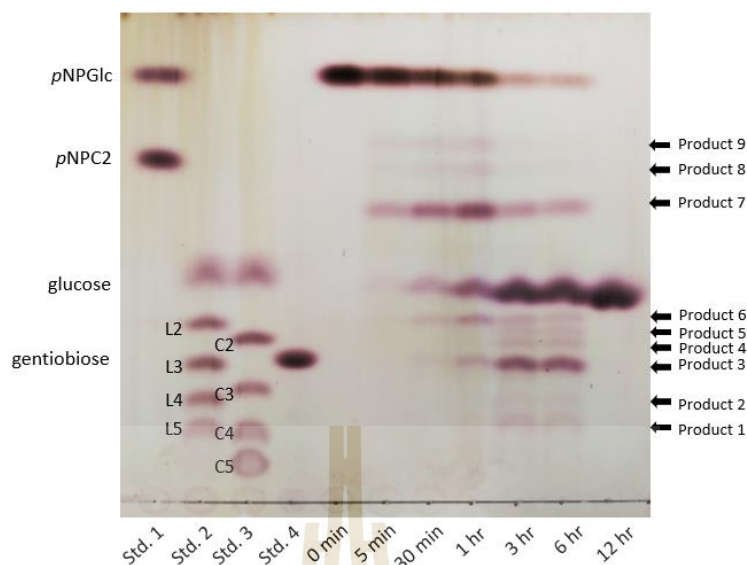


**Figure 4.30** TLC analysis of the transglucosylation of *p*NPGlc by OsExo2. Standards contain *p*NPGlc and *p*NP-cellobiose (std. 1), glucose and L2-L5 (std. 2), glucose and C2-C5 (std. 3), and gentiobiose (std. 4). The reaction products with unknown structures are indicated as Product 1–9. The reaction times are indicated below the lanes.

During the HIC purification of OsExo2, it was apparent that the activity increased when increasing ethylene glycol concentration. Therefore, we tested the transglucosylation activity by using *p*NPGlc as a glucosyl donor substrate, while ethylene glycol was used as a glucosyl acceptor substrate and visualized by TLC. The new spot can be seen between the positions of *p*NPGlc and glucose, consistent with an ethylene glycol glucoside product. From this result, we tested the transglucosylation activity toward various alcohols, including methanol, ethanol, *n*-propanol, isopropanol, 1-butanol, 3-methyl-1-butanol, octanol, glycerol, propargyl alcohol, 4-hydroxybenzyl alcohol, and  $\beta$ -mercaptoethanol. OsExo1 (glycosylated and deglycosylated forms) and OsExo2 can transfer glucosyl moieties from *p*NPGlc to methanol, ethanol, *n*-propanol, butanol, 3-

methyl-1-butanol, ethylene glycol, propargyl alcohol, 4-hydroxybenzyl alcohol, and  $\beta$ -mercaptoethanol, as show in Figures 4.31 – 4.33 but not to isopropanol, glycerol, and octanol. These results suggest that OsExo1 and OsExo2 transfer glucose only to primary hydroxyls of short-chain alcohols. The glucoside products were produced by OsExo2, purified, and characterized by NMR analysis as described in Section 4.11.

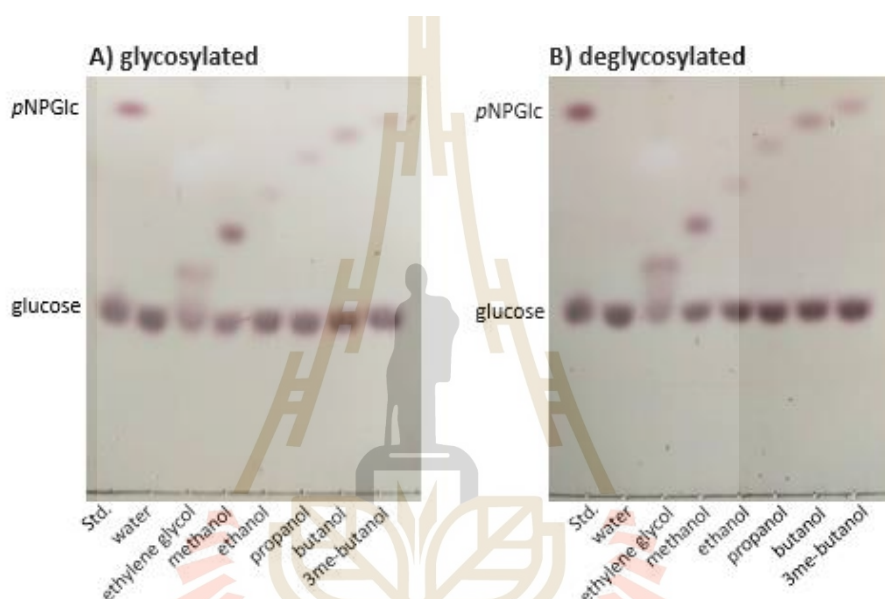


**Figure 4.31** TLC analysis of the transglucosylation by OsExo1. A) glycosylated, B) deglycosylated enzyme from *pNPGlc* to alcohols, including ethylene glycol, methanol, ethanol, propanol, butanol, and 3-methyl-1-butanol and water as a control reaction. Standards contain glucose and *pNPGlc* (std.).

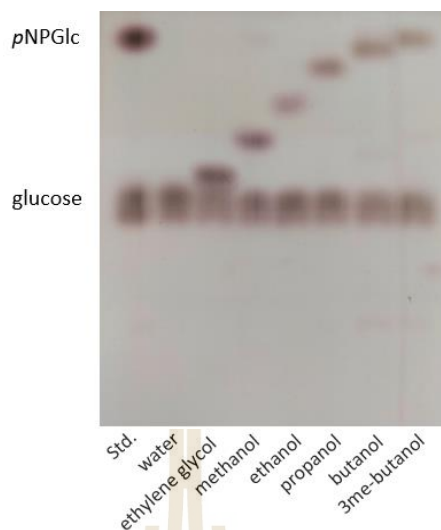


**Figure 4.32** TLC analysis of the transglucosylation by OsExo2 from *p*NPGlc to alcohols, including ethylene glycol, methanol, ethanol, propanol, butanol, and 3-methyl butanol and water as a control reaction. The standard contained glucose and *p*NPGlc (Std.).

Due to OsExo1 and OsExo2 having high activity toward  $\beta$ -1,3- and  $\beta$ -1,4-linked gluco-oligosaccharides and polysaccharides (Prawisut, 2018), which is similar the HvExo1 and HvExo2 (Hrmova et al., 1996; Hrmova and Fincher, 1998), different glucosyl donor substrates were tested on the transglucosylation activity. As shown in Figure 4.33, the spots of new products can be seen in similar positions between 2 glucosyl donors, *p*NPGlc and cellobiose. To test other glucosyl donor substrates, methanol was used as a glucosyl donor with cello-oligosaccharides (C2-C5), laminari-oligosaccharides (L2-L5), and polysaccharides laminarin, barley glucan, and lichenan. As shown in Figures 4.34 - 4.37, C2-C5, L2-L5, laminarin, barley glucan, and lichenan can act as glucosyl donors for OsExo1 and OsExo2. The enzyme N-glycosylation does not seem to have a significant effect on the transglucosylation activity of the rice exoglucanases.

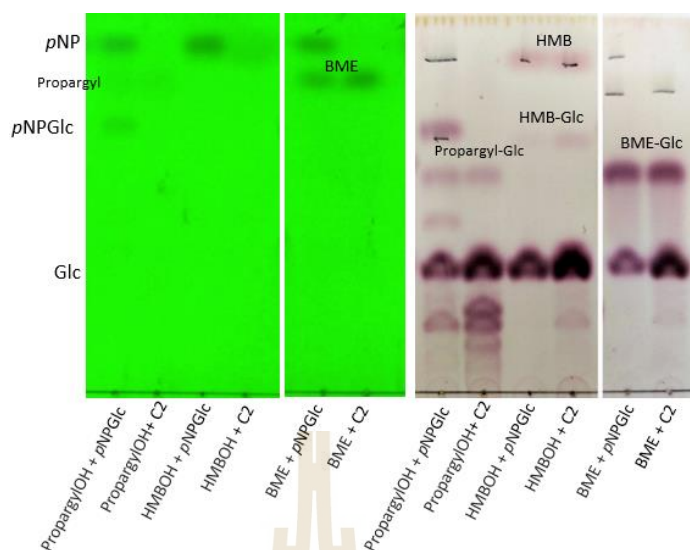


**Figure 4.33** TLC analysis of the transglucosylation of alcohols by OsExo2 with *p*NPGlc and cellobiose donors. The acceptors included propargyl alcohol, 4-hydroxybenzyl alcohol (HMBOH), and  $\beta$ -mercaptoethanol (BME).

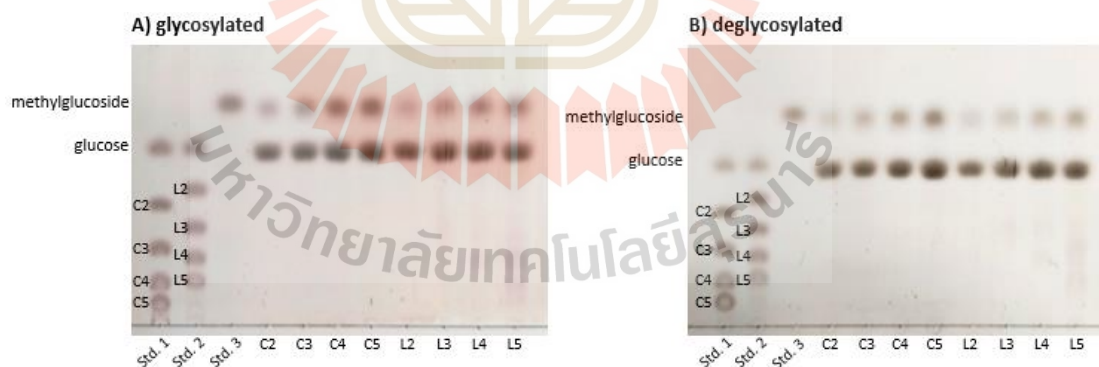


**Figure 4.34** TLC analysis of the transglucosylation from oligosaccharides to methanol by OsExo1. A) glycosylated, B) deglycosylated enzyme. Standards contain glucose and C2-C5 (Std. 1), glucose and L2-L5 (Std. 2), and methyl  $\beta$ -D-glucopyranoside (Std. 3). Glucosyl donor cello-oligosaccharides included C2, C3, C4, and C5, laminari-oligosaccharides including L2, L3, L4, and L5.

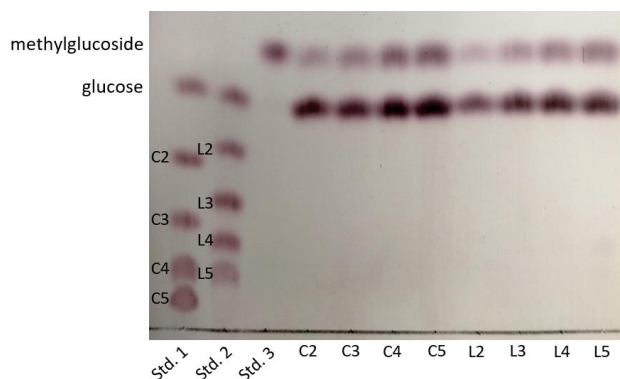


**Figure 4.35** TLC analysis of the transglucosylation from oligosaccharides to methanol by OsExo2. Standards contain glucose and C2-C5 (Std. 1), glucose and L2-L5 (Std. 2), and methyl  $\beta$ -D-glucopyranoside (Std. 3). Glucosyl donor cello-oligosaccharides included C2, C3, C4, and C5, laminari-oligosaccharides including L2, L3, L4, and L5.

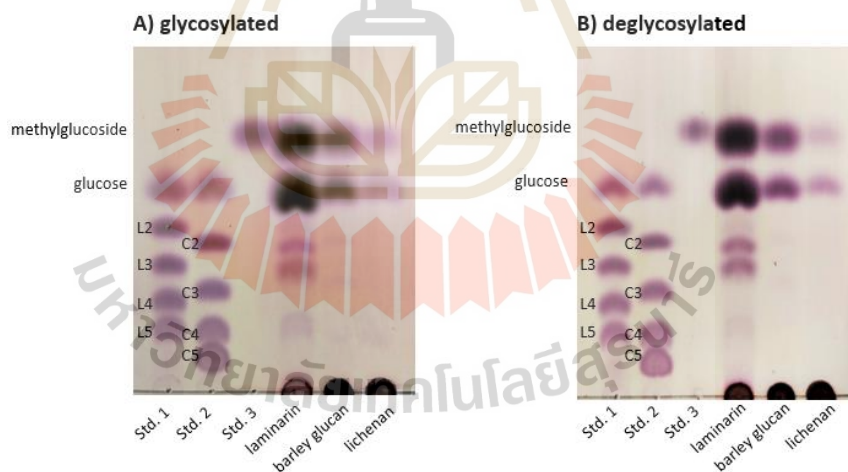


**Figure 4.36** TLC analysis of the transglucosylation from polysaccharides to methanol by OsExo1. A) glycosylated, B) deglycosylated forms. Standards contain glucose and L2-L5 (Std. 1), glucose and C2-C5 (Std. 2), and methyl  $\beta$ -D-glucopyranoside (Std. 3). Glucosyl donor polysaccharides included laminarin, barley glucan, and lichenan.

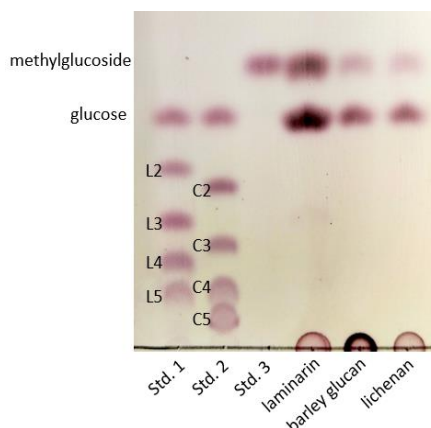


**Figure 4.37** TLC analysis of the transglucosylation from polysaccharides to methanol by OsExo2. Standards contain glucose and L2-L5 (Std. 1), glucose and C2-C5 (Std. 2), and methyl  $\beta$ -D-glucopyranoside (Std. 3). Glucosyl donor polysaccharides included laminarin, barley glucan, and lichenan.

The transglucosylation by  $\beta$ -glucosidase is a kinetically controlled reaction. It depends on the properties of the enzyme more than the conditions or thermodynamic equilibrium (Feng et al., 2005). Thus, mutagenesis is the most common approach for improving transglucosylation rate in  $\beta$ -glycosidases, i.e. increased stability of acceptor in aglycone +1 subsites together with decreased in stabilization in the glycone subsite by mutation in a highly conserved amino acid that located at -1 subsite around the active site of GH1 Ttb-gly can be improved synthetic activity (Feng et al., 2005; Teze et al., 2014). The mutation of *P. furiosus* CelB at F426Y significantly increased the transglucosylation ratio over hydrolysis in producing hexyl- $\beta$ -glucoside (Hansson and Adlercreutz, 2001).

In general, the enzymatic reaction is conducted in aqueous solution following their natural surroundings. However, disadvantage of aqueous media is often



challenging between water and other glycosyl donors, which rise to unwanted reactions such as hydrolysis rather than transglycosylation. Therefore, technique for reducing water activity is necessary such as addition of co-solvents. The oligosaccharide synthetic activity of *A. oryzae*  $\beta$ -galactosidase is significantly increased in a triethyl phosphate co-solvent system with cyclodextrin (Srisimararat and Pongsawasdi, 2008). The synthetic behavior of *E. coli*  $\beta$ -galactosidase in glycerol-based solvents takes place without noticeable hydrolytic activity and with total regioselectivity, exhibiting an improvement over the use of aqueous buffer (Perez-Sanchez et al., 2011).

Increasing substrate concentration is one of the significant parameters to improve the ratio of transglycosylation by  $\beta$ -glycosidases. The competition between water and acceptor dictate the ratio between transglycosylation and hydrolysis activity directly, then the transglycosylation product should be proportional to acceptor concentration (Richard et al., 1995).

#### **4.12 Purification of transglycosylation products of OsExo2**

The transglycosylation products of *p*NPGlc by OsExo2 were isolated by 3-step purification. The first step was silica gel column chromatography in chloroform and methanol, from which a mixture of *p*NPGlc, *p*NPG1, *p*NPG2, *p*NPG3, and *p*NPG4 was collected together. The second step was purification by C18 reverse-phase column chromatography in water and methanol. In this step, we can eliminate *p*NPGlc then the mixture of *p*NP-oligosaccharide products: *p*NPG1, *p*NPG2, *p*NPG3, and *p*NPG4, which came together. The products were assumed to be *p*NP conjugates since they could be seen by absorbance of UV light. Since their polarities are similar, those



products were further purified by TLC with butanol: acetic acid: water (2:1:1 v/v) as solvent. The active UV single spot was scraped from the TLC, as shown in Figure 4.38. The number of glucosyl residues and their linkage in each product were then confirmed by NMR.

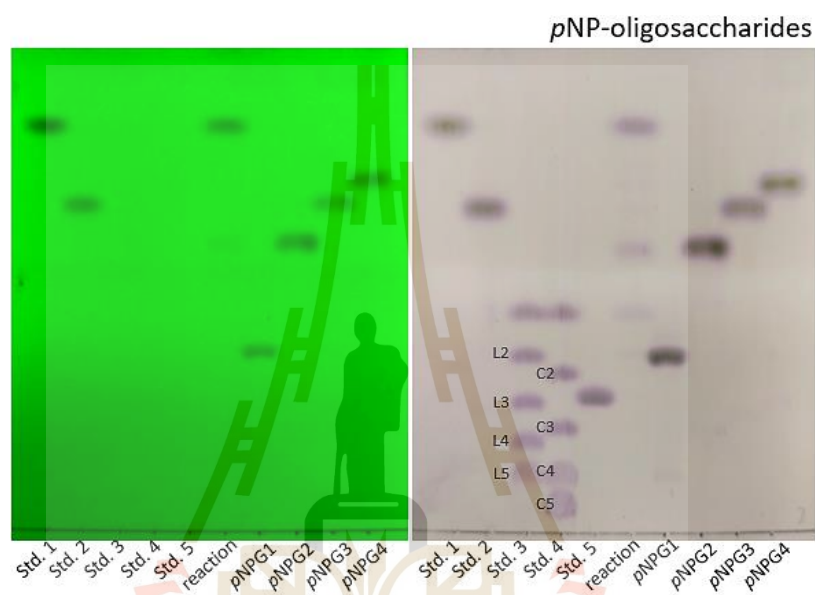


**Figure 4.38** TLC analysis of purification of transglucosylation products of *pNPGlc* generated by OsExo2. Standards contain, *pNPGlc* (Std. 1), *pNPC2* (Std. 2), glucose and laminari-oligosaccharides L2-L5 (Std. 3), glucose and cello-oligosaccharides C2-C5 (Std. 4).

The glucoside products of short-chain alcohols including methanol, ethanol, *n*-propanol, 1-butanol, 3-methyl-1-butanol propargyl alcohol,  $\beta$ -mercaptoethanol, and 4-hydroxymethyl benzyl alcohol were purified by silica gel column chromatography. The products that gave a single spot on TLC were collected and their structures confirmed by NMR (Figure 4.39).

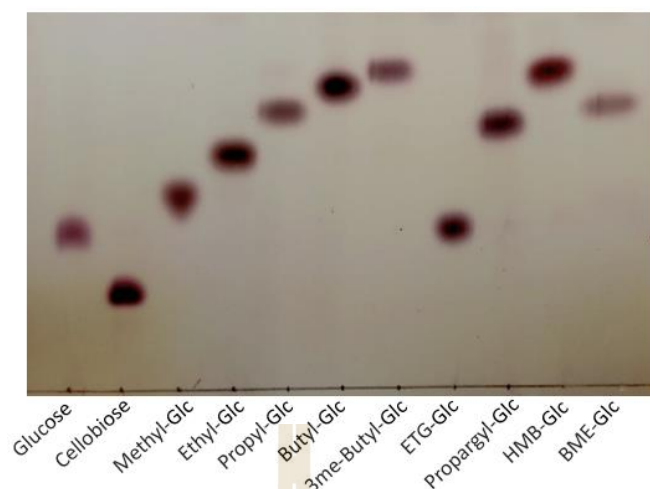


**Figure 4.39** TLC analysis of purification of transglucosylation products of alcohols generated by OsExo2. The transglucosylation products include with methanol, ethanol, *n*-propanol, 1-butanol, 3-methyl-1-butanol (3me-Butyl), ethylene glycol (ETG), propargyl alcohol, 4-hydroxybenzyl alcohol (HMB), and  $\beta$ -mercaptoethanol. Standards include glucose and cellobiose.

#### 4.13 Transglucosylation product structural confirmation

The transglucosylation products' structures were confirmed by NMR spectrometry with  $D_2O$  as solvent. The key correlations to construct the linkage in oligosaccharides of the 4 isolated *pNP*-oligosaccharide compounds (*pNPG1-pNPG4*), as show in Figure 4.35, were initially identified as tri- and di-saccharides by analysis of  $^1H$  and  $^{13}C$  NMR spectra. The anomeric protons and anomeric carbon peaks were identified in the  $^1H$  and  $^{13}C$  NMR spectra, in which the anomeric proton coupling constant values were between 7.5 – 8 Hz, which suggested that the anomeric glycosidic linkages were in  $\beta$  configuration, as expected. Based on the polarity of oligosaccharide standards on TLC

analysis in Figure 4.35, *p*NPG1-*p*NPG4 would be different between their linkages. Therefore, the glycosidic linkages in di and tri-saccharides were analyzed by using 2D NMR. The -CH<sub>2</sub> protons using C-H correlations were identified from HSQC spectra and the key glycosidic linkages presented in tri and di-saccharides using two and three C-H bond correlations were identified from HMBC spectra.

#### 4.13.1 *p*NP-β-D-gentiotrioside (*p*NPG1)

The product *p*NPG1 was identified as *p*NP-β-D-gentiotrioside with the following data:  $R_f = 0.36$  (silica gel TLC with BuOH: acetic acid: water 4: 1: 1 v/v as solvent); <sup>1</sup>H NMR (D<sub>2</sub>O, 500 MHz): δ 8.26 (d,  $J = 9.5$  Hz, 2H), 7.29 (d,  $J = 9.5$  Hz, 2H), 5.29 (d,  $J = 7.5$  Hz, 1H), 4.47 (d,  $J = 8$  Hz, 1H), 4.43 (d,  $J = 8$  Hz, 1H), 4.18 (appt,  $J = 10.5$  Hz, 2H), 3.95-3.88 (m, 2H), 3.86-3.80 (m, 2H), 3.64-3.61 (m, 3H), 3.55-3.47 (m, 3H), 3.45-3.41 (m, 2H), 3.39-3.35 (m, 1H), 3.29 (appt,  $J = 8.5$  Hz, 2H), and 3.25-3.21 ppm (m, 1H); <sup>13</sup>C NMR (D<sub>2</sub>O, 125 MHz) δ 161.5, 142.6, 126.1, 116.6 102.9, 102.7, 99.2, 75.8, 75.6, 75.5, 75.2, 74.7, 73.08, 73.02, 72.6, 69.6, 69.3, 69.2, 68.9, 62.4, 60.7, 48.8, and 38.6 ppm.

HSQC: H-6, 4.20 ppm (m, 1H), H-6' 3.83 (m, 1H), H-12 4.16 (m, 1H), H-12' 3.92 (m, 1H), H-18 3.86 (m, 1H), H-18' 3.62 (m, 1H); C-6, 68.9, C-12, 69.2, and C-18, 60.7. H-6 and H6' showed correlation with C-6 at 68.9 ppm. H-12 and H-12' having correlation with C-12 at 69.2 ppm. Similarly, H-18 and H-18' showed correlations with C-18 at 60.7 ppm. The HSQC C-H single bond correlation suggested us to find out the C-6, C-12, and C-18 (Appendix B, Figure B.3).

HMBC: H-1 5.29 (d,  $J = 7.5$  Hz, 1H), H-6, 4.20 ppm (m, 1H), H-6' 3.83 (m, 1H), H-7, 4.43 ppm (d,  $J = 8$  Hz, 1H), H-12 4.16 (m, 1H), H-12' 3.92 (m, 1H), H-13, 4.47

ppm (d,  $J = 8$  Hz, 1H); C-6, 68.9, C-7, 102.7, C-12, 69.2, C-18, 60.7, C-13, 102.9, and C-19, 161.5 ppm.

We observed the first anomeric proton [H-1] at 5.29 (d,  $J = 7.5$ Hz, 1H) having three bond correlation with C-19 at 161.5 ppm, which indicates the *p*-nitrophenol connected with the glucosyl moiety (Appendix B, Figure B.4A). The second anomeric proton [H-7] at 4.43 ppm (d,  $J = 8$ Hz, 1H) showed correlation with C-6 at 68.9 ppm, and also H-6 having correlation with C-7 at 102.7 ppm. These correlations guided us to construct the  $\beta$ -1-6 glycosidic linkage. The third anomeric proton [H-13] at 4.47 ppm (d,  $J = 8$ Hz, 1H) showed correlation with C-12 at 69.2 ppm, and also H-12 having correlation with C-13 at 102.9 ppm. These correlations guided us to construct the second  $\beta$ -1-6 glycosidic linkage (Appendix B, Figure B.4B). The two  $\beta$ -1-6 glycosidic linkages suggested pNPG1 is *p*NP- $\beta$ -D-gentiotrioside (Figure 4.40).

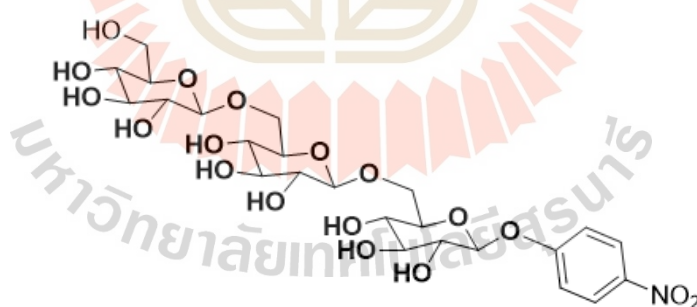


**Figure 4.40** Chemical structure of *p*NP- $\beta$ -D-gentiotrioside.

#### 4.13.2 *p*NP- $\beta$ -D-gentiobioside (*p*NPG2)

The data for *p*NPG2 suggested it is *p*NP- $\beta$ -D-gentiobioside, as follows:  $R_f = 0.60$  (silica gel TLC with BuOH: acetic acid: water 4: 1: 1 v/v as solvent);  $^1\text{H}$  NMR ( $\text{D}_2\text{O}$ , 500 MHz):  $\delta$  8.26 (d,  $J = 9$  Hz, 2H), 7.24 (d,  $J = 9.5$  Hz, 2H), 5.27 (d,  $J = 7.5$  Hz, 1H), 4.54 (d,  $J = 8$  Hz, 1H), 4.21 (d,  $J = 10$  Hz, 1H), 3.90-3.85 (m, 3H), 3.68-3.65 (m, 1H), 3.64-3.62 (m, 2H), 3.58-3.56 (m, 1H), 3.44-3.40 (m, 1H), 3.38-3.33 (m, 2H), and 3.28 (appt,  $J = 8$  Hz, 1H);  $^{13}\text{C}$  NMR ( $\text{D}_2\text{O}$ , 125 MHz)  $\delta$  161.6, 142.6, 126.0, 116.4, 120.5, 99.2, 78.1, 75.9, 75.4, 75.0, 73.9, 73.1, 72.5, 69.4, 60.5, and 59.7 ppm.

HSQC: H-6, 4.21 ppm (d,  $J = 10$  Hz, 1H), H-6' 3.90 (m, 1H), H-12 3.85 (m, 1H), and H-12' 3.67 (m, 1H); C-6, 68.3 and C-12, 60.6. H-6 and H6' showed correlation with C-6 at 68.3 ppm. H-12 and H-12' were correlated with C-12 at 60.6 ppm. The HSQC C-H single bond correlations suggested the C-6 and C-12 (Appendix B, Figure B.7).

HMBC; H-1, 5.29 (d,  $J = 7.5$  Hz, 1H), H-6, 4.21 ppm (d,  $J = 10$  Hz, 1H), H-6', 3.90 (m, 1H), H-7, 4.54 (d,  $J = 8$  Hz, 1H); C-1, 99.2, C-6, 68.3, C-7, 102.7, and C-13, 161.5 ppm.

We observed the first anomeric proton [H-1] having three bond correlation with C-19 at 161.5 ppm, which indicates the *p*-nitrophenol connected with glucose molecule (Appendix Figure B.8A). The second anomeric proton [H-7] at 4.54 ppm (d,  $J = 8$  Hz, 1H) showed correlation with C-6 at 68.3 ppm, and also H-6 having correlation with C-7 at 102.7 ppm (Appendix B, Figure B.8B). These correlations guided us to construct the  $\beta$ -1-6 glycosidic linkage. The one  $\beta$ -1-6 glycosidic linkage suggested the disaccharide was *p*NP- $\beta$ -D-gentiobioside (Figure 4.41).

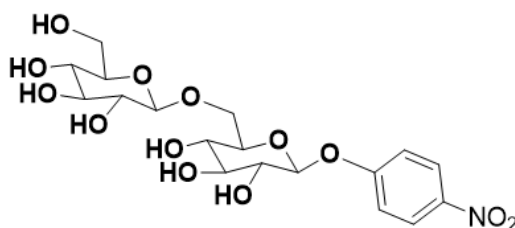


**Figure 4.41** Chemical structure of *p*NP- $\beta$ -D-gentiobioside (*p*NPG2).

#### 4.13.3 *p*NP- $\beta$ -D-cellobioside (*p*NPG3)

The NMR and chromatographic data suggested that product *p*NPG3 is *p*NP- $\beta$ -D-cellobiose, as follows:  $R_f = 0.68$  (silica gel TLC with BuOH: acetic acid: water 4: 1: 1 v/v as solvent);  $^1\text{H}$  NMR ( $\text{D}_2\text{O}$ , 500 MHz):  $\delta$  8.26 (d,  $J = 9$  Hz, 2H), 7.24 (d,  $J = 9.5$  Hz, 2H), 5.29 (d,  $J = 7.5$  Hz, 1H), 4.54 (d,  $J = 8$  Hz, 1H), 4.01-3.99 (m, 1H), 3.92 (dd,  $J = 2, 12.5$  Hz, 1H), 3.87-3.83 (m, 2H), 3.78-3.3.76 (m, 2H), 3.73-3.64 (m, 2H), 3.53-3.47 (m, 2H), 3.43-3.38 (m, 1H), and 3.33 ppm (appt,  $J = 8$  Hz, 1H);  $^{13}\text{C}$  NMR ( $\text{D}_2\text{O}$ , 125 MHz):  $\delta$  161.6, 142.6, 126.0, 116.4, 120.5, 99.2, 78.1, 75.9, 75.4, 75.0, 73.9, 73.1, 72.5, 69.4, 60.5, and 59.7 ppm.

Based on the migration rate of *p*NPG3 relative to *p*NP- $\beta$ -D-cellobioside (*p*NPG2) standard, we suspected it was *p*NP- $\beta$ -D-cellobioside. We dissolved both *p*NP- $\beta$ -D-cellobioside standard and the isolated *p*NPG3 sample in  $\text{D}_2\text{O}$  and then ran  $^1\text{H}$ -NMR. The superimposed  $^1\text{H}$ -NMR spectra of the commercial *p*NP- $\beta$ -D-cellobioside and isolated *p*NPG3 matched each other, as shown in Figure 4.42. This superimposed spectrum confirmed that *p*NPG3 is *p*NP- $\beta$ -D-cellobioside (Figure 4.43).

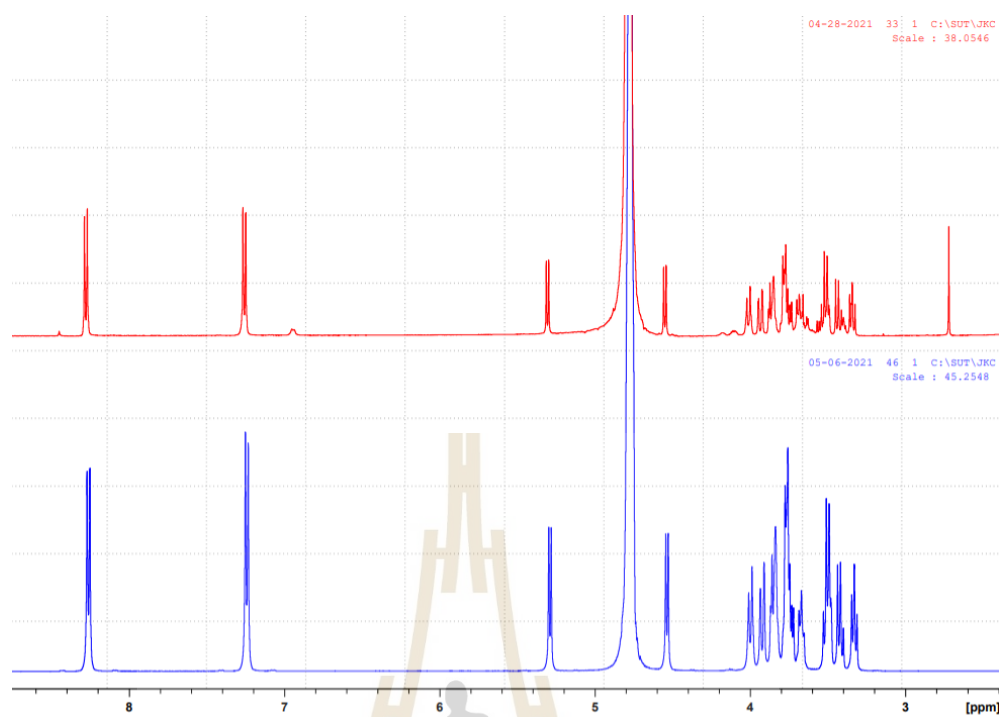


**Figure 4.42** Superimposed <sup>1</sup>H-NMR spectra of *p*NP-β-D-cellobioside standard (blue) and *p*NP-β-D-cellobioside isolated sample (red).

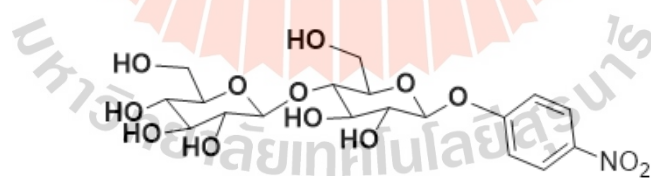


**Figure 4.43** Chemical structure of *p*NP-β-D-cellobioside.



#### 4.13.4 *p*NP- $\beta$ -D-laminaribioside (*p*NPG4)

The *p*NPG4 product was identified as *p*NP- $\beta$ -D-laminaribioside based on the following data:  $R_f = 0.71$  (silica gel TLC with BuOH: acetic acid: water 4: 1: 1 v/v as solvent);  $^1\text{H NMR}$  ( $\text{D}_2\text{O}$ , 500 MHz):  $\delta$  8.27 (d,  $J = 9$  Hz, 2H), 7.25 (d,  $J = 9$  Hz, 2H), 5.30 (d,  $J = 7.5$  Hz, 1H), 4.72 (anomeric proton merged with  $\text{D}_2\text{O}$ , 1H), 3.95-3.87 (m, 3H) 3.83 (appt,  $J = 8$  Hz, 1H), 3.78 (dd,  $J = 5.5, 12.5$  Hz, 1H), 3.74-3.37 (m, 2H), 3.63 (appt,  $J = 9.5$  Hz, 2H), 3.54-3.47 (m, 2H), 3.43-3.33 ppm (m, 3H);  $^{13}\text{C NMR}$  ( $\text{D}_2\text{O}$ , 125 MHz)  $\delta$  161.6, 126.0, 116.4, 120.7, 99.1, 83.7, 75.9, 75.5, 73.4, 72.5, 69.5, 67.7, 60.6, and 60.3 ppm.

HSQC: H-1, 5.30 (d,  $J = 7.5\text{Hz}$ , 1H), H-3 3.95 (m, 1H), and H-7 4.72 (anomeric proton merged with  $\text{D}_2\text{O}$ , 1H); C-1, 99.1, C-3, 83.7, and C-7, 102.7 ppm. H-3 at 3.95 ppm (m, 1H) showed a correlation with C-3 at 88.7 ppm. H-7 had a correlation with C-7 at 103.7 ppm. The HSQC C-H single bond correlations suggested identities of the C-3 and C-7 peaks.

HMBC: H-3 3.95 (m, 1H) and H-7 4.72 ppm (anomeric proton merged with  $\text{D}_2\text{O}$ , 1H); C-3, 83.7 and C-7, 102.7 ppm.

We observed the first anomeric proton [H-1] having a three-bond correlation with the C-19 peak at 161.5 ppm, which indicates the *p*-nitrophenol connected with glucosyl moiety (Appendix B, Figure B.13). The second anomeric proton [H-7] peak at 4.72 ppm showed a correlation with the C-3 peak at 83.7 ppm, and also the H-3 peak had a correlation with the C-7 peak at 102.7 ppm (Appendix B, Figure B.14). These correlations guided us to construct the  $\beta$ -1-3 glycosidic linkage. The one  $\beta$ -1-3 glycosidic linkage suggested that *p*NPG4 was the disaccharide glycoside *p*NP- $\beta$ -D-laminaribioside (Figure 4.44).

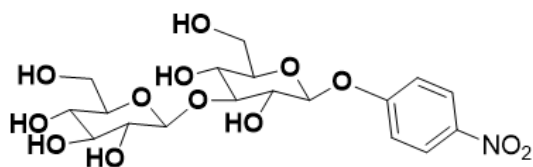


**Figure 4.44** Chemical structure of *p*NP- $\beta$ -D-laminaribioside.

#### 4.13.5 Methyl- $\beta$ -D-glucopyranoside

The product of the transglycosylation product of methanol was confirmed with the following data.  $R_f = 0.37$  (silica gel TLC with  $\text{CHCl}_3$ : MeOH 9:1 v/v as solvent);  $^1\text{H NMR}$  ( $\text{D}_2\text{O}$ , 500 MHz):  $\delta$  4.35 (d,  $J = 8$  Hz, 1H), 3.90 (dd,  $J = 2, 12.5$  Hz, 1H), 3.70 (dd,  $J = 5.5, 12.5$  Hz, 1H), 3.55 (s, 3H), 3.49-3.42 (m, 2H), 3.37-3.32 (m, 1H) and 3.24 ppm (appt,  $J = 3.2$  Hz);  $^{13}\text{C NMR}$  ( $\text{D}_2\text{O}$ , 125 MHz)  $\delta$  103.2, 75.9, 75.7, 73.0, 69.6, 60.6, and 57.1 ppm.

The anomeric protons coupling constant value was 8 Hz at 4.35 ppm (Figure B.15), and anomeric carbon peak was at 103.2 ppm (Figure B.16) which confirmed that the anomeric glycosidic linkage was in  $\beta$  configuration. The chemical structure of methyl- $\beta$ -D-glucopyranoside is shown in Figure 4.45.

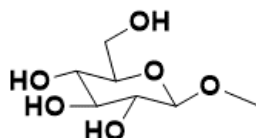


**Figure 4.45** Chemical structure of methyl- $\beta$ -D-glucopyranoside.

#### 4.13.6 Ethyl- $\beta$ -D-glucopyranoside

The product of the transglycosylation product of ethanol was confirmed with the following data.  $R_f = 0.44$  (silica gel TLC with  $\text{CHCl}_3$ : MeOH 9:1 v/v as solvent);  $^1\text{H}$  NMR ( $\text{D}_2\text{O}$ , 500 MHz):  $\delta$  4.45 (d,  $J = 8$  Hz, 1H), 3.99-3.92 (m, 1H), 3.90 (dd,  $J = 2, 12$  Hz, 1H), 3.74-3.68 (m, 2H), 3.49-3.42 (m, 2H), 3.36 (appt,  $J = 9.5$ Hz, 1H), 3.23 (appt,  $J = 8.5$  Hz, 1H) and 1.22 ppm (t,  $J = 7$  Hz, 3H);  $^{13}\text{C}$  NMR ( $\text{D}_2\text{O}$ , 125 MHz)  $\delta$  101.8, 75.8, 75.7, 73.1, 69.6, 66.1, 60.7 and 14.2 ppm.

The anomeric protons coupling constant value was 8 Hz at 4.45 ppm (Figure B.17), and the anomeric carbon peak was at 101.8 ppm (Figure B.18), which confirmed the anomeric glycosidic linkage was in  $\beta$  configuration. The chemical structure of ethyl- $\beta$ -D-glucopyranoside is shown in Figure 4.46.

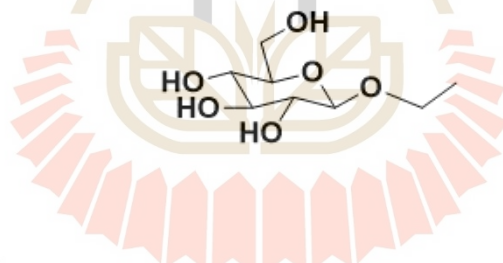


**Figure 4.46** Chemical structure of ethyl- $\beta$ -D-glucopyranoside.

#### 4.13.7 Propyl- $\beta$ -D-glucopyranoside

The product of the transglycosylation product of n-propanol was confirmed as n-propyl- $\beta$ -D-glucopyranoside with the following data.  $R_f = 0.57$  (silica gel TLC with  $\text{CHCl}_3$ : MeOH 9:1 v/v as solvent);  $^1\text{H}$  NMR ( $\text{D}_2\text{O}$ , 500 MHz):  $\delta$  4.44 (d,  $J = 8$  Hz, 1H), 3.91-3.83 (m, 2H), 3.70 (dd,  $J = 6, 12.5$  Hz, 1H), 3.64-3.59 (m, 1H), 3.48-3.41 (m, 2H), 3.36 (appt,  $J = 9$ Hz, 1H), 3.24 (appt,  $J = 8.5$ Hz, 1H), 1.60 (sx,  $J = 7.5$ Hz, 2H), and

0.90 ppm (t,  $J = 7\text{Hz}$ , 3H);  $^{13}\text{C}$  NMR ( $\text{D}_2\text{O}$ , 125 MHz):  $\delta$  102.1, 75.8, 75.7, 73.1, 72.2, 69.6, 60.7, 22.1 and 9.5 ppm.

The anomeric proton coupling constant value was 8 Hz for the peak at 4.44 ppm (Figure B.19) and anomeric carbon peak was at 102.1 ppm (Figure B.20) which confirmed that the anomeric glycosidic linkage was in  $\beta$  configuration. The chemical structure of *n*-propyl- $\beta$ -D-glucopyranoside is shown in Figure 4.47.

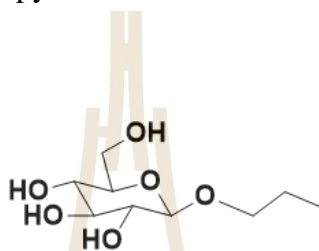


**Figure 4.47** Chemical structure of *n*-propyl- $\beta$ -D-glucopyranoside.

#### 4.13.8 *n*-Butyl- $\beta$ -D-glucopyranoside

The product of the transglycosylation product of *n*-butanol was confirmed as *n*-butyl- $\beta$ -D-glucopyranoside with the following data.  $R_f = 0.62$  (silica gel TLC with  $\text{CHCl}_3:\text{MeOH}$  9:1 v/v as solvent);  $^1\text{H}$  NMR ( $\text{D}_2\text{O}$ , 500 MHz):  $\delta$  4.44 (d,  $J = 8\text{ Hz}$ , 1H), 3.939-3.887 (m, 2H), 3.721-3.654 (m, 2H), 3.486-3.417 (m, 2H), 3.62 (appt,  $J = 9.5\text{ Hz}$ , 1H), 3.239 (appt,  $J = 8.5\text{ Hz}$ , 1H), 1.621-1.564 (m, 2H), 1.380-1.320 (m, 2H), and 0.89 ppm (t,  $J = 7.5\text{ Hz}$ , 3H);  $^{13}\text{C}$  NMR ( $\text{D}_2\text{O}$ , 125 MHz):  $\delta$  102.1, 75.87, 75.80, 73.1, 70.3, 69.6, 60.7, 30.8, 18.4 and 13.0 ppm.

The anomeric proton coupling constant value was 8 Hz for the peak at 4.44 ppm (Figure B.21), and anomeric carbon peak was at 102.1 ppm (Figure B.22), which

confirmed that the anomeric glycosidic linkage was in  $\beta$  configuration. The chemical structure of *n*-butyl- $\beta$ -D-glucopyranoside is shown in Figure 4.48.

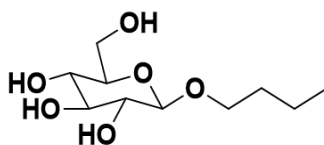


**Figure 4.48** Chemical structure of *n*-butyl- $\beta$ -D-glucopyranoside.

#### 4.13.9 3-Methyl-1-butyl- $\beta$ -D-glucopyranoside

The product of the transglycosylation product of 3-methyl-1-butanol was confirmed as 3-Methyl-1-butyl- $\beta$ -D-glucopyranoside with the following data.  $R_f$  = 0.64 (silica gel TLC with  $\text{CHCl}_3$ : MeOH 9:1 v/v as solvent);  $^1\text{H}$  NMR ( $\text{D}_2\text{O}$ , 500 MHz):  $\delta$  4.43 (d,  $J$  = 8 Hz, 1H), 3.97-3.93 (m, 1H), 3.90 (dd,  $J$  = 2, 12 Hz, 1H), 3.72-3.65 (m, 2H), 3.46 (appt,  $J$  = 9 Hz, 1H), 3.44-3.41 (m, 1H), 3.38-3.33 (m, 1H), 3.23 (appt,  $J$  = 9 Hz, 1H), 1.70-1.63 (m, 1H), 1.55-1.45 (m, 2H) and 0.88 ppm (d,  $J$  = 6.5 Hz, 6H);  $^{13}\text{C}$  NMR ( $\text{D}_2\text{O}$ , 125 MHz):  $\delta$  102.1, 75.86, 75.80, 73.1, 69.6, 69.1, 60.7, 37.5, 24.1, 21.73, and 21.72 ppm.

The anomeric proton coupling constant value was 8 Hz for the peak at 4.43 ppm (Appendix B, Figure B.23), and anomeric carbon peak was at 102.1 ppm (Figure B.24), which confirmed that the anomeric glycosidic linkage was in  $\beta$  configuration. The chemical structure of 3-methyl-1-butyl- $\beta$ -D-glucopyranoside is shown in Figure 4.49.

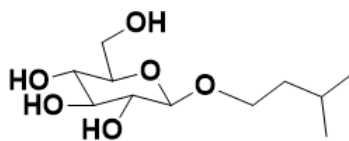


**Figure 4.49** Chemical structure of 3-methyl-1-butyl- $\beta$ -D-glucopyranoside.

#### 4.13.10 2-Hydroxyethyl- $\beta$ -D-glucopyranoside

The product of the transglycosylation product of ethylene glycol was confirmed as 2-hydroxyethyl- $\beta$ -D-glucopyranoside with the following data.  $R_f = 0.17$  (silica gel TLC with  $\text{CHCl}_3:\text{MeOH}$  9:1 v/v as solvent);  $^1\text{H}$  NMR ( $\text{D}_2\text{O}$ , 500 MHz):  $\delta$  4.48 (d,  $J = 8$  Hz, 1H), 4.01-3.96 (m, 1H), 3.90 (dd,  $J = 2, 12.5$  Hz, 1H), 3.78-3.76 (m, 3H), 3.71 (dd,  $J = 6, 12$  Hz, 1H), 3.49 (appt,  $J = 9$  Hz, 1H), 3.46-3.43 (m, 1H), 3.39-3.34 (m, 1H), 3.30 ppm (appt,  $J = 8$  Hz, 1H);  $^{13}\text{C}$  NMR ( $\text{D}_2\text{O}$ , 125 MHz):  $\delta$  102.3, 75.8, 75.6, 73.1, 71.1, 69.6, 60.9, and 60.2 ppm.

The anomeric proton coupling constant value was 8 Hz for the peak at 4.48 ppm (Appendix B, Figure B.25), and the anomeric carbon peak was at 102.3 ppm (Appendix B, Figure B.26) which confirmed that the anomeric glycosidic linkage was in  $\beta$  configuration. The chemical structure of 2-hydroxy-ethyl-1- $\beta$ -D-glucoside is shown in Figure 4.50.

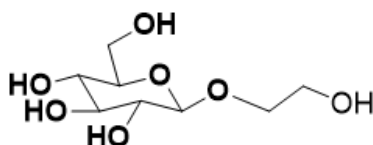


**Figure 4.50** Chemical structure of 2-hydroxyethyl- $\beta$ -D-glucopyranoside.

#### 4.13.11 Propargyl- $\beta$ -D-glucopyranoside.

The product of the transglycosylation product of propargyl alcohol was confirmed as propargyl- $\beta$ -D-glucopyranoside with the following data.  $R_f = 0.44$  (silica gel TLC with  $\text{CHCl}_3$ :MeOH 9:1 v/v as solvent);  $^1\text{H NMR}$  ( $\text{D}_2\text{O}$ , 500 MHz):  $\delta$  4.62 (d,  $J = 8$  Hz, 1H), 4.49-4.42 (m, 2H), 3.90 (dd,  $J = 2, 12$  Hz, 1H), 3.26-3.69 (m, 1H), 3.55-3.49 (m, 1H), 3.47-3.44 (m, 1H), 3.37 (appt,  $J = 9$ Hz, 1H), 3.28 (appt,  $J = 8.5$  Hz, 1H) and 2.90 ppm (t,  $J = 2.5$  Hz, 1H [proton exchanged]);  $^{13}\text{C NMR}$  ( $\text{D}_2\text{O}$ , 125 MHz):  $\delta$  100.5, 76.2, 75.9, 75.6, 72.8, 69.5, 62.4, 60.3, and 56.4 ppm.

The anomeric proton coupling constant value was 8 Hz for the peak at 4.62 ppm (Appendix B, Figure B.27), and the anomeric carbon peak was at 100.5 ppm (Appendix B, Figure B.28), which confirmed that the anomeric glycosidic linkage is in  $\beta$  configuration. The chemical structure of propargyl- $\beta$ -D-glucopyranoside is shown in Figure 4.51.

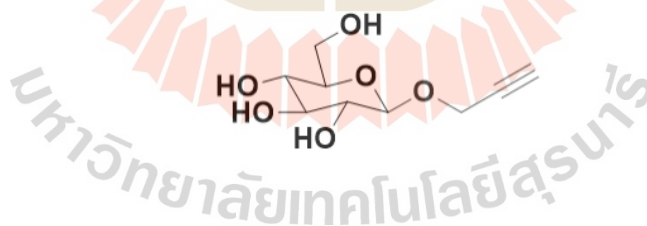


**Figure 4.51** Chemical structure of propargyl- $\beta$ -D-glucopyranoside.

#### 4.13.12 Ethylene-disulfide- $\beta$ -D-glucopyranoside

The product of the transglycosylation product of  $\beta$ -mercaptoethanol was identified as ethylene-disulfide- $\beta$ -D-glucopyranoside with the following data.  $R_f = 0.4$  (silica gel TLC with  $\text{CHCl}_3$ :MeOH 9:1 v/v as solvent);  $^1\text{H NMR}$  ( $\text{D}_2\text{O}$ , 500 MHz):  $\delta$  4.50 (d,  $J = 8$  Hz, 1H), 4.18-4.13 (m, 1H), 3.99-3.95(m, 1H), 3.90 (dd,  $J = 2, 12.5$  Hz,



1H), 3.86 (t, 6Hz, 2H), 3.71 (dd,  $J = 6, 12.5$  Hz, 1H), 3.50-3.43 (m, 2H), 3.29-3.25 (m, 1H), 3.27 (appt,  $J = 8.5$  Hz, 1H), 2.98 (t, 6.5 Hz, 2H), and 2.90 (t, 6 Hz, 2H);  $^{13}\text{C}$  NMR ( $\text{D}_2\text{O}$ , 125 MHz):  $\delta$  102.3, 75.9, 75.6, 73.0, 69.5, 67.8, 60.6, 59.1, 39.9, and 37.4 ppm.

The anomeric proton coupling constant value was 8 Hz for the peak at 4.50 ppm with total 15 H atoms (Appendix B, Figure B.29), and the anomeric carbon peak was at 102.3 ppm, with total 10 carbon atoms (Appendix B, Figure B.30) which, confirmed that the anomeric glycosidic linkage was in  $\beta$  configuration and present disulfide bond of  $\beta$ -mercaptoethanol in the molecule. The chemical structure of ethylene-disulfide- $\beta$ -D-glucopyranoside is shown in Figure 4.52.

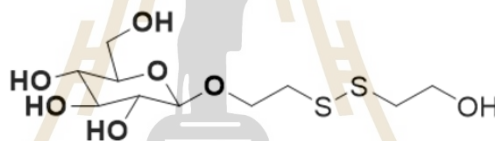


**Figure 4.52** Chemical structure of ethylene-disulfide- $\beta$ -D-glucopyranoside

#### 4.13.13 4-Hydroxy-benzyl- $\beta$ -D-glucopyranoside

The product of the transglycosylation product of 4-hydroxy-benzyl alcohol was identified as 4-hydroxy-benzyl- $\beta$ -D-glucopyranoside with the following data.  $R_f = 0.44$  (silica gel TLC with  $\text{CHCl}_3:\text{MeOH}$  9:1 v/v as solvent);  $^1\text{H}$  NMR ( $\text{D}_2\text{O}$ , 500 MHz):  $\delta$  7.38-7.28 (m, 2H), 6.99-6.94 (m, 2H), 4.93 (d,  $J = 11.5$  Hz, 1H), 4.53 (d,  $J = 8$  Hz, 1H), 3.90 (dd,  $J = 2, 12.5$  Hz, 1H), 3.71 (dd,  $J = 6, 12.5$  Hz, 1H), 3.46-3.41 (m, 2H), 3.39-3.33 (m, 1H), and 3.28 ppm (appt,  $J = 8.5$  Hz, 1H);  $^{13}\text{C}$  NMR ( $\text{D}_2\text{O}$ , 125 MHz):  $\delta$  154.3, 131.3, 130.3, 123.0, 120.5, 115.7, 101.2, 75.9, 75.6, 73.0, 69.6, 67.0, and 60.7 ppm.

The anomeric proton coupling constant value was 8 Hz for the peak at 4.53 ppm (Appendix B, Figure B.31), and the anomeric carbon peak was at 101.2 ppm (Appendix B, Figure B.32), which confirmed that the anomeric glycosidic linkages are  $\beta$  configuration. When the benzyl is alcohol glycosylated, the benzylic protons become diastereotopic and split into two different peaks and appears at different chemical shifts. From the NMR, the peak for the benzylic proton splits into two different doublets (one proton peak seems to be merged with the solvent peak) and the other proton peak appears at 4.93 ppm (d,  $J = 11.5$  Hz). The chemical structure of 4-hydroxy-benzyl- $\beta$ -D-glucoside is shown in Figure 4.53.

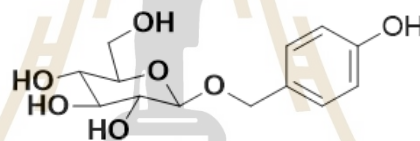


**Figure 4.53** Chemical structure of 4-hydroxy-benzyl- $\beta$ -D-glucopyranoside

#### 4.14 Summary and future directions

The GH1 Os9BGlu31 transglucosylation works by the same mechanism as retaining glycoside hydrolases (Ketudat-Cairns, and Esen, 2010), and can transfer glucose from *p*NPGlc to phenolic acids, and carboxylic acids. The effects of various substitution mutations of Os9BGlu31 were explored to improve use of different donor and acceptor substrates. Unfortunately, no activity could be detected from these enzymes. However, the previously characterized variants that exhibited highest activity were used in this study to produce glucoconjugate of antibiotics and other potential

medicinal compounds. Among the tested acceptor substrates, six acceptors resulted in apparently glycosylated products, including chloramphenicol, nybomycin, ampicillin, amoxicillin, tetracycline, and doxorubicin. Chloramphenicol glucoside was produced and its structure determined by NMR. The structure of other the antibiotic glucosides could be confirmed and their bioactivity tested in the future.

The GH3 OsExo1 and OsExo2 also have a retaining catalytic mechanism, which removes single monosaccharides from the non-reducing end of their substrate, with retention of anomeric configuration (Ketudat-Cairns, and Esen, 2010). GH enzymes often have low regioselectivity (Komvongsa et al., 2015), which leads to a mixture of products when the acceptor contains more than one hydroxyl group (Tran et al., 2019), but OsExo1 and OsExo2 have specificity to primary alcohols, as demonstrated in this work, such as the hydroxyl groups on methanol, ethanol, *n*-propanol, isopropanol, 1-butanol, 3-methyl-1-butanol, propargyl alcohol, 4-hydroxybenzyl alcohol, and  $\beta$ -mercaptoethanol. However, the transglycosylation activity of the enzymes also can transfer a glucosyl moiety to a glycon portion in glycoside in different linkages, which led to detectable *p*NP-oligosaccharides, including *p*NP- $\beta$ -D-gentiotrioside, *p*NP- $\beta$ -D-gentiobioside, *p*NP- $\beta$ -D-cellobioside, and *p*NP- $\beta$ -D-laminaribiose. Moreover, OsExo1 and OsExo2 can utilize various glucosyl donor substrates, due to their broad specificity toward (1,3)- $\beta$ -D-glucans, (1,4)- $\beta$ -D-glucans, (1,3;1,4)- $\beta$ -D-glucans and (1,6)- $\beta$ -D-glucans (Hrmova and Fincher, 1998). These properties make these enzymes applicable to environmentally friendly glucoside production in reactions with crude oligosaccharides from biomass breakdown as the glucose donors, which may be explored in the future.

## CHAPTER V

### CONCLUSION

This thesis studied the use of glycoside hydrolase family 1 and 3 enzymes in transglycosylation of compounds of interest. The effects of various substitution mutations of Os9BGlu31 were explored to improve use of different donor and acceptor substrates. The transglycosylation properties of GH3 exoglucanases OsExo1 and OsExo2 were investigated as well to produce glycosides of various alcohols. The purification and structural confirmation of the transglycosylation products is also described. The description was separated into two parts starting from Os9BGlu31 engineering and transglycosylation of medicinal compounds, then followed by OsExo1 and OsExo2 characterization as catalysts for transglycosylation reactions.

The Os9BGlu31 amino acid substitutions were based on molecular docking to in *silico* mutated enzymes and were introduced into the Os9BGlu31W243L variants. The resulting variants included Os9BGlu31 H123E/W243L, Y313H/W243L, Y313Q/W243L, Y313S/W243L, E441T/W243L, and E441H/W243L. Unfortunately, no activity could be detected from these enzymes. Therefore, we studied the transglucosylation of antibiotics and other potential medicinal compounds by Os9BGlu31 variants W243H, W243K, W243L, W243N, and W243R, which were previously generated and characterized (Komvongsa et al., 2015; Tran et al., 2019). The production of glucoconjugates of the medicinal compounds was assessed by UPLC. Among the tested acceptor substrates, six acceptors resulted in apparently glycosylated

products, including chloramphenicol, nybomycin, ampicillin, amoxicillin, tetracycline, and doxorubicin. Chloramphenicol glucoside was produced with Os9BGlu31W243N as catalyst and characterized by NMR, and the coupling constant value of the anomeric proton peak of 8 Hz at 4.45 ppm and anomeric carbon peak at the chemical shift of 102.8 ppm confirmed that the anomeric glycosidic linkage was in  $\beta$  configuration. Chloramphenicol contains one primary and one secondary alcohol that can be glycosylated, but the primary hydroxyl is most amenable to glycosylation.

The GH3 enzyme OsExo1 was produced as a secreted protein from *P. pastoris*, as previously described by Prawisut, 2019. The protein was purified from culture media by  $\text{Ni}^{2+}$  IMAC and SEC over an S200 column. The OsExoI was found to be glycosylated in different levels, and the carbohydrate could be removed by digestion with endoglycosidase H. The glycosylation sites in OsExoI were predicted to be Asn210, Asn322 and Asn520 by NetNGlyc (Blom et al., 2004). The highest glycosylation fraction was found to have the highest specific activity at  $17.81 \text{ U}\cdot\text{mg}^{-1}$ , the medium glycosylation fraction had  $9.76 \text{ U}\cdot\text{mg}^{-1}$ , and low glycosylation fraction had  $4.02 \text{ U}\cdot\text{mg}^{-1}$ , while the deglycosylated form had a specific activity of  $9.47 \text{ U}\cdot\text{mg}^{-1}$ . The pH dependence of N-deglycosylated OsExo1 activity was similar to that of glycosylated OsExo1, OsExo2, and rHvExo1 (glycosylated and N-deglycosylated forms), which showed bell-shaped activity versus pH curves, and highest activities detected at pH 5.0. The temperature optimum for the glycosylated OsExo1 enzyme was  $45 \text{ }^\circ\text{C}$ . The temperature stability of OsExo1 N-deglycosylated was similar to that of glycosylated OsExo1, OsExo2 and the N-deglycosylated rHvExo1 (Prawisut et al., 2020; Prawisut, 2019; and Luang et al., 2010). Thus, the glycosylation does not seem to be critical for the stability of rice OsExo1.

OsExo2 was produced in *E. coli*, as described by Prawisut, 2019. The protein was purified by Ni<sup>2+</sup> IMAC, SEC over an S200 column, and HIC over a phenyl sepharose column, respectively. During the purification of OsExo2, it was apparent that the activity increased when ethylene glycol was present in the elution step of HIC purification. Therefore, we tested the transglucosylation activity by using *p*NPGlc as a glucosyl donor substrate, while ethylene glycol was used as a glucosyl donor substrate and the reaction products were visualized by TLC. The new spot could be seen between the positions of *p*NPGlc and glucose, consistent with an ethylene glycol glucoside product.

The transglucosylation activity of OsExo1 and OsExo2 toward various alcohols, including methanol, ethanol, *n*-propanol, isopropanol, 1-butanol, 3-methyl-1-butanol, *n*-octanol, glycerol, propargyl alcohol, 4-hydroxybenzyl alcohol, and  $\beta$ -mercaptoethanol were tested, and all of these could be glycosylated, except for isopropanol, glycerol, and octanol. This suggests that OsExo1 and OsExo2 can transfer glucose only to primary alcohols of short-chain or aromatic molecules. The structures of the products with ethylene glycol and the short-chain alcohols, methanol, ethanol, *n*-propanol, 1-butanol, 3-methyl-1-butanol, propargyl alcohol, 4-hydroxybenzyl alcohol, and  $\beta$ -mercaptoethanol were confirmed by NMR. These products were 2-hydroxy-1-ethyl- $\beta$ -D-glucopyranoside methyl- $\beta$ -D-glucopyranoside, ethyl- $\beta$ -D-glucopyranoside, *n*-propyl- $\beta$ -D-glucopyranoside, 1-butyl- $\beta$ -D-glucopyranoside, 3-methyl-1-butyl- $\beta$ -D-glucopyranoside, propargyl- $\beta$ -D-glucopyranoside, 4-hydroxybenzyl- $\beta$ -D-glucopyranoside, and di- $\beta$ -mercaptoethyl- $\beta$ -D-glucoside, respectively.

The transglucosylation activities toward *p*NPGlc were observed at various times. During the initial stages of the reaction, a small amount of glucose was observed, in

addition to *p*NP-oligosaccharide products. As the reaction progressed, transient transglycosylation products were detected comprising *p*NP-oligosaccharides and oligosaccharides. In a complete reaction, the *p*NP-oligosaccharides and oligosaccharides had been hydrolyzed, and only glucose was present as the final hydrolysis product. The four *p*NP-oligosaccharide products were produced by OsExo2 and their structures were characterized by NMR. The NMR results identified the clearly detectable *p*NP-oligosaccharides as *p*NP- $\beta$ -D-gentiotriose, *p*NP- $\beta$ -D-gentiobiose, *p*NP- $\beta$ -D-cellobiose, and *p*NP- $\beta$ -D-laminaribiose.

To test other glucosyl donor substrates, methanol was used as a glucosyl donor with cello-oligosaccharides (C2-C5), laminari-oligosaccharides (L2-L5), and the polysaccharides laminarin, barley glucan, and lichenan. The results showed that C2-C5, L2-L5, laminarin, barley glucan, and lichenan can serve as glucosyl donors for OsExo1 and OsExo2. The enzyme N-glycosylation state does not seem to have a significant impact on the transglycosylation activity of the rice exoglucanases. This information suggests the efficient catalytic routes to produce useful glycoconjugates.

Further work that can be done in the future would be engineering improved soluble protein expression of rice exoglucanase 2 in *E. coli* by site directed mutagenesis, due to its capability to use of different glucosyl donor substrates. The structure of antibiotic glucosides can be confirmed and the bioactivity tested. Nonetheless, the current work contributes substantially to our ability to apply plant GH1 and GH3 enzymes for production of useful gluco-conjugates.





**REFERENCES**

มหาวิทยาลัยเทคโนโลยีสุรนารี

## REFERENCES

- Adari, B. R., Alavala, S., George, S. A., Meshram, H. M., Tiwari, A. K., and Sarma, A. V. (2016). Synthesis of rebaudioside-A by enzymatic transglycosylation of stevioside present in the leaves of *Stevia rebaudiana* Bertoni. **Food Chem.** 1(200): 154 - 158.
- Bartnik, M., and Facey, P. C. (2017). Chapter 8-Glycosides. In S. Badal, and R. Delgoda, (Ed.), Pharmacognosy, **Academic Press.** 101 - 161.
- Baumann, M. J., Eklo, J. M., Michel, G., Kallas, A. M., Teeri, T. T., Czjzek, M., and Brumer, H. (2007). **The Plant Cell.** 19: 1947 - 1963.
- Bissaro, B., Durand, J., Biarnés, X., Planas, A., Monsan, P. F., O'Donohue, M. J., and Faure, R. (2015). Molecular design of non-Leloir furanose-transferring enzymes from an  $\alpha$ -L-arabinofuranosidase: a rationale for the engineering of evolved transglycosylases. **ACS Catalysis.** 5(8): 4598 - 4611.
- Blom, N., Sicheritz-Pontén, T., Gupta, R., Gammeltoft, S., and Brunak, S. (2004). Prediction of post-translational glycosylation and phosphorylation of proteins from the amino acid sequence. **Proteomics.** 4: 1633 - 1649.
- Bowles, D. (2005) Glycosyltransferases: managers of small molecules. **Current Opinion in Plant Biology.** 8(3): 254 - 263.
- Bunzel, M., Ralph, J., Kim, H., Lu, F., Ralph, S. A., Marita, J., Hatfield, R., and Steinhart, H. (2003). "Sinapate dehydrodimers and sinapate-ferulate heterodimers in cereal dietary fibre". **Journal of Agricultural and Food Chemistry.** 51(5): 1427 - 1434.

- Cantarel, B. L., Coutinho, P. M., Rancurel, C., Bernard, T., Lombard, V., and Henrissat, B. (2009). The Carbohydrate-Active EnZymes database (CAZy): an expert resource for glyco-genomics. **Nucleic Acids Research**. 37: 233 - 238.
- Cardini, C. E., Paladini, A. C., and Caputto, L. F. (1950). Leloir, Uridine diphosphate glucose - the coenzyme of the galactose glucose phosphate isomerization, **Nature**. 165: 192 - 192.
- Charoenwattanasatien, R., Pengthaisong, S., Breen, I., Mutoh, R., Sansenya, S., Hua, Y., Tankrathok, A., Wu, L., Songsiriritthigul, C., Tanaka, H., Williams, S. J., Davies, G. J., Kurisu, G., and Ketudat Cairns, J. R. (2016). Bacterial  $\beta$ -glucosidase reveals the structural and functional basis of genetic defects in human glucocerebrosidase 2 (GBA2). **ACS Chemical Biology**. 11(7): 1891 - 1900.
- Chuenchor, W., Pengthaisong, S., Robinson, R. C., Yuvaniyama, J., Svasti, J., and Ketudat Cairns, J. R. (2011). The structural basis of oligosaccharide binding by rice BGlu1 beta-glucosidase. **Journal of Structural Biology** .173: 169 - 179.
- Clark, G. F., Oehninger, S., and Seppala, M. (1996). Role for glycoconjugates in cellular communication in the human reproductive system. **Molecular Human Reproduction**. 2(7): 513 - 517.
- Cressey, P., and Reeve, J. (2019). Metabolism of cyanogenic glycosides: A review. **Food and Chemical Toxicology**. 125: 223 - 232.
- Cournoyer, B., and Faure, D. (2003). Radiation and functional specialization of the family 3 glycoside hydrolase. **Journal of Molecular Microbiology and Biotechnology**. 5: 190 - 198.

- Davies, G. J., Ducros, V. M. A., Varrot, A., and Zechel, D. L. (2003). Mapping the conformational itinerary of  $\beta$ -glycosidases by X-ray crystallography. **Biochemical Society Transactions**. 31: 523 - 527.
- Davies, G. J., and Henrissat, B. (1995). Structures and mechanisms of glycosyl hydrolases. **Structure**. 3: 853 - 859.
- Desmet, T., Soetaert, W., Bojarová, P., Křen, V., Dijkhuizen, L., Eastwick-Field, V., and Schiller, A. (2012). Enzymatic glycosylation of small molecules: challenging substrates requires tailored catalysts. **Chemistry-A European Journal**. 18: 10786 - 10801.
- Escamilla-Treviño, L. L., Chen, W., Card, M. L., Shih, M. C., Cheng, C. L., and Poulton, J. E. (2006). Arabidopsis thaliana beta-glucosidases BGLU45 and BGLU46 hydrolyse monolignol glucosides. **Phytochemistry**. 67: 1651 - 1560.
- Fan, J. Q., Takegawa, K., Iwahara, S., Kondo, A., Kato, I., Abeygunawardana, C., and Lee, Y. C. (1995). Enhanced transglycosylation activity of *Arthrobacter protophormiae* Endo- $\beta$ -N-acetylglucosamine in media containing organic solvents. **Journal of Biological Chemistry**. 270(30): 17723 - 17729.
- Flynn, V. A., Pedram, K., Malaker, S. A., Batista, P. J., Smith, B. A. H., Johnson, A. G., George, B. M., Majzoub, K., Villalta, P. W., Carette, J. E., and Bertozzi, C. R. (2021). Small RNAs are modified with N-glycans and displayed on the surface of living cells. **Cell**. 184(12): 3109 - 3124.
- Gachon, C. M., Langlois-Meurinne, M., and Saindrenan, P. (2005). Plant secondary metabolism glycosyltransferases: The emerging functional analysis. **Trends in Plant Science**. 10(11): 542 - 549.

- Hansson, T., and Adlercreutz, P. (2001). Enhanced transglucosylation/hydrolysis ratio of mutants of *Pyrococcus furiosus* beta-glucosidase: effects of donor concentration, water content, and temperature on activity and selectivity in hexanol. **Biotechnology Bioengineering**. 75(6): 656 - 665.
- Harvey, A. J., Hrmova, M., Gori, R., Varghese, J. N., and Fincher, G. B. (2000). Comparative modeling of the three-dimensional structures of family 3 glycoside hydrolases. **Proteins: Structure, Function, and Bioinformatics**. 41(2): 257 - 269.
- Henrissat, B. (1991). A classification of glycosyl hydrolases based on amino acid sequence similarities. **Biochemical Journal**. 280: 309 - 316.
- Henrissat, B. and Bairoch, A. (1996). Updating the sequence-based classification of glycosyl hydrolases. **Biochemical Journal**. 316: 695 - 696.
- Hommalai, G., Withers, S. G., Chuenchor, W., Ketudat Cairns, J. R., and Svasti, J. (2007). Enzymatic synthesis of cello-oligosaccharides by rice BGlu1  $\beta$ -glucosidase glycosynthase mutants. **Glycobiology**. 17(7): 744 - 753.
- Hrmova, M., DeGori, R., Smith, B. J., Driguez, H., Varghese, J. N., and Fincher, G. B. (2002). Structural basis for a broad specificity in higher plant  $\beta$ -D-glucan glucohydrolases. **Plant Cell**. 14: 1033 - 1052.
- Hrmova, M., and Fincher, G. B. (2001). Structure-function relationships of beta-D-glucan endo- and exohydrolases from higher plants. **Plant Molecular Biology**. 47(1-2): 73 - 91.
- Hrmova, M., and Fincher, G. B. (1998). Barley  $\beta$ -D-glucan exohydrolases. Substrate specificity and kinetic properties. **Carbohydrate Research**. 305: 209 - 221.

- Hrmova, M., Harvey, A. J., Wang, J., Shirley, N. J., Jones, G. P., Høj, P. B., and Fincher, G. B. (1996). Barley  $\beta$ -D-glucan exohydrolases with  $\beta$ -D-glucosidase activity. Purification and determination of primary structure from a cDNA clone. **Journal of Biological Chemistry**. 271: 5277 - 5286.
- Ismail, A., Sultani, S., and Ghoul, M. (1999). Enzymatic-catalyzed synthesis of alkyl glycosides in monophasic and biphasic systems I. The transglycosylation reaction. **Journal of Biotechnology**. 69: 135 - 143.
- Jain, M., Kaur, N., Tyagi, A. K., and Khurana, J. P. (2006). The auxin-responsive GH3 gene family in rice (*Oryza sativa*). **Functional and Integrative Genomics**. 6(1): 36 - 46.
- Jenkins, J., Lo-Leggio, L., Harris, G., and Pickersgill, R. (1995). Beta-glucosidase, beta-galactosidase, family A cellulases, family F xylanases and two barley glycanases form a superfamily of enzymes with 8-fold beta/alpha architecture and with two conserved glutamates near the carboxy-terminal ends of beta-strands four and seven. **FEBS Letters**. 362: 281 - 285.
- Jones, P., and Vogt, T. (2001). Glycosyltransferases in secondary plant metabolism: tranquilizers and stimulant controllers. **Planta**. 213(2): 164 - 174.
- Ketudat Cairns, J. R., and Esen, A. (2010).  $\beta$ -Glucosidases review. **Cellular and Molecular Life Sciences**. 67: 3389 - 3405.
- Kitaoka, M., and Hayashi, K. (2002). Carbohydrate-processing phosphorolytic enzymes. **Trends in Glycoscience and Glycotechnology**. 14(75): 35 - 50.
- Komvongsa, J., Luang, S., Marques, J. V., Phasai, K., Davin, L. B., Lewis, N. G., and Ketudat Cairns, J. R. (2015). Active site cleft mutants of Os9BGlu31 transglucosidase modify acceptor substrate specificity and allow production of multiple kaempferol glycosides. **Biochimica et Biophysica Acta**. 1850: 1405 - 1414.

- Koshland, D. E. Jr. (1953). Stereochemistry and mechanism of enzymatic reaction. **Biological Reviews.** 28: 416 - 436.
- Kumar, S., Stecher, G., Li, M., Knyaz, C., and Tamura, K. (2018). MEGA X: Molecular Evolutionary Genetics Analysis across computing platforms. **Molecular Biology and Evolution.** 35: 1547 - 1549.
- Kren, V., and Martinkova, L. (2001). Glycosides in Medicine: "The Role of Glycosidic Residue in Biological Activity". **Current Medicinal Chemistry.** 8: 1303 - 1328.
- Kren, V., and Režanka, T. (2008). Sweet antibiotics - the role of glycosidic residues in antibiotic and antitumor activity and their randomization. **FEMS Microbiology Reviews.** 32(5): 858 - 889.
- Kytidou, K., Artola, M., Overkleeft, H. S., and Aerts, J. M. F. G. (2020). Plant glycosides and glycosidases: a treasure-trove for therapeutics. **Frontiers in Plant Science.** 11(357).
- Laemmli, U. K. (1970). Cleavage of structural proteins during the assembly of the head of bacteriophage T4. **Nature.** 227(5259): 680 - 685.
- Lairson, L. L., Henrissat, B., Davies, G. J., and Withers, S. G. (2008). Glycosyltransferases: structures, functions, and mechanisms. **Annual Review of Biochemistry.** 77: 521 - 555.
- Lee, K. H., Piao, H. L., Kim, H. Y., Choi, S. M., Jiang, F., Hartung, W., Hwang, I., Kwak, J. M., Lee, I. J., and Hwang, I. (2006). Activation of glucosidase via stress-induced polymerization rapidly increases active pools of abscisic acid. **Cell.** 126: 1109 - 1120.



- Lim, E. K., Doucet, C. J., Hou, B., Jackson, R. G., Abrams, S. R., and Bowles, D. J. (2005). Resolution of (+)-abscisic acid using *Arabidopsis* glycosyltransferase. *Tetrahedron: Asymmetry*. 16: 143 - 147.
- Ljunger, G., Adlercreutz, P., and Mattiasson, B. (1994). Enzymatic synthesis of octyl- $\beta$ -D-glucoside in octanol at controlled water activity. **Enzyme and Microbial Technology**. 16: 751 - 755.
- Lombard, V., Golaconda, R. H., Drula, E., Coutinho, P. M., and Henrissat, B. (2014). The Carbohydrate-Active EnZymes database (CAZy) in 2013. **Nucleic Acids Research**. 42: 490 - 495.
- Luang, S., Cho, J. I., Mahong, B., Opassiri, R., Akiyama, T., Phasai, K., Komvongsa, J., Sasaki, N., Hua, Y., Matsuba, Y., Ozeki, Y., Jeon, J. S., and Ketudat Cairns, J. R. (2013). Os9BGlu31 is a transglucosidase with the capacity to equilibrate phenolpropenoid, flavonoid and phytohormone glycoconjugates. **Journal of Biological Chemistry**. 288: 10111 - 10123.
- Lundemo, P. (2015). Transglycosylation by Glycoside Hydrolases - Production and modification of alkyl glycosides (Doctoral dissertation). **Lund University, Sweden**.
- Matsuba, Y., Sasaki, N., Tera, M., Okamura, M., Abe, Y., Okamoto, E., Nakamura, H., Funabashi, H., Takatsu, M., Saito, M., Matsuoka, H., Nagasawa, K., and Ozeki, Y. (2010). A novel glucosylation reaction on anthocyanins catalyzed by acyl-glucose-dependent glycosyltransferase in the petals of carnation and delphinium. **The Plant Cell**. 22: 3374 - 3389.
- McCarter, J., and Withers, S. G. (1994). Mechanisms of enzymatic glycoside hydrolysis. **Current Opinion in Structural Biology**. 4: 885 - 892.

- Mestrom, L., Przypis, M., Kowalczykiewicz, D., Pollender, A., Kumpf, A., Marsden, S. R., Bento, I., Jarzebski, A. B., Szymańska, K., Arkadiusz Chruściel, A., Tischler, D., Schoevaart, R., Hanefeld, U., and Hagedoorn, P. L. (2019). Leloir glycosyltransferases in applied biocatalysis: a multidisciplinary approach. **International Journal of Molecular Sciences**. 20: 5263.
- Miller, M. B., Brulc, J. M., Bayer, E. A., Lamed, R., Flint, H. J., and White, B. A. (2010). Chapter 10-Advanced technologies for biomass hydrolysis and saccharification using novel enzymes. In A. Vertès, N. Qureshi, H. P. Blaschek, and H. Yukawa (Ed.), *Biomass to Biofuels: Strategies for Global Industries*, **John Wiley & Sons, Ltd.**
- Moellering, E. R., and Benning, C. (2010). Galactoglycerolipid metabolism under stress: a time for remodeling. **Trends in Plant Science**. 16(2): 98 - 107.
- Morant, A. V., Jørgensen, K., Jørgensen, C., Paquette, S. M., Sánchez-Pérez, R., Møller B. L., and Bak, S. (2008). Beta-glucosidases as detonators of plant chemical defense. **Phytochemistry**. 69(9): 1795 - 1813.
- Nam, S. H., Park, J., Jun, W., Kim, D., Ko, J. A., Abd El-Aty, A. M., Choi, J. Y., Kim, D. I., and Yang, K. Y., (2017). Transglycosylation of gallic acid by using *Leuconostoc glucansucrase* and its characterization as a functional cosmetic agent. **AMB Express**. 7(24).
- Nishimura, T., Kometani, T., Okada, S., Ueno, N., and Yamamoto, T. (1995). Inhibitory effects of hydroquinone- $\alpha$ -glucoside on melanin synthesis. **Journal of the Pharmaceutical Society of Japan**. 115(8): 626 - 632.

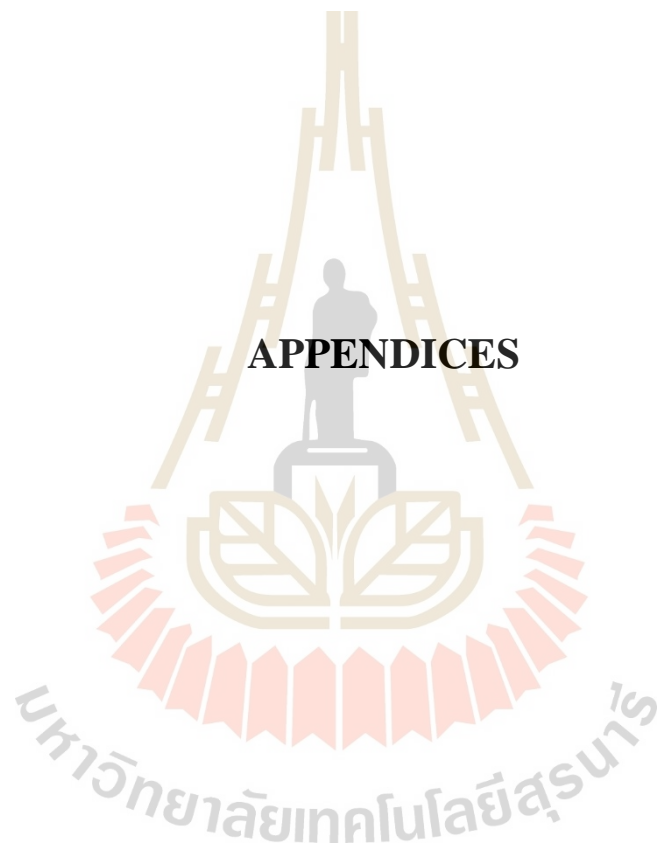
- Opassiri, R., Pomthong, B., Onkoksoong, T., Akiyama, T., Esen, A., and Ketudat Cairns J. R. (2006). Analysis of rice glycosyl hydrolase family 1 and expression of Os4BGlu12 beta-glucosidase. **BMC Plant Biology**. 6: 33.
- Opassiri, R., Hua, Y., Wara-Aswapati, O., Akiyama, T., Svasti, J., Esen, A., and Ketudat Cairns, J. R. (2004).  $\beta$ -Glucosidase, exo- $\beta$ -glucanase and pyridoxine transglucosylase activities of rice BGlu1. **Biochemical Journal**. 379: 125 - 131.
- O'Neill, E. C., and Field, R. A. (2015). Enzymatic synthesis using glycoside phosphorylases. **Carbohydrate Research**. 403: 23 - 37.
- Pandey, R. P., Parajuli, P., Koirala, N., Lee, J. H., Park, Y. I., and Sohng, J. K. (2014). Glucosylation of isoflavonoids in engineered *Escherichia coli*. **Molecules and Cells**. 37(2): 172 - 177.
- Pengthaisong, S., Withers, S. G., Kuaprasert, B., Svasti, J., and Ketudat Cairns, J. R. (2011). The role of the oligosaccharide binding cleft of rice BGlu1 in hydrolysis of cellooligosaccharides and in their synthesis by rice BGlu1 glycosynthase. **Protein Science**. 21: 362 - 372.
- Perez-Sanchez, M., Cabrera, C. A., García-Martín, H., Sinisterra, J. V., García, J. I., and Hernaiz, M. J. (2011). Improved synthesis of disaccharides with *Escherichia coli*  $\beta$ -galactosidase using bio-solvents derived from glycerol. **Tetrahedron**. 67: 7708 - 7712.
- Prawisut, A., Choknud, S., and Ketudat Cairns, J. R. (2020). Expression of rice  $\beta$ -exoglucanase II (OsExoII) in *Escherichia coli*, purification, and characterization. **Protein Expression and Purification**. 175: 105708.

- Prawisut, A. (2018) Expression, purification and characterization of rice beta-glucan exoglucanase (Doctoral dissertation). **Suranaree University of Technology, Thailand.**
- Polayes, D. A. (1998). Application of TEV Protease in Protein Production. **Methods in Molecular Medicine.** 13: 169 - 183.
- Puchart, V. (2015). Glycoside phosphorylases: Structure, catalytic properties and biotechnological potential. **Biotechnology Advances.** 33: 261 - 276.
- Rather, M. Y., and Mishra, S. (2013).  $\beta$ -Glycosidases: An alternative enzyme based method for synthesis of alkyl-glycosides. **Sustainable Chemical Processes.** 1(7).
- Richard, J. P., Westerfeld, J. G., Lin, S., and Beard, J. (1995). Structure-reactivity relationships for beta-galactosidase (*Escherichia coli*, *lac Z*). 2. Reactions of the galactosyl-enzyme intermediate with alcohols and azide ion. **Biochemistry.** 34(37): 11713 - 11724.
- Romero-Télllez, S., Lluch José, M., González-Lafont, À., and Masgrau, L. (2019). Comparing hydrolysis and transglycosylation reactions catalyzed by *Thermus thermophilus*  $\beta$ -Glycosidase. A Combined MD and QM/MM Study. **Frontiers in Chemistry.** 7: 200.
- Rye, C. S., and Withers, S. G. (2000). Glycosidase mechanisms. **Current Opinion in Chemical Biology.** 4: 573 - 580.
- Sinnott, M. L. (1990). Catalytic mechanism of enzymatic glycosyl transfer. **Chemical Reviews.** 90: 1171 - 1202.
- Song, J., Zhang, H., Lia, L., Bi, Z., Chen, M., Wang, W., Yao, Q., Guo, H., Tian, M., Li, H., Yi, W., and Wang, P. G. (2006). Enzymatic biosynthesis of oligosaccharides and glycoconjugates. **Current Organic Synthesis.** 3: 159 - 168.

- Srisimararat, W. and Pongsawasdi, P. (2008). Enhancement of the oligosaccharide synthetic activity of  $\beta$ -galactosidase in organic solvents by cyclodextrin. **Enzyme and Microbial Technology**. 43: 436 - 441.
- Stick, R. V., and Williams, S. J. (2009). Chapter 4 - Formation of the glycosidic linkage. In R. V. Stick, and S. J. Williams. (Ed.), *Carbohydrates: the essential molecules of life* (second edition), **Elsevier**. 133 - 202.
- Streltsov, V. A., Luang, S., Peisley A., Varghese J. N., Ketudat Cairns, J. R., Fort, S., Hijnen, M., Tvaroska, I., Arda, A., Jimenez-Barbero, J., Alfonso-Prieto, M., Rovira, C., Mendoza, F., Tiessler, L., Sanchez-Aparicio, J., Rodrigue-Guerra, J., Lluch, J. M., Marechal, J. D., Masgrau, L., and Hrmova, M. (2019). Discovery of processive catalysis by an exo-hydrolase with a pocket-shaped active site. **Nature Communications**. 10: 2222.
- Sua, C., Allum, A. J., Aizawa, Y., and Kato, T. A. (2016). Novel glyceryl glucoside is a low toxic alternative for cryopreservation agent. **Biochemical and Biophysical Research Communications**. 476(4): 359 - 364.
- Teze, D., Hendrickx, J., Czjzekj, M., Ropartz, D., Sanejouand, Y. H., Tran, V., Tellier, C., and Dion, M. (2014) Semi-rational approach for converting a GH1  $\beta$ -glycosidase into a  $\beta$ -transglycosidase. **Protein Engineering, Design & Selection**. 27(1): 13 - 19.
- Thenchartanan, P., Pitchayatanakorn, P., Wattana-Amorn, P., Ardá, A., Svasti, J., Jiménez-Barbero, J., and Kongsaree, P. T. (2020). Synthesis of long-chain alkyl glucosides via reverse hydrolysis reactions catalyzed by an engineered  $\beta$ -glucosidase. **Enzyme and Microbial Technology**. 140: 109591.

- Tran, L. T., Blay, V., Luang, S., Eurtivong, C., Choknud, S., González-Díazi, H., and Ketudat Cairns, J. R. (2019). Engineering faster transglycosidases and their acceptor specificity. **Green Chemistry**. 21: 2823 - 2836.
- Trott, O., and Olson, A. J. (2010). AutoDock Vina: improving the speed and accuracy of docking with a new scoring function, efficient optimization and multithreading. **Journal of Computational Chemistry**. 31(2): 455 - 461.
- Waterhouse, A., Bertoni, M., Bienert, S., Studer, G., Tauriello, G., Gumienny, R., Heer, F. T., de Beer, T. A. P., Rempfer, C., Bordoli, L., Lepore, R., and Schwede, T. (2018). SWISS-MODEL: homology modelling of protein structures and complexes. **Nucleic Acids Research**. 46(1): 296 - 303.
- Vaistij, F. E., Lim, E. K., Edwards, R., and Bowles, D. J. (2009). Glycosylation of secondary metabolites and xenobiotics. In A. E. Osbourn, and V. Lanzotti (Ed.), *Plant Derived Natural Products*, **Springer Nature**. 209 - 228.
- Vetter, J. (2000). Plant Cyanogenic Glycosides. **Toxicon**. 38: 11 - 36.
- Vinholes, J., Silva, M. B., and Silva, L. R. (2015). Hydroxycinnamic acids (HCAs): structure, biological properties and health effects. *Advances in Medicine and Biology*. **Nova Science Publishers**. 105 - 130.
- Zechel, D. L., and Withers, S. G. (2000). Glycosidase mechanisms: anatomy of a finely tuned catalyst. **Accounts of Chemical Research**. 33: 11 - 18.
- Zhang, C., Zhang, L., Wang, D., Ma, H., Liu, B., Shi, Z., Ma, X., Yue-Chen, Y., and Chen, Q. (2018). Evolutionary history of the glycoside hydrolase 3 (GH3) family based on the sequenced genomes of 48 plants and identification of jasmonic acid-related GH3 proteins in *Solanum tuberosum*. **International Journal of Molecular Sciences**. 19: 1850.

**APPENDICES**





# APPENDIX A

## PROTEIN PURIFICATION

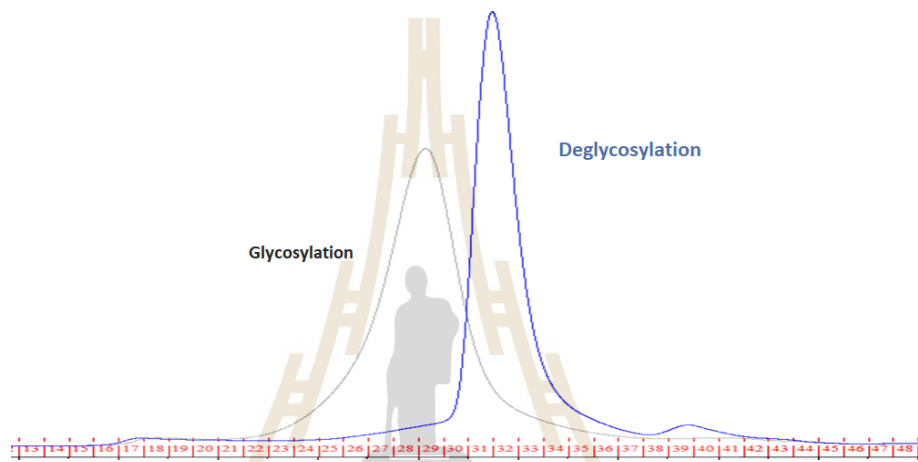


**Figure A.1** HPLC chromatogram of SEC purification of OsExo1.

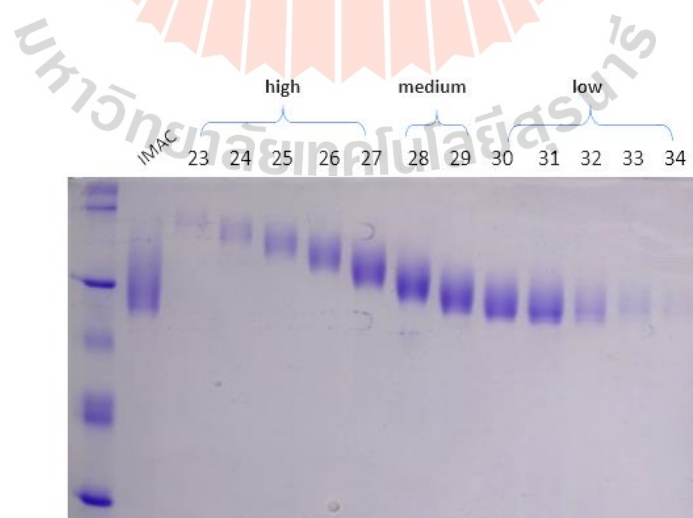


**Figure A.2** SDS-PAGE analysis of SEC purification of OsExo1 glycosylation form.

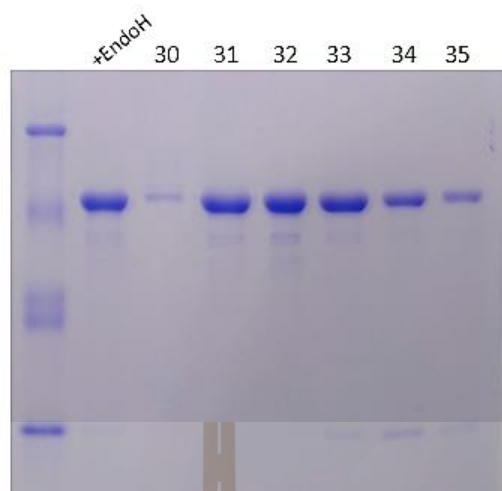


**Figure A.3** SDS-PAGE analysis of SEC purification of OsExo1 deglycosylated form.

**Table A.1** OsExo1 activity during SEC purification.

Fraction No.	Form	Glycosylated	Deglycosylated
23		0.310	-
24		0.639	-
25		0.959	-
26		1.198	-
27		1.574	-
28		2.060	-
29		1.868	-
30		1.855	0.410
31		1.645	2.069
32		1.116	2.142
33		0.238	1.792
34		0.105	1.143
35		-	0.713
36		-	0.470

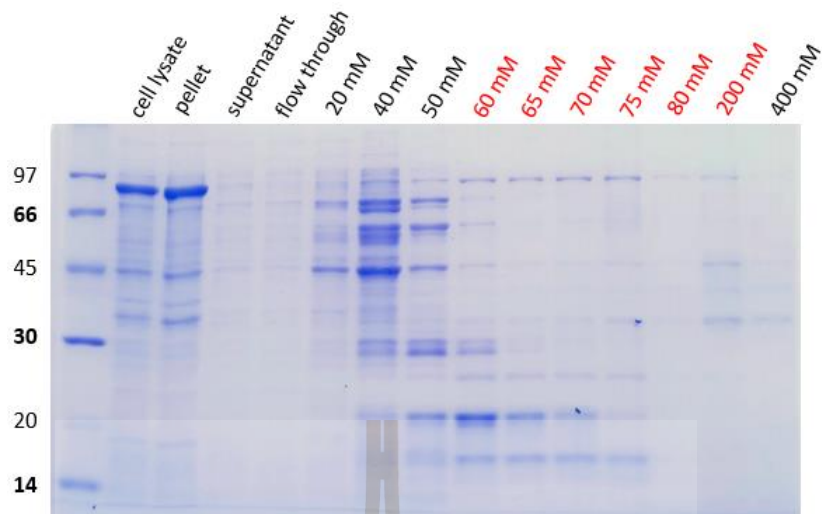


**Figure A.4** SDS-PAGE analysis of IMAC purification of OsExo2.

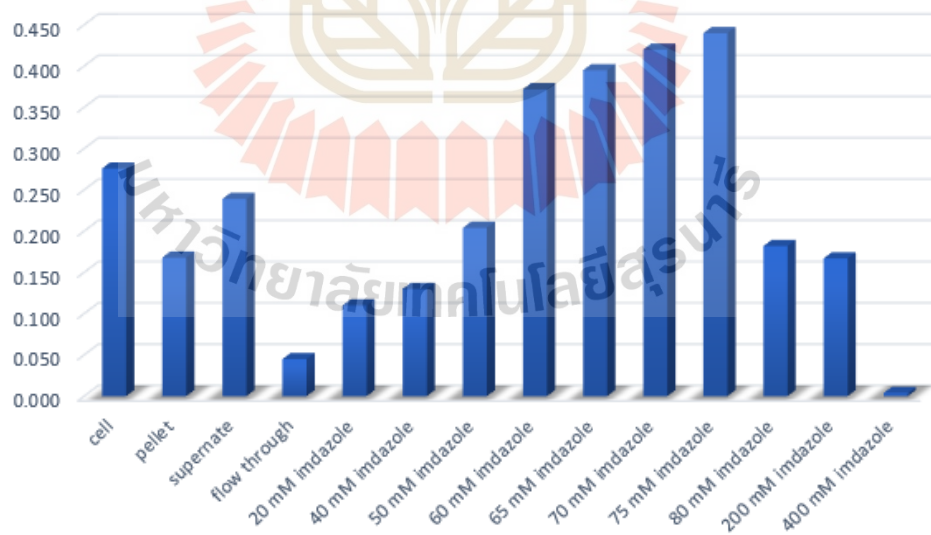


**Figure A.5** OsExo2 activity during IMAC purification.

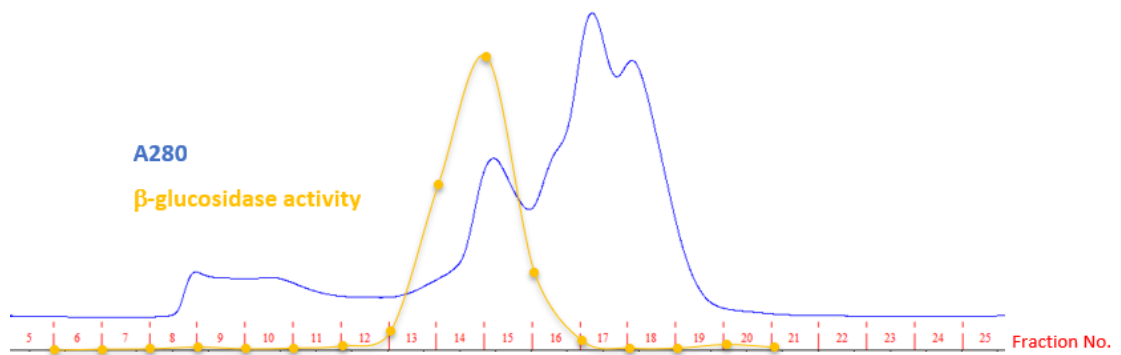


**Figure A.6** HPLC chromatogram of SEC purification and its activity of OsExo2.

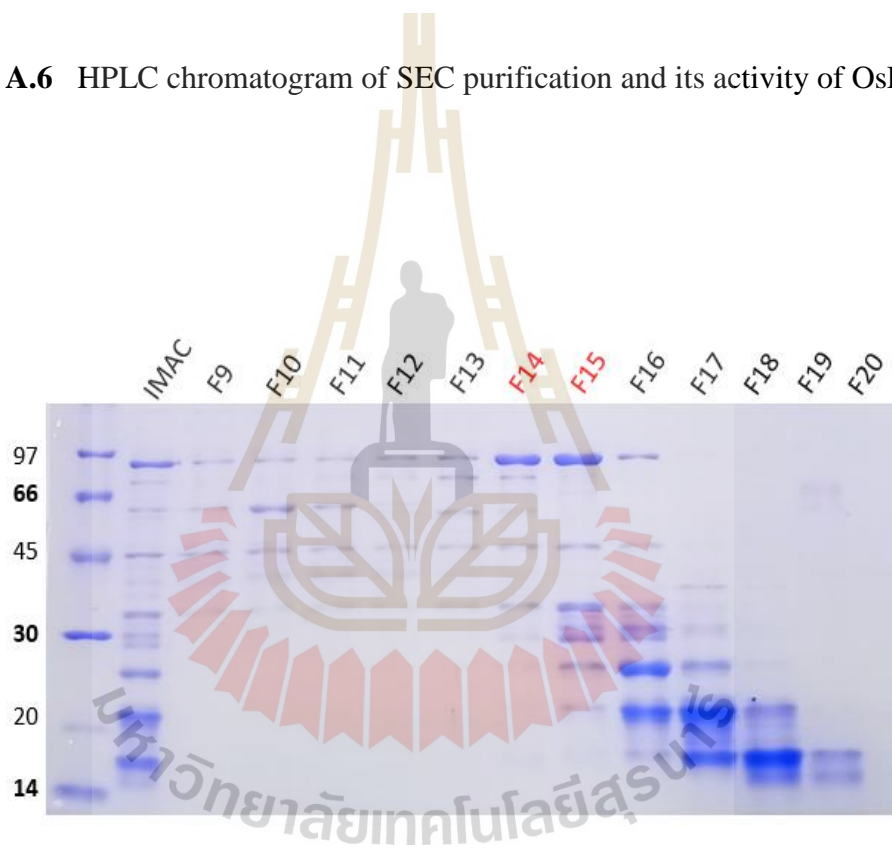


**Figure A.7** SDS-PAGE analysis of SEC purification of OsExo2.

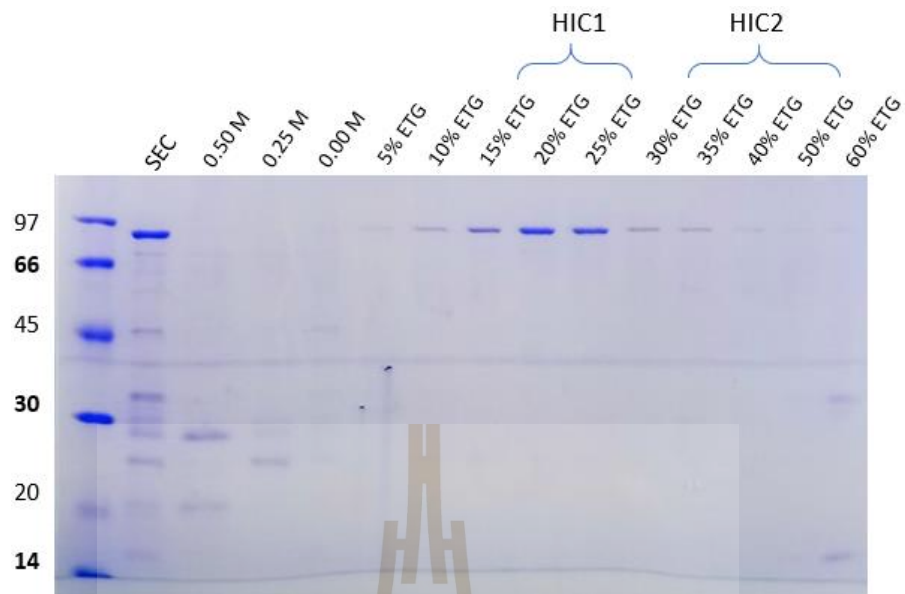


**Figure A.8** SDS-PAGE analysis of HIC purification of OsExo2.

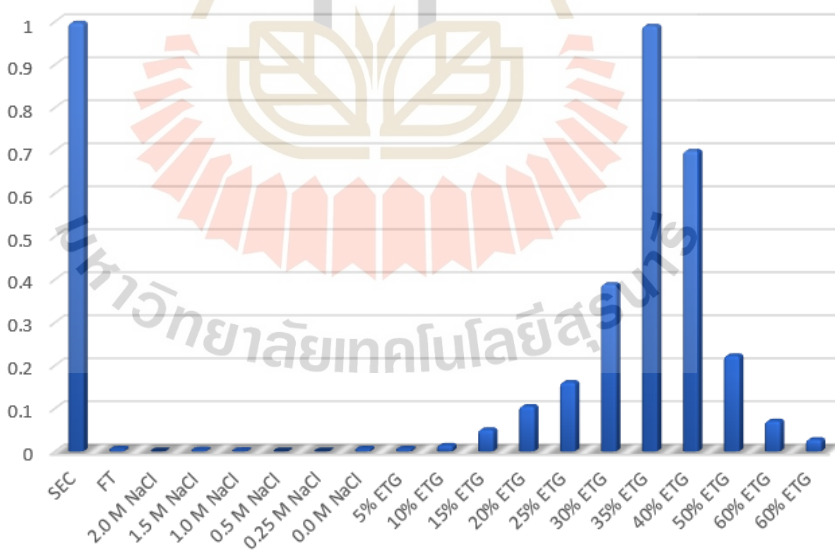


**Figure A.9** OsExo2 activity during HIC purification.

## ***Pfu* polymerase Production**

1. Starter culture: I inoculated 1 ml of the frozen stock of the selected *Pfu* DNA-polymerase clone into 10 ml LB containing 100 µg/ml ampicillin and 34 µg/ml chloramphenicol (LBA<sub>100</sub>C<sub>34</sub>) and incubated in shaking incubator at 180-200 rpm, at 37 °C, overnight (12-18 hr).

2. To scale up, the starter culture (10 ml) was added to 400 ml of LBA<sub>100</sub>C<sub>34</sub> and incubated in a shaking incubator at 180-200 rpm, at 37 °C, overnight (12-18 hr).

3. A 10% v/v portion of scaled up culture was inoculated into 1 L of LB containing LBA<sub>100</sub>C<sub>34</sub> and the culture was incubated in a shaking incubator at 180-200 rpm, at 37 °C until the A<sub>600</sub> reached 1.0. The temperature of the bacterial culture was decreased to 23 °C.

4. IPTG was added to a final concentration of 1 mM to the 23 °C culture from step 3, to induce the expression of T7 polymerase for recombinant protein expression under the control of the T7 promoter for 18 h at 23 °C.

5. The *E. coli* cells were harvested by centrifugation at 4,500 rpm for 30 min.

6. The pellet was resuspended in 100 ml of Ni<sup>2+</sup>-Binding buffer (50 mM Tris-HCl, pH 8.0, 500 mM NaCl, and 20 mM imidazole).

7. The cells were disrupted by sonication for 20 seconds for 3 times, always keep on ice (optional: the cells were treated with lysozyme at a final concentration of 1 mg/ml for 1 h at 37 °C before sonication).

8. The cell debris was removed by centrifugation at 18,000 rpm for 45 min, and the supernatant collected.

9. Ni-NTA beads (3 mL, slurry) were added to the supernatant and mixed continuously for 30 min at 4 °C.

10. The cells were resuspended in His-binding/washing buffer: 50mM Tris, pH 8.0, 500 mM NaCl, 20 mM imidazole.

11. The resuspended sample/resin was loaded into a 10 ml disposable column, the resin beads were washed with His-wash buffer 30-150 ml (50 mM Tris, pH 7.2, 0.5 M NaCl, 20 mM imidazole) until the OD<sub>280</sub> was stable (as measured by Nano-drop spectrophotometer).

12. The protein sample was eluted by His-elution buffer: 50 mM Tris, pH 7.2, 0.5 M NaCl, 250 – 500 mM imidazole, 5-10 2-ml fractions were kept until the OD<sub>280</sub> was stable (as measured by Nano-drop spectrophotometer).

13. The protein sample (1 ml in 1.5 ml microfuge tube) was incubated in boiling water 30 second or until the solution became milky white.

14. The tube was centrifuged at 13,000xg by microcentrifuge for 5-10 minutes to remove the precipitated protein (pellet).

15. The solution was concentrated by 50 kDa MWCO ultrafiltration membrane, and kept in storage buffer (50 mM Tris-HCl (pH 8.0), 0.1 mM EDTA, 1 mM DTT, and 50% glycerol) at 40 °C.

16. The **10X Reaction Buffer with MgSO<sub>4</sub>** for *Pfu* polymerase was prepared as follows: 200 mM Tris-HCl (pH 8.8 at 25°C), 100 mM KCl, 100 mM (NH<sub>4</sub>)<sub>2</sub>SO<sub>4</sub>, 20 mM MgSO<sub>4</sub>, 1.0% Triton® X-100 and 1 mg/ml nuclease-free BSA.



# APPENDIX B

## NMR SPECTRA

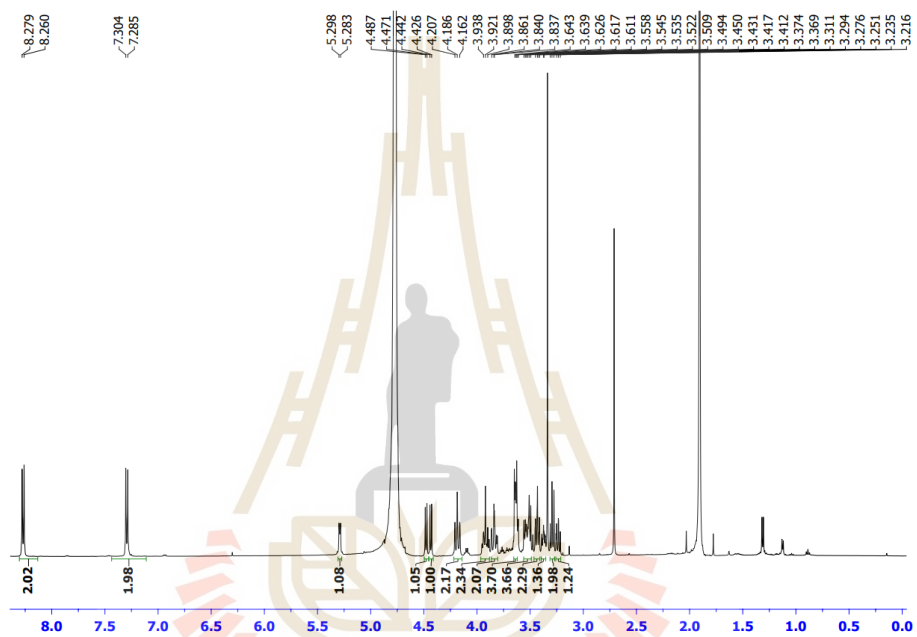
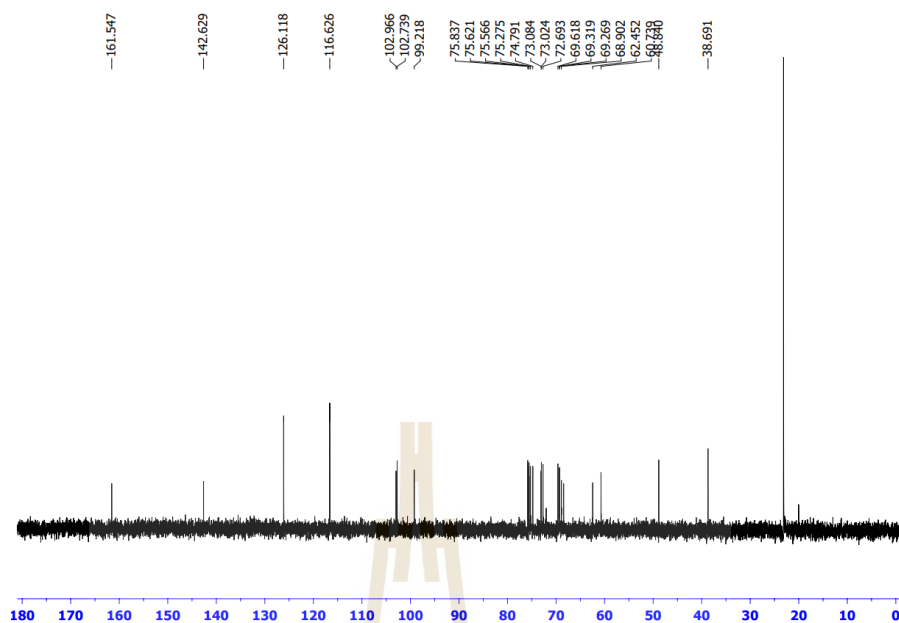
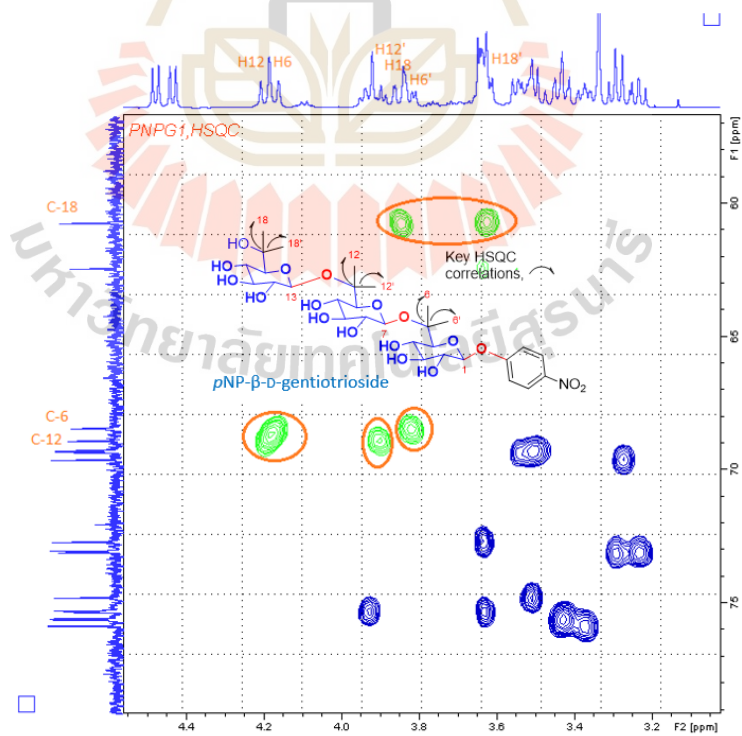


Figure B.1  $^1\text{H-NMR}$  spectrum of *p*NP- $\beta$ -D-gentiotrioside.



**Figure B.2**  $^{13}\text{C}$ -NMR spectrum of *p*NP- $\beta$ -D-gentiotriose.



**Figure B.3** HSQC spectrum of *p*NP- $\beta$ -D-gentiotriose.

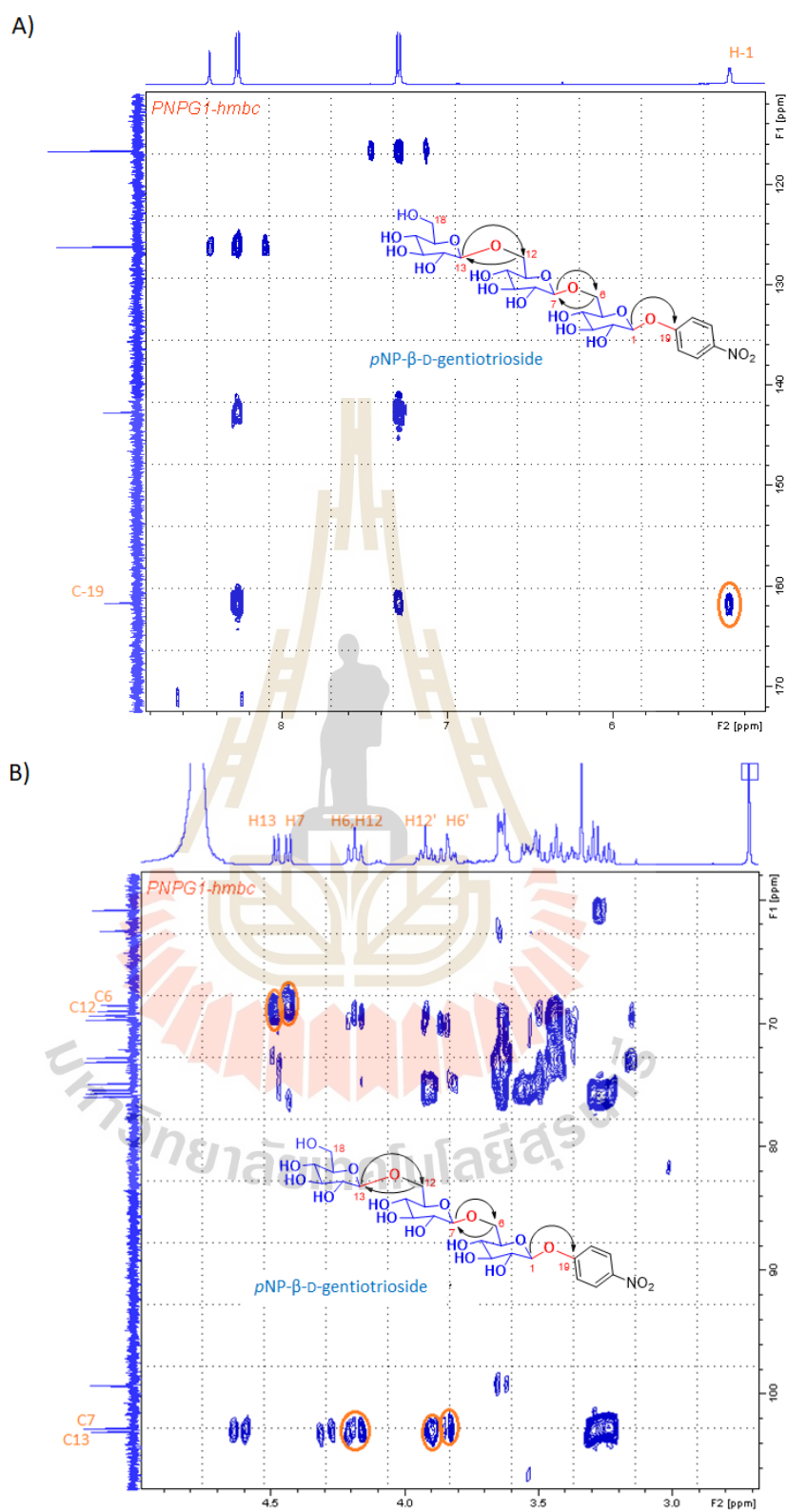


**Figure B.4** HMBC spectrum of *p*NP- $\beta$ -D-gentiatrioside.

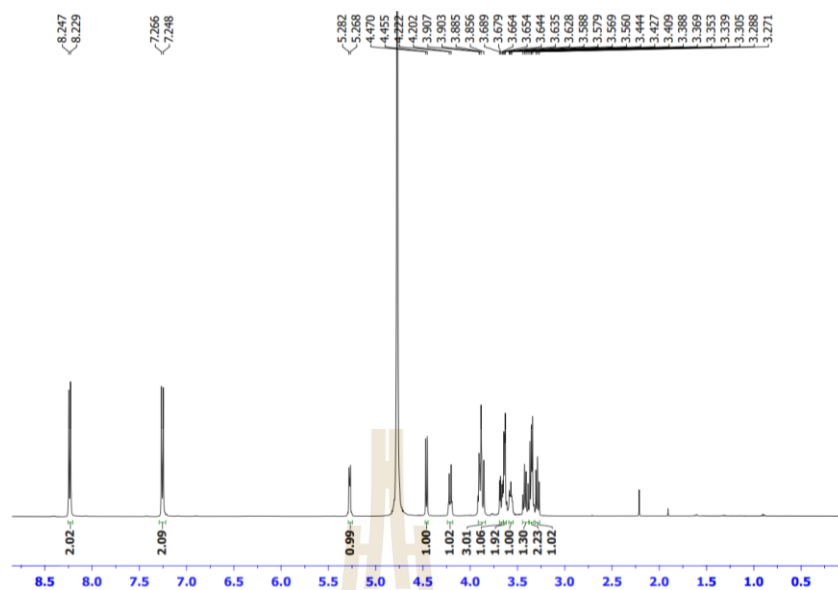


Figure B.5  $^1\text{H-NMR}$  spectrum of *pNP*- $\beta$ -D-gentiobioside.

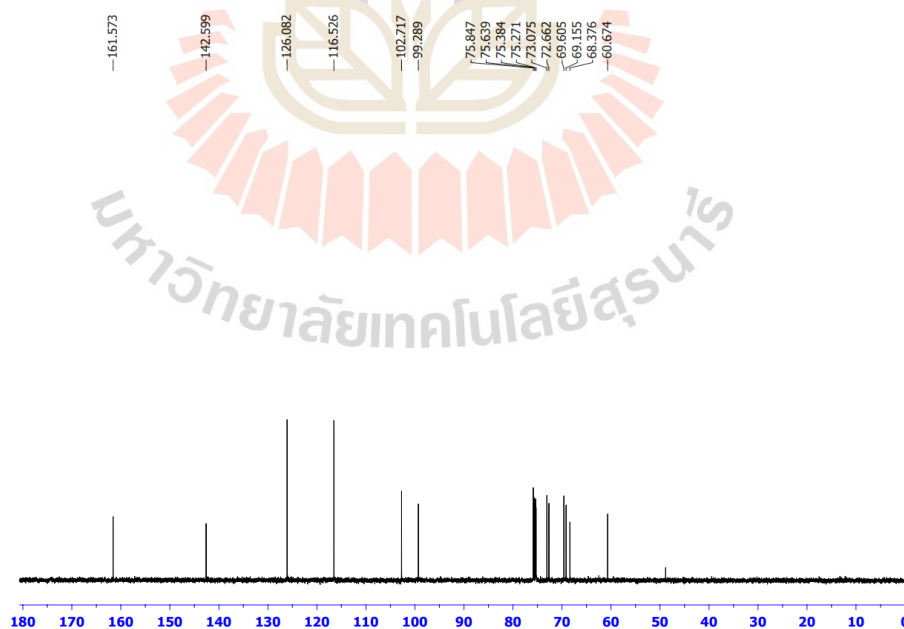


Figure B.6  $^{13}\text{C-NMR}$  spectrum of *pNP*- $\beta$ -D-gentiobioside.

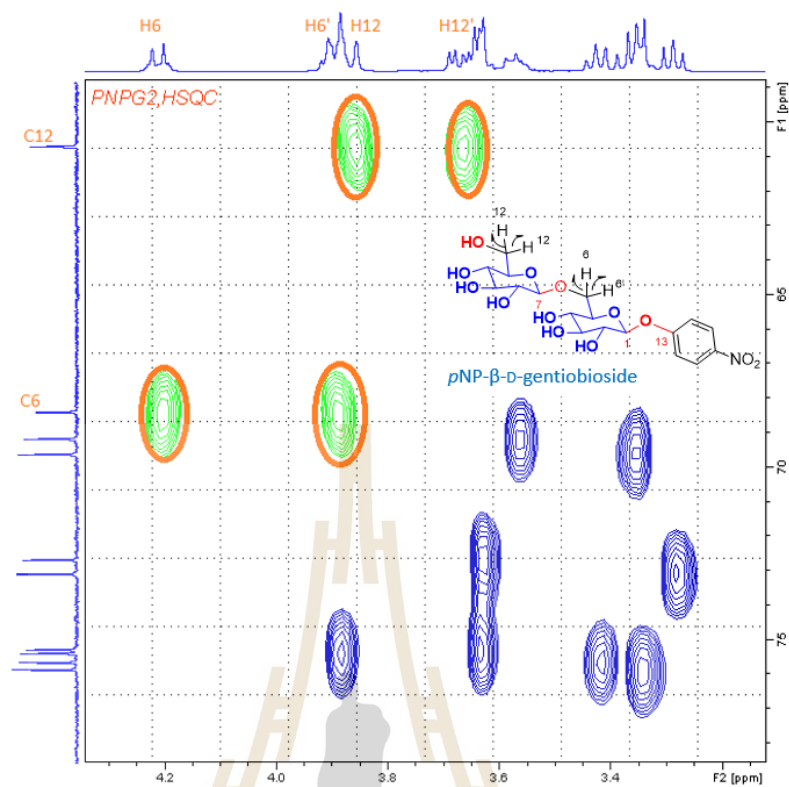


Figure B.7 HSQC spectrum of *p*NP- $\beta$ -D-gentiobioside.

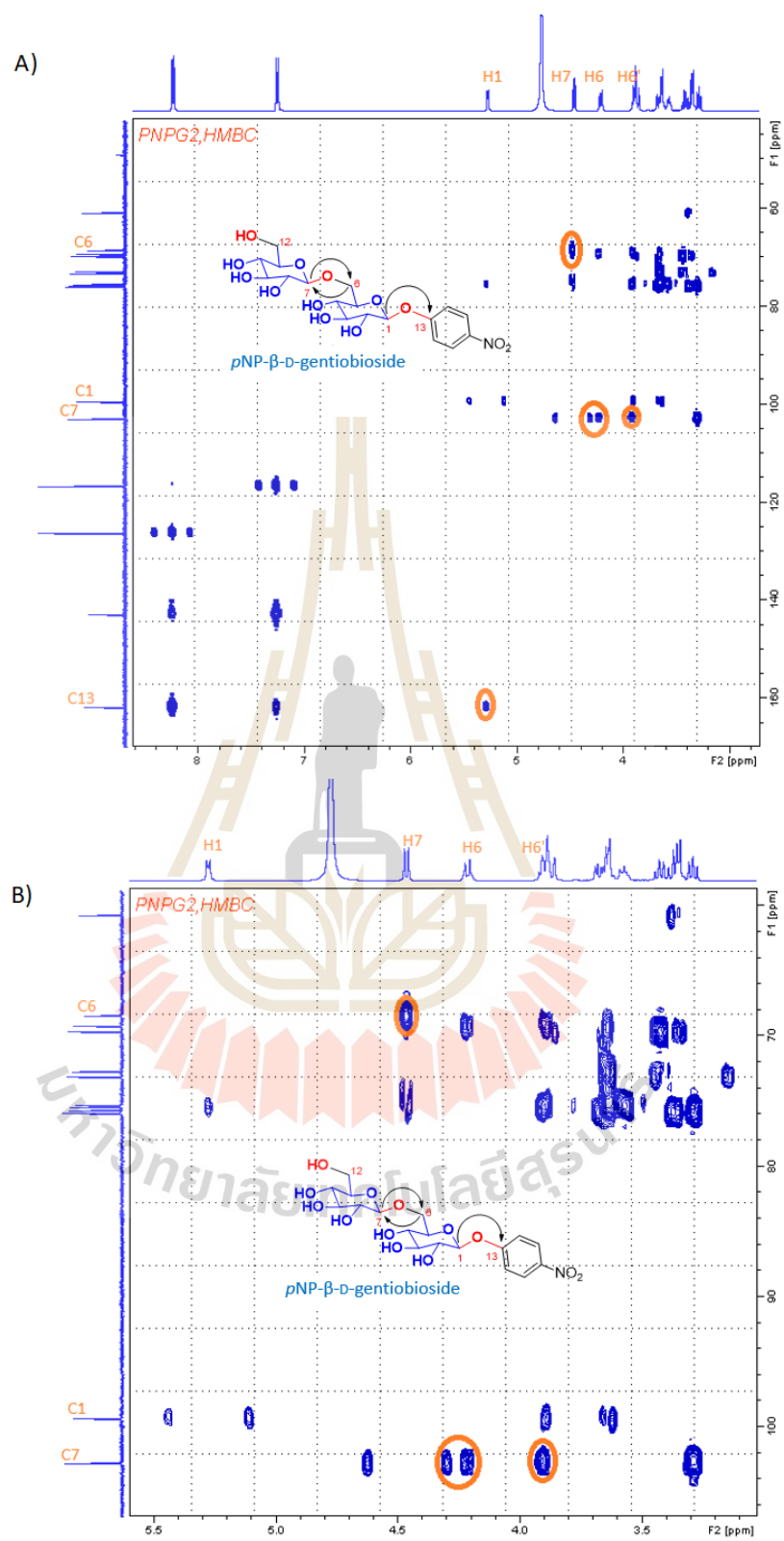
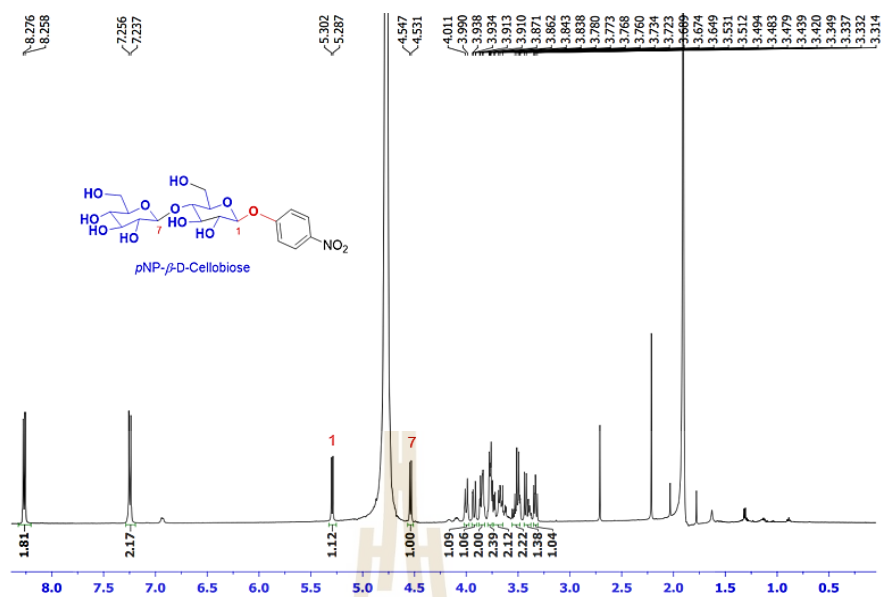
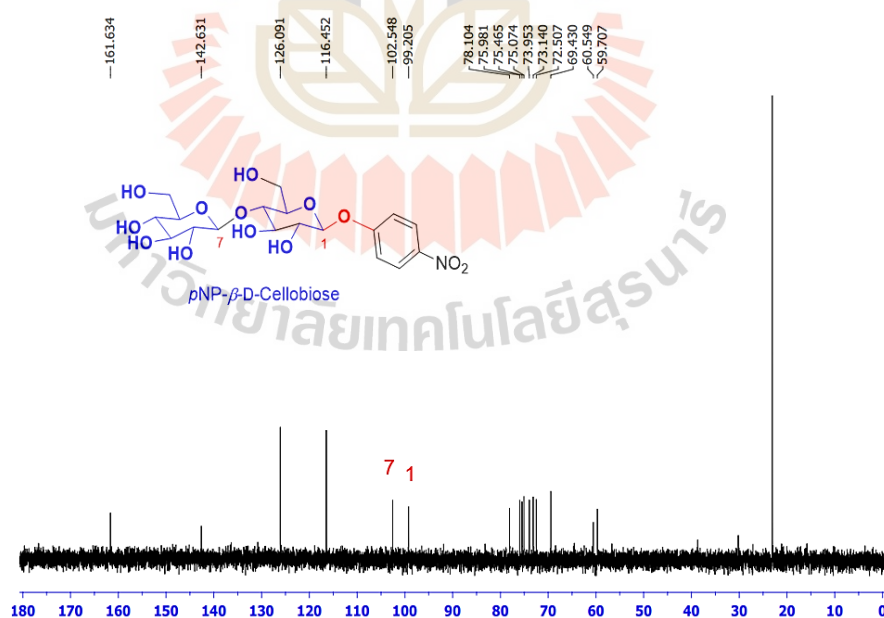


Figure B.8 HMBC spectrum of *p*NP- $\beta$ -D-gentiobioside.



**Figure B.9** <sup>1</sup>H-NMR spectrum of pNP-β-D-cellobioside.



**Figure B.10** <sup>13</sup>C-NMR spectrum of pNP-β-D-cellobioside.



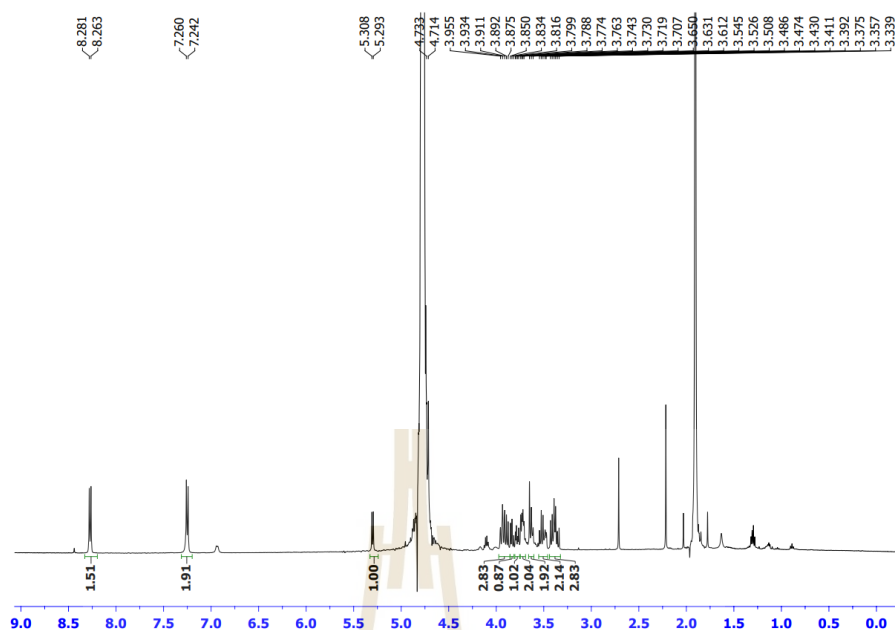


**Figure B.11**  $^1\text{H}$ -NMR spectrum of *p*NP- $\beta$ -D-laminaribioside.

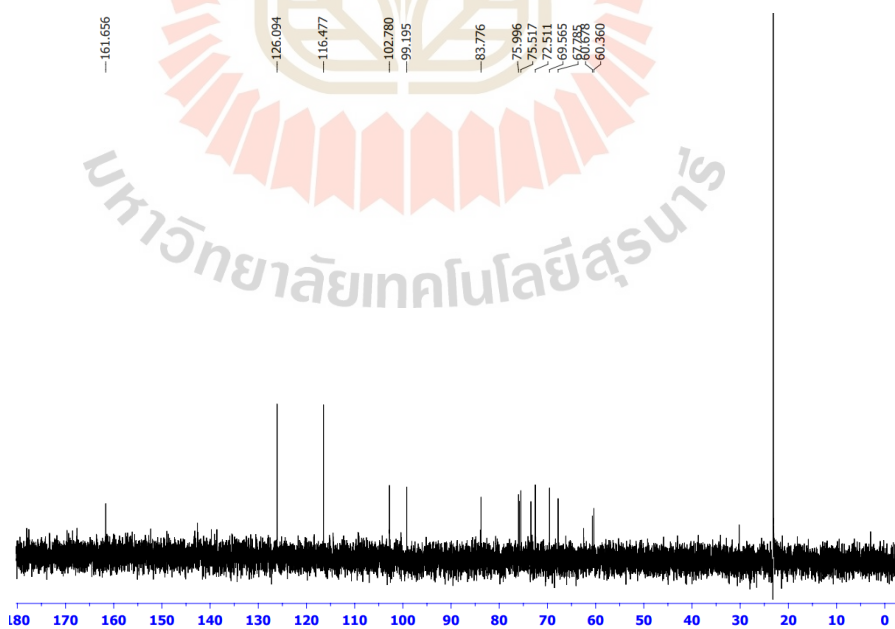


**Figure B.12**  $^{13}\text{C}$ -NMR spectrum of *p*NP- $\beta$ -D-laminaribioside.

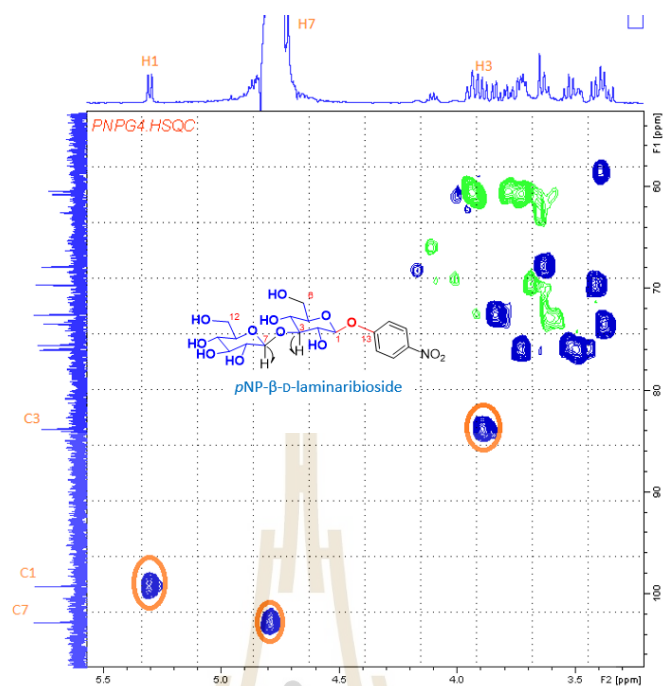


Figure B.13 HSQC spectrum of *p*NP- $\beta$ -D-laminaribioside.

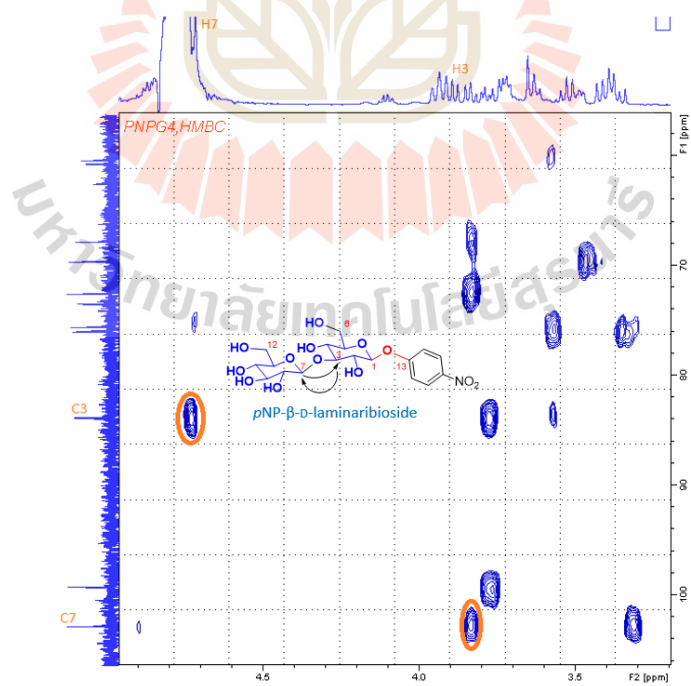
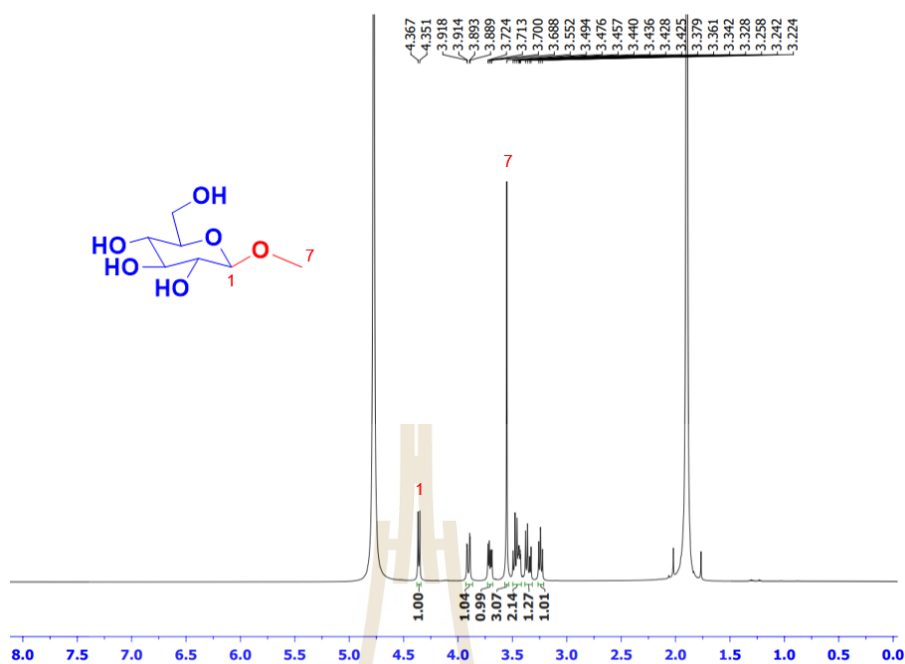
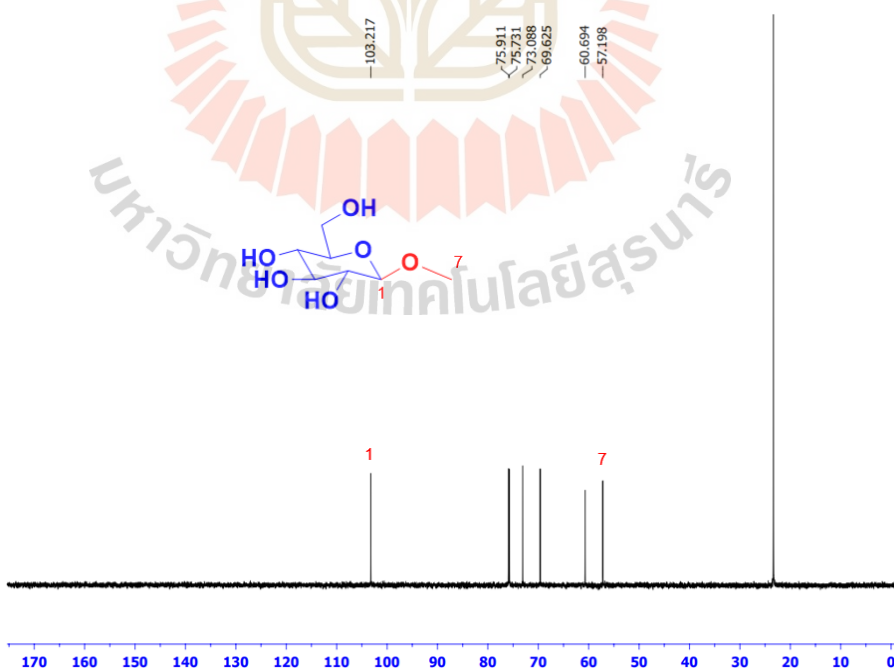


Figure B.14 HMBC spectrum of *p*NP- $\beta$ -D-laminaribioside.



**Figure B.15**  $^1\text{H-NMR}$  spectrum of methyl- $\beta$ -D-glucopyranoside.



**Figure B.16**  $^{13}\text{C-NMR}$  spectrum of methyl- $\beta$ -D-glucopyranoside.

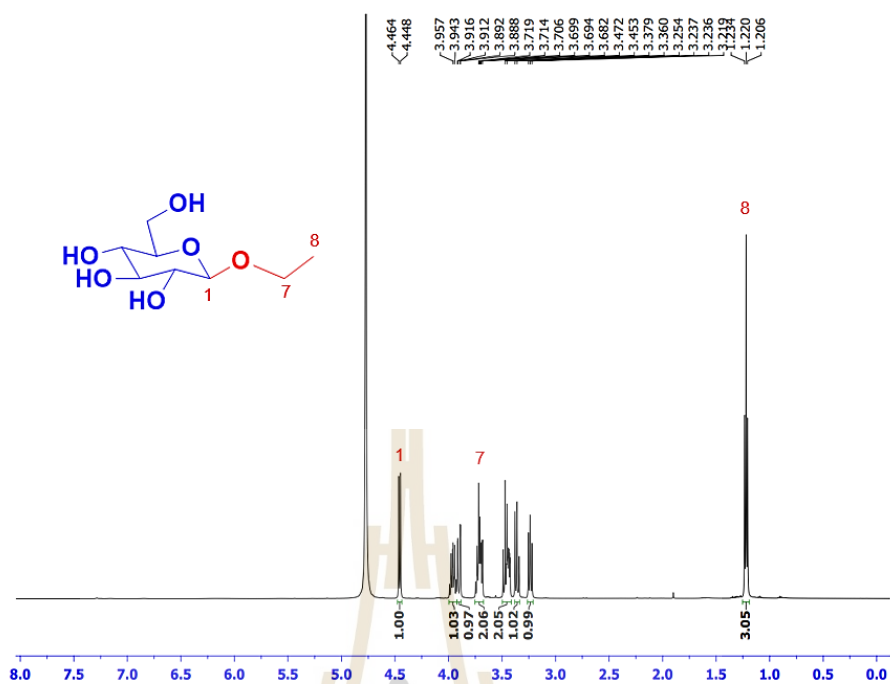


**Figure B.17**  $^1\text{H}$ -NMR spectrum of ethyl- $\beta$ -D-glucopyranoside.

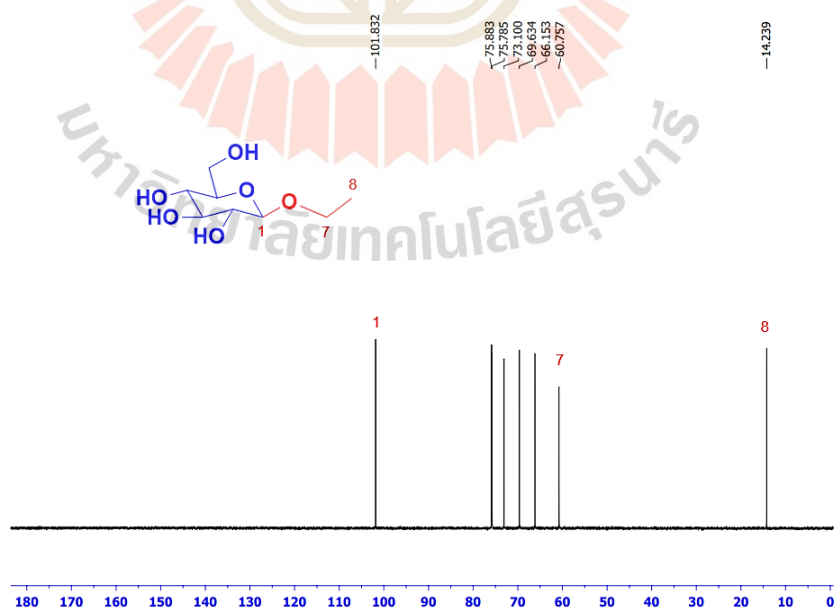


**Figure B.18**  $^{13}\text{C}$ -NMR spectrum of ethyl- $\beta$ -D-glucopyranoside.

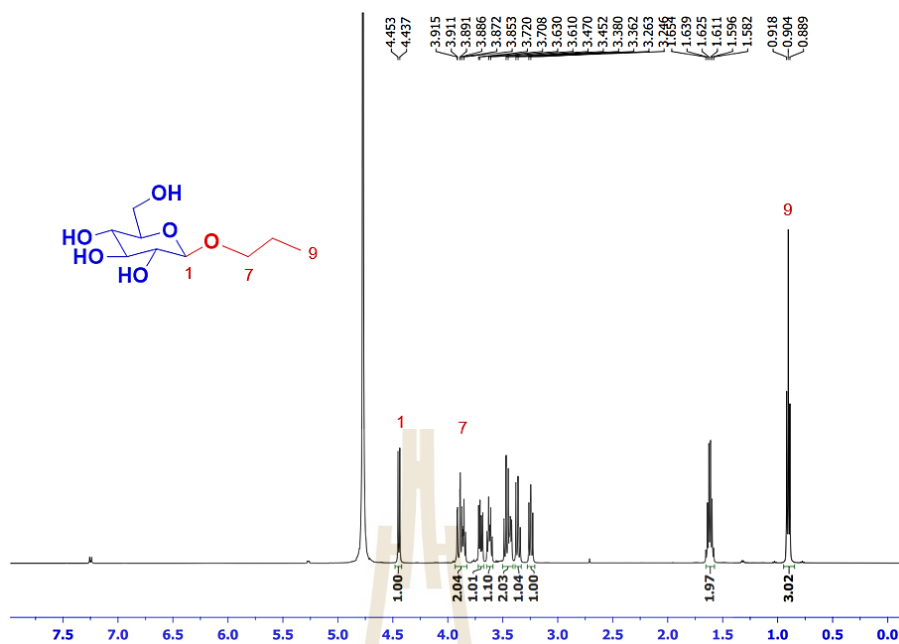


**Figure B.19**  $^1\text{H-NMR}$  spectrum of *n*-propyl- $\beta$ -D-glucopyranoside.

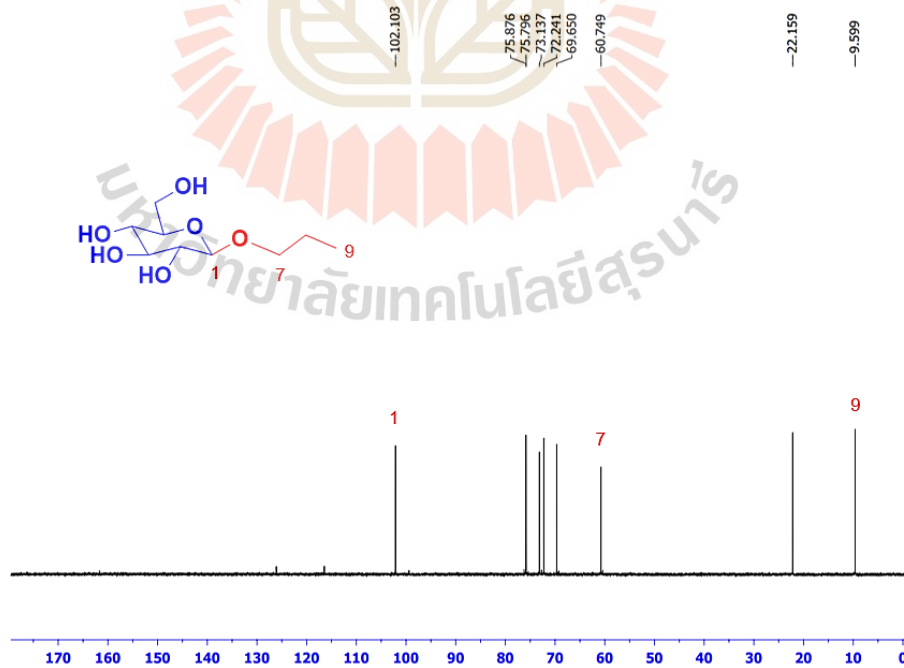


**Figure B.20**  $^{13}\text{C-NMR}$  spectrum of *n*-propyl- $\beta$ -D-glucopyranoside.

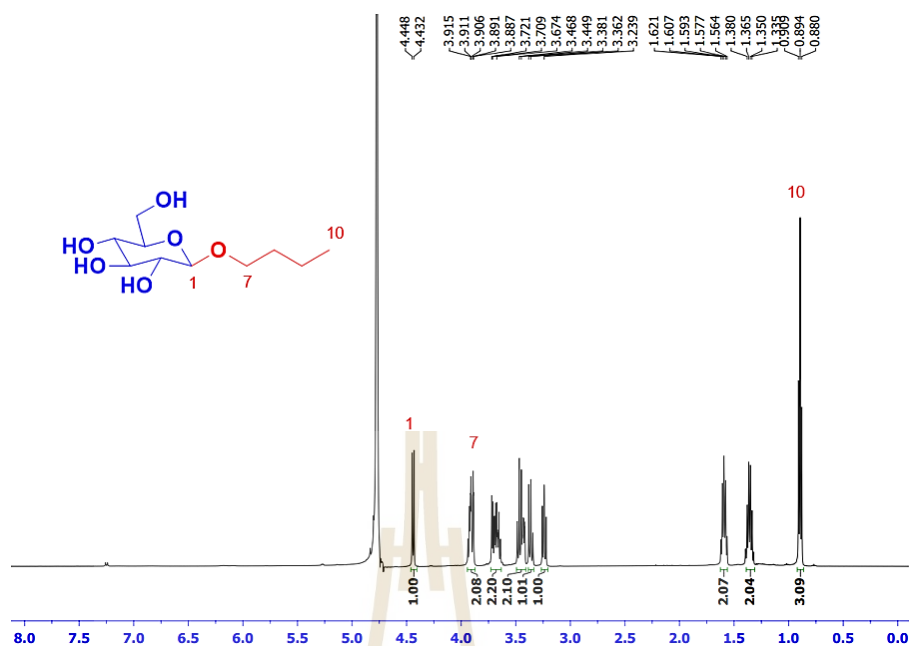


**Figure B.21**  $^1\text{H}$ -NMR spectrum of *n*-butyl- $\beta$ -D-glucopyranoside.

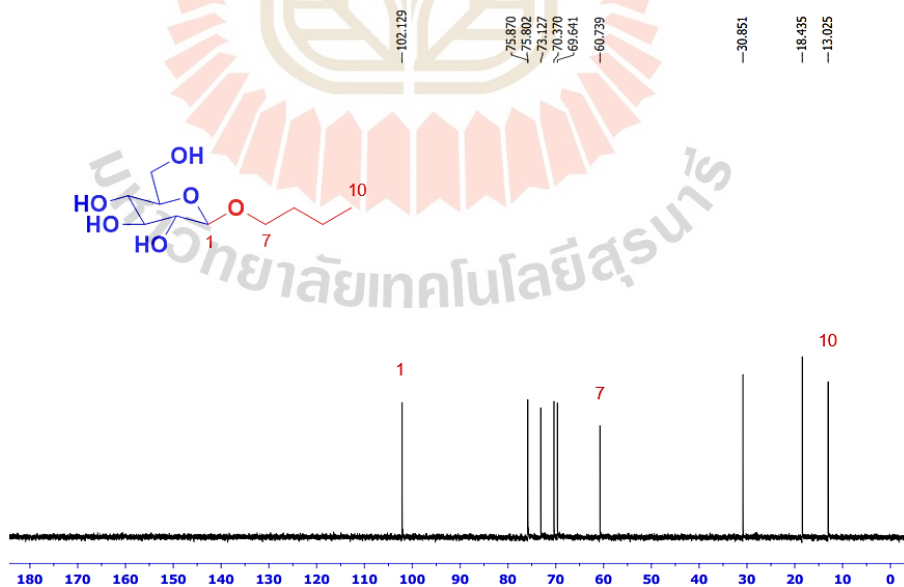


**Figure B.22**  $^{13}\text{C}$ -NMR spectrum of *n*-butyl- $\beta$ -D-glucopyranoside.

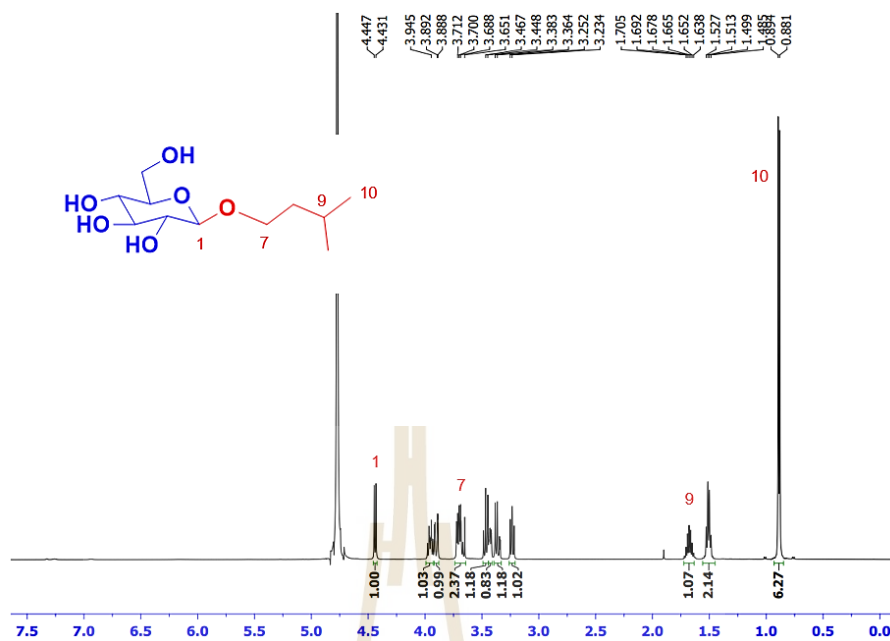


**Figure B.23**  $^1\text{H-NMR}$  spectrum of 3-methyl-1-butyl- $\beta$ -D-glucopyranoside.

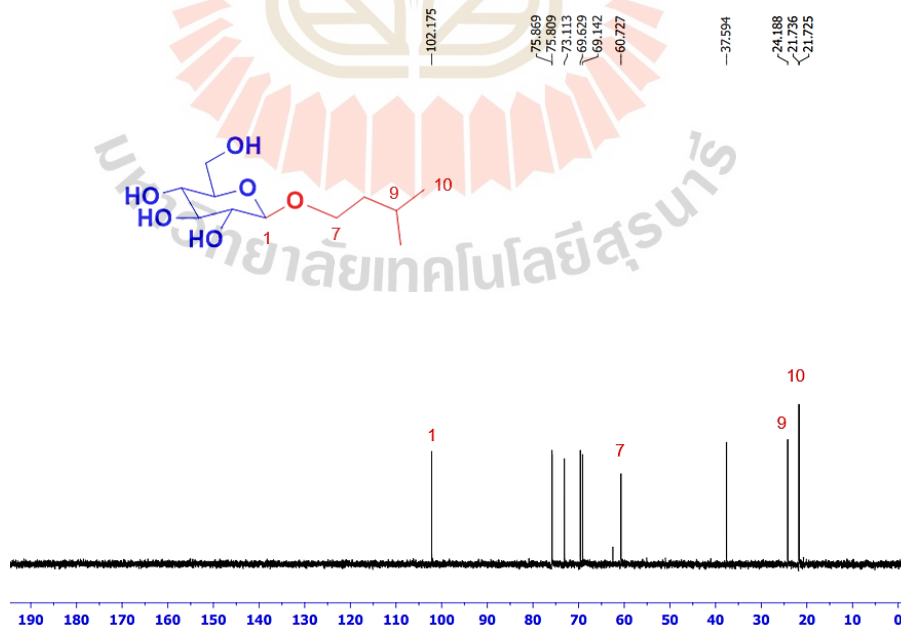


**Figure B.24**  $^{13}\text{C-NMR}$  spectrum of 3-methyl-1-butyl- $\beta$ -D-glucopyranoside.



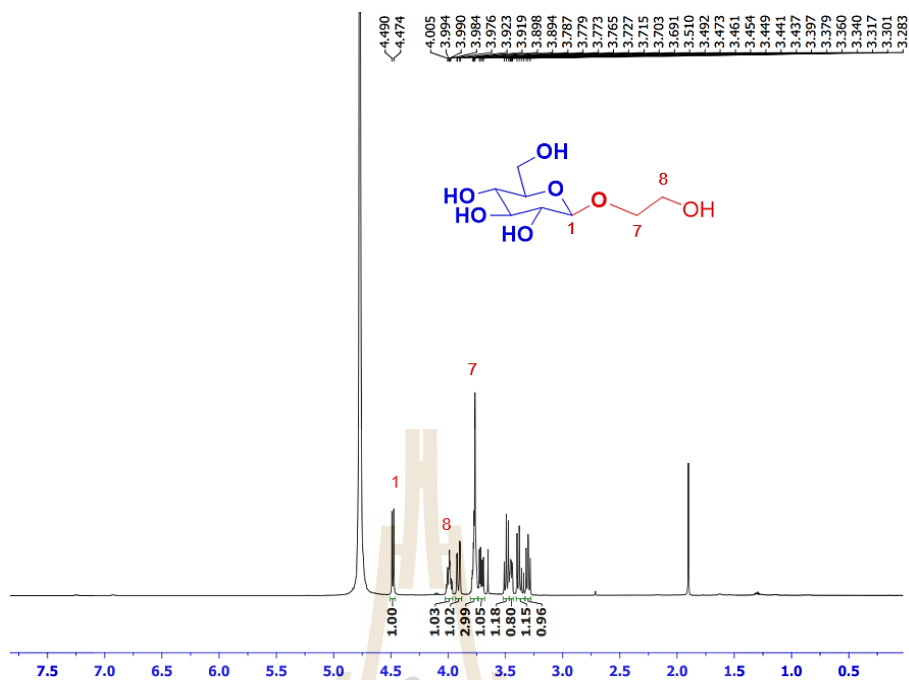


**Figure B.25** <sup>1</sup>H-NMR spectrum of 2-Hydroxyethyl-β-D-glucopyranoside.

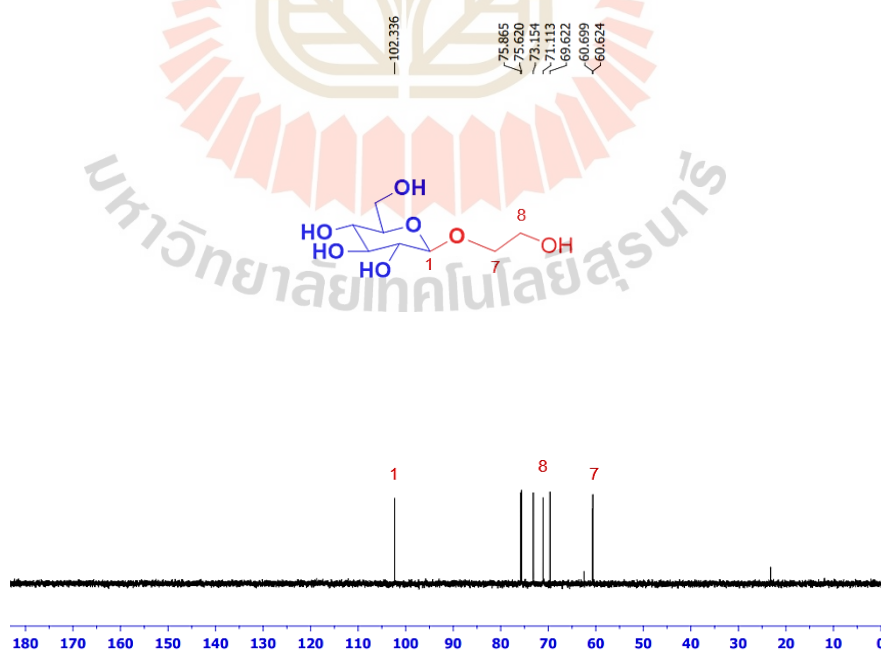


**Figure B.26** <sup>13</sup>C-NMR spectrum of 2-Hydroxyethyl-β-D-glucopyranoside.

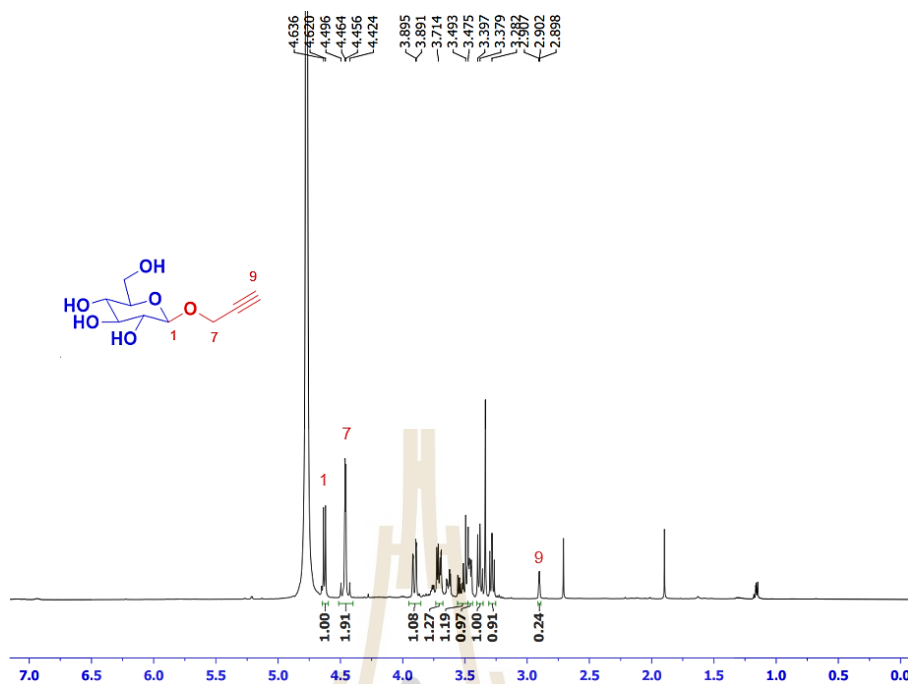


**Figure B.27**  $^1\text{H-NMR}$  spectrum of propargyl- $\beta$ -D-glucopyranoside.

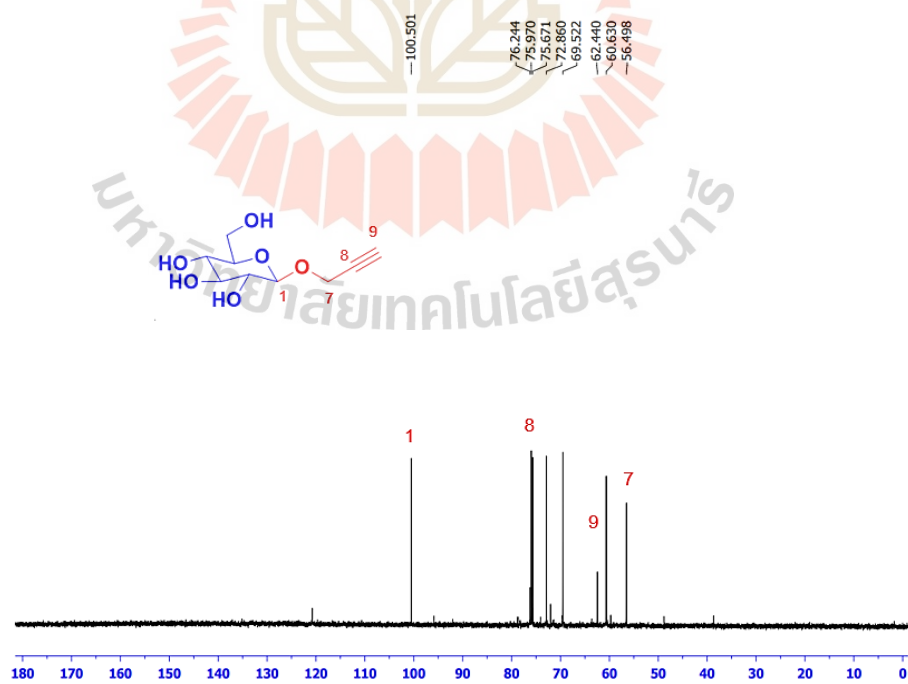


**Figure B.28**  $^{13}\text{C-NMR}$  spectrum of propargyl- $\beta$ -D-glucopyranoside.

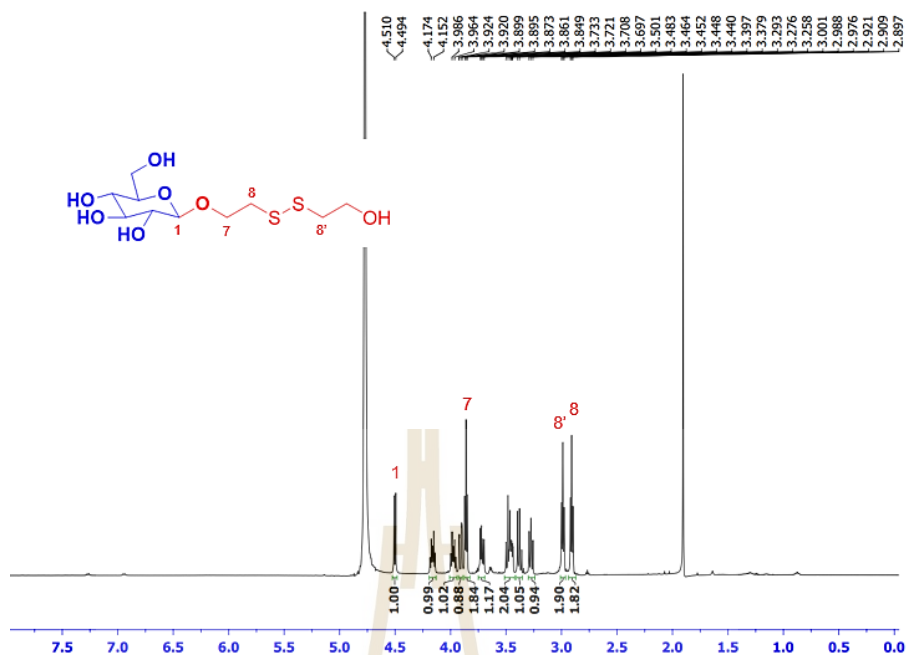


**Figure B.29**  $^1\text{H}$ -NMR spectrum of ethylene-disulfide- $\beta$ -D-glucopyranoside.

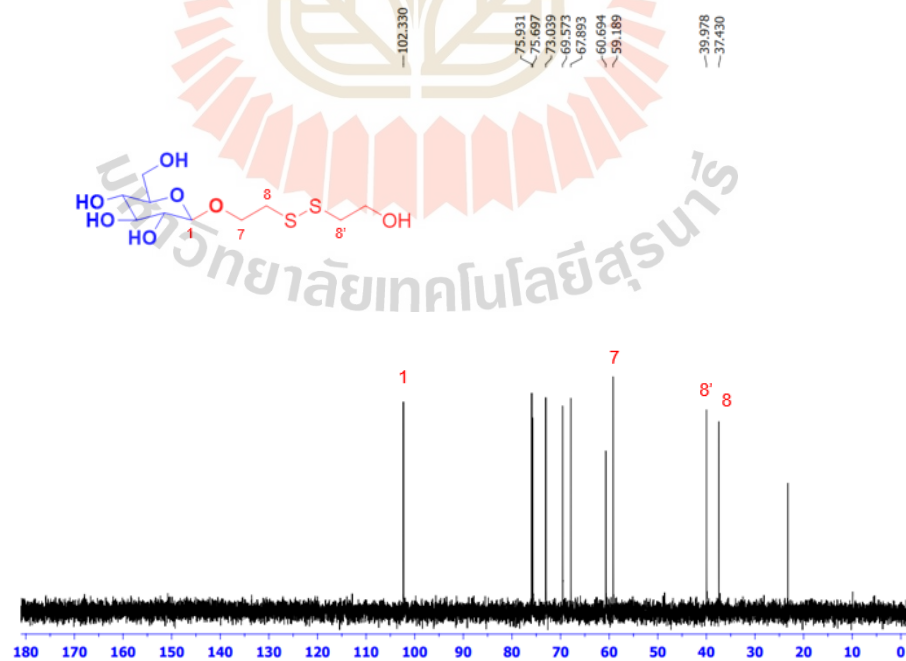


**Figure B.30**  $^{13}\text{C}$ -NMR spectrum of ethylene-disulfide- $\beta$ -D-glucopyranoside.

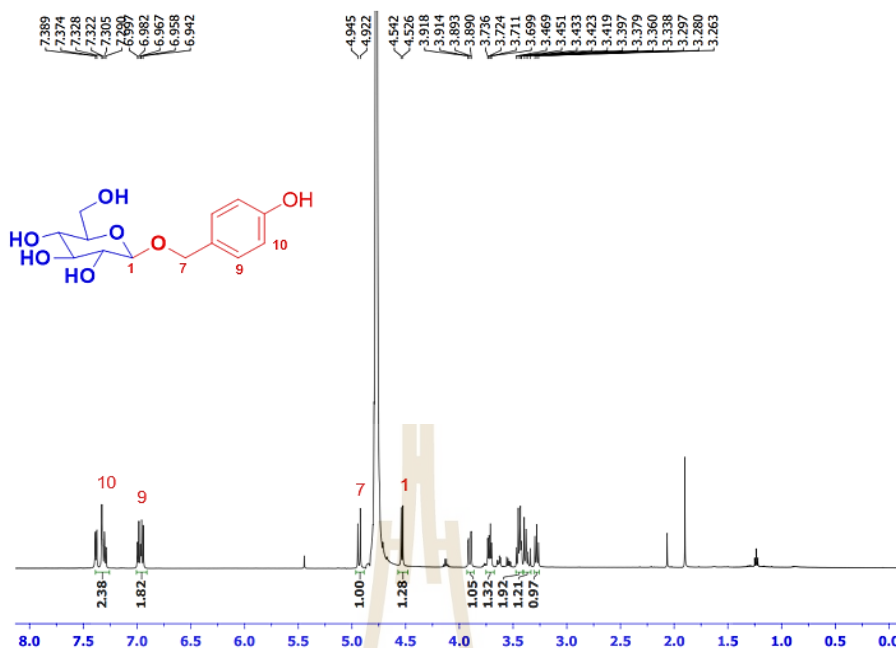


**Figure B.31**  $^1\text{H}$ -NMR spectrum of 4-hydroxybenzyl alcohol  $\beta$ -D-glucopyranoside.

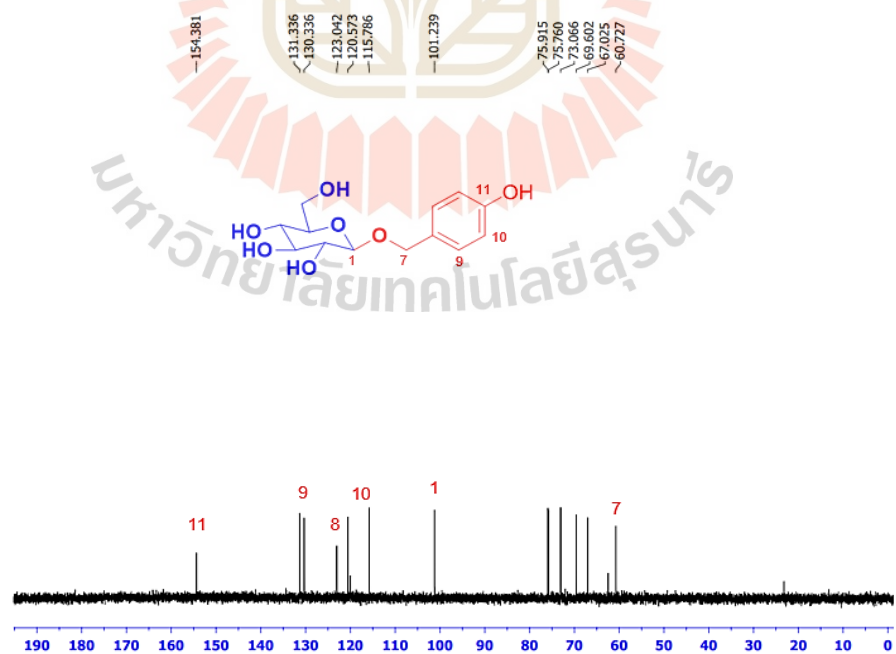


**Figure B.32**  $^{13}\text{C}$ -NMR spectrum of 4-hydroxybenzyl alcohol  $\beta$ -D-glucopyranoside.

## APPENDIX C

### PUBLICATIONS

#### PUBLICATIONS

Akkarawit Prawisut, **Sunaree Choknud**, and James Ketudat Cairns (2020). Expression of rice  $\beta$ -exoglucanase II (OsExoII) in *Escherichia coli*, purification, and characterization. **Protein Expression and Purification**. 175:105708.

Linh Thuy Tran, Vincent Blay, Sukanya Luang, Chatchakorn Eurtivong, **Sunaree Choknud**, Humberto G. Díaz, and James Ketudat Cairns (2019). Engineering faster transglycosidases and their acceptor specificity. **Green Chemistry**. 21(10).

Jaggaiyah Naidu Gorantla, Salila Pengthaisong, **Sunaree Choknud**, Teadkai Kaewpuang, Tanaporn Manyum, Vinich Promarak, and James Ketudat Cairns (2019). Gram scale production of 1-azido- $\beta$ -D-glucose via enzyme catalysis for the synthesis of 1,2,3-triazole-glucosides. **RSC Advances**. 9(11): 6211 - 6220.

**Sunaree Choknud**, Oratai Saisa-ard, and Kenneth J. Haller. (2012). Preparation and characterization of carboxylic acid adducts of gabapentin. **Engineering Journal**. 16(3): 29 - 36.

#### PROCEEDINGS

Phoprasat, P., Yutaekool, N., **Choknud, S.**, Wongthanutkul, R., Jaroonphan, B., Chaiyachit, P., Kamonsuttipaijit, N., and Chamnarnsilapa, S. (2020). Study of calcium-controlled conformation in the N-terminal half of gelsolin by SAXS.

**SUT International Virtual Conference on Science and Technology.** August 28<sup>th</sup>, Nakhon-Ratchasima, Thailand: 215 - 221.

**Sunaree Choknud** and Sakesit Chumnarnsilpa (2016). Screening of natural products effect on GTP hydrolysis of bacillus subtilis FtsZ. **The 11<sup>th</sup> international Symposium of the Protein Society of Thailand.** August 3 - 5, Bangkok, Thailand: 215 - 221.

**Sunaree Choknud**, Chomphonuch Songsiriritthigul, and Sakesit Chumnarnsilpa (2015). The structural study of the c-terminal half of gelsolin. **The 10<sup>th</sup> International Symposium of the Protein Society of Thailand.** July 15 - 17, Bangkok, Thailand: 167 - 172.

#### **PATENT APPLICATIONS**

James Ketudat Cairns and **Sunaree Choknud**. Suranaree University of Technology. Method for production of plant phytohormone abscisic acid glucose ester with transglucosidase. **Thailand patent TH.** Publication No. 1801003832(45/2563), 09 Nov 2020.

James Ketudat Cairns, Jaggaiah Naidu Gorantla, Salila Pengthaisong, and **Sunaree Choknud**. The Thailand Research Fund and Suranaree University of Technology. Low cost process for the gram scale production of 1-azido- $\beta$ -D-glucose for click sugar conjugation reactions via enzymatic catalysis. **Thailand patent TH.** Application No. 1801005294, 05 Sep 2018.

## CURRICULUM VITAE

**NAME** Acting Sub-Lieutenant Sunaree Choknud

**DATE OF BIRTH** December 06, 1989

**PLACE OF BIRTH** Ubon Ratchathani

**EDUCATION**

<b>2021</b>	<b>Ph.D. in Biochemistry and Biochemical Technology</b> , School of Chemistry, Institute of Science, Suranaree University of Technology, Nakhon Ratchasima, Thailand
<b>2015</b>	<b>M.Sc. in Biochemistry</b> , School of Chemistry, Institute of Science, Suranaree University of Technology, Nakhon Ratchasima, Thailand
<b>2012</b>	<b>B.Sc. in Chemistry</b> , Department of Chemistry, Faculty of Science, Ubon Ratchathani Rajabhat University, Ubon Ratchathani, Thailand

